AD-A213 729

RT DOCUMENTATION PAGE

Form Approved
OMB No. 0704-0188

1a. REPORT SECURITY CLASSIFICATION UNCLASSIFIED	1b. RESTRICTIVE MARKINGS NONE
2a. SECURITY CLASSIFICATION AUTHORITY	3. DISTRIBUTION/AVAILABILITY OF REPORT APPROVED FOR PUBLIC RELEASE; DISTRIBUTION UNLIMITED.
2b. DECLASSIFICATION/DOWNGRADING SCHEDULE	
4. PERFORMING ORGANIZATION REPORT NUMBER(S)	5. MONITORING ORGANIZATION REPORT NUMBER(S) AFIT/CI/CIA-88-230
6a. NAME OF PERFORMING ORGANIZATION AFIT STUDENT AT TEXAS A&M UNIVERSITY 6b. OFFICE SYMBOL (If applicable)	7a. NAME OF MONITORING ORGANIZATION AFIT/CIA
6c. ADDRESS (City, State, and ZIP Code)	7b. ADDRESS (City, State, and ZIP Code) Wright-Patterson AFB OH 45433-6583
8a. NAME OF FUNDING/SPONSORING ORGANIZATION 8b. OFFICE SYMBOL (If applicable)	9. PROCUREMENT INSTRUMENT IDENTIFICATION NUMBER
8c. ADDRESS (City, State, and ZIP Code)	10. SOURCE OF FUNDING NUMBERS PROGRAM ELEMENT NO. / PROJECT NO. / TASK NO / WORK UNIT ACCESSION NO.

11. TITLE (Include Security Classification) (UNCLASSIFIED) See Title Page
~~IDENTIFICATION AND QUALIFICATION OF STRUCTURE IN SIMULATED TIROS N RADIANCE SURROUNDINGS~~

12. PERSONAL AUTHOR(S)
G. ANDERSON WHITE, III

13a. TYPE OF REPORT	13b. TIME COVERED	14. DATE OF REPORT (Year, Month, Day)	15. PAGE COUNT
~~THESIS~~/DISSERTATION	FROM _____ TO _____	1988	163

16. SUPPLEMENTARY NOTATION
APPROVED FOR PUBLIC RELEASE IAW AFR 190-1
ERNEST A. HAYGOOD, 1st Lt, USAF
Executive Officer, Civilian Institution Programs

17. COSATI CODES			18. SUBJECT TERMS (Continue on reverse if necessary and identify by block number)
FIELD	GROUP	SUB-GROUP	

19. ABSTRACT (Continue on reverse if necessary and identify by block number)

89 10 24 158

20. DISTRIBUTION/AVAILABILITY OF ABSTRACT ☒ UNCLASSIFIED/UNLIMITED ☐ SAME AS RPT. ☐ DTIC USERS	21. ABSTRACT SECURITY CLASSIFICATION UNCLASSIFIED
22a. NAME OF RESPONSIBLE INDIVIDUAL ERNEST A. HAYGOOD, 1st Lt, USAF	22b. TELEPHONE (Include Area Code) (513) 255-2259 / 22c. OFFICE SYMBOL AFIT/CI

DD Form 1473, JUN 86 — Previous editions are obsolete. — SECURITY CLASSIFICATION OF THIS PAGE

AFIT/CI "OVERPRINT"

1 Sep 88

MEMO FOR RECORD

SUBJ: Dissertation information for entry into annual Air University Abstract of Research Reports

TO: AFIT/CIR
Wright Patterson AFB OH 45433-6583

The following information accompanies the abstract of my dissertation:

a. Author: G. Anderson White, III

b. Title: Identification and Quantification of Synoptic Structure in Simulated TIROS N Radiance Soundings

c. Military rank: Captain (Major selectee)

d. Service branch: USAF

e. Date: 1988

f. Number of pages: 149

g. Degree awarded: Ph.D.

h. Name of institution: Texas A&M University

G. ANDERSON WHITE, III, Capt, USAF

IDENTIFICATION AND QUANTIFICATION OF SYNOPTIC STRUCTURE IN SIMULATED TIROS N RADIANCE SOUNDINGS

A Dissertation

by

G. ANDERSON WHITE, III

Submitted to the Office of Graduate Studies
Texas A&M University
in partial fulfillment of the requirements for the degree of

DOCTOR OF PHILOSOPHY

December 1988

Major Subject: Meteorology

IDENTIFICATION AND QUANTIFICATION OF SYNOPTIC STRUCTURE IN SIMULATED TIROS N RADIANCE SOUNDINGS

A Dissertation

by

G. ANDERSON WHITE, III

Approved as to style and content by:

James P. McGuirk
(Chairman)

Steven W. Lyons
(Member)

George L. Huebner
(Member)

Rudolf J. Freund
(Member)

Kenneth L. White
(Member)

James R. Scoggins
(Head of Department)

December 1988

ABSTRACT

Identification and Quantification of Synoptic Structure in Simulated TIROS N Radiance Soundings. (December 1988)

G. Anderson White, III, B.S., University of North Carolina at Chapel Hill;

M.S., Texas A&M University

Chairman of Advisory Committee: Dr. James P. McGuirk

There has been continual improvement in the accuracy of retrieved atmospheric soundings from satellite radiance measurements; however, satellite data still provide an overly smooth product which is of limited use for synoptic scale analysis. Considerable smoothing occurs when information present in satellite radiance measurements is lost in the retrieval process. This research describes and develops techniques which (1) identify synoptic features and (2) quantify their fine structures directly from TIROS N satellite radiance data.

A series of nine, overlapping, synthetic temperature and moisture soundings is constructed which contains synoptic features representative of the tropical eastern Pacific Ocean. Each of the soundings in the series is perturbed randomly, within limits, to create a statistically meaningful training data set. The training data set is processed through a radiative transfer algorithm to generate equivalent TIROS N satellite observations.

The variance of the training set is partitioned into a portion accounting for synoptic class and a portion describing synoptic feature variation within a class. The variance structure of feature quantification differs strongly from that associated with classification.

In a two-step process, the training data observations first are separated according to synoptic feature, and, second, the fine structure of the synoptic feature is quantified. Three classification techniques are developed to partition the training data observations into synoptic groups and to classify new soundings: a subjective, graphical, interpretative procedure; canonical discriminant analysis; and, discriminant analysis. Accurate classification was accomplished until atmospheric sounding perturbations exceeded 12% of the observed temperatures of the synoptic class means.

Two experiments of feature quantification are described: a prediction of trade wind and frontal inversion height and strength using both synthetic and observed soundings; and, a prediction of frontal structure based on discriminant analysis of a training data set containing frontal inversion soundings. Positive skill, with some ambiguity, was demonstrated in both experiments.

DEDICATION

I dedicate this part of my life to my family. I now realize the that completion of the Ph.D. degree is not an individual accomplishment; it is the result of work and sacrifice by many with the credit wrongfully attributed to one.

To my wonderful wife and eternal companion, Ronda, I offer simply my thanks. You gave up so many hours we could have had together. To our children, Becky, Sarah, Amy and Joshua, I owe you more than I can repay. I cannot count the times you cheerfully sent me "off to school" when we needed to be with each other.

I am indebted to my parents, Gail and Delta White, who encouraged me throughout my life to extend my reach.

Thank you for believing in me. I love you all. To you all, this work is dedicated.

ACKNOWLEDGEMENTS

I am grateful to the faculty of Texas A&M University, the Department of Meteorology and especially the members of my committee for their guidance and support. I owe a particular debt of gratitude to Dr. James P. McGuirk, who treated me as a colleague, and, in doing so, brought forth more effort from me than I thought possible. He never criticized; instead, he communicated, and I learned to criticize myself. I thank Dr. Aylmer H. Thompson for sharing his knowledge of satellite, tropical and synoptic meteorology. His organizational and writing skills are legendary; he helped me immensely. Retirement kept Dr. Thompson's name from the signature page of this document; he deserves recognition nonetheless. Dr. Steven W. Lyons assumed Dr. Thompson's committee duties and made significant contributions to analysis and discussion of results. I appreciate the contributions of Dr. George L. Huebner in the field of remote sensing. Dr. Rudolf J. Freund was my sounding board and statistical mentor; much of the early work was hatched in his office. Dr. Kenneth L. White added thought and innovation to my computations and computer-generated graphics. Dr. William B. Smith introduced me to multivariate statistical methods; what wasn't accomplished in Dr. Freund's office was in Dr. Smith's. Ms. Kay Claybourn and Mr. Roger Sorrells guided me through the mysteries of the university computer system. Dr. Herman Chernoff of the Department of Statistics, Harvard University, offered many helpful suggestions for analysis of my data; I think he was intrigued by yet another application of Chernoff faces.

The radiative transfer model was provided by Drs. Joel Susskind and Dennis Reuter of NASA Goddard Laboratory for the Atmospheres. The model importation, modifications and program additions were successful largely

through the efforts of Messrs. Roger Sorrells, Eddie Rieger and Rob Liles, and Miss Charlotte Atwater. Mrs. Nicole Streetman spent countless hours scripting the manuscript and preparing many of the figures.

I acknowledge the sponsorship of the United States Air Force Institute of Technology, and especially Lt Col John P. Cipriano, for making possible and administering my studies. My work was a small part of a larger effort supported by NASA's George C. Marshall Space Flight Center, contract No. NAS8-37284.

TABLE OF CONTENTS

TABLE OF CONTENTS (Continued)

LIST OF TABLES

LIST OF FIGURES

LIST OF FIGURES (Continued)

LIST OF FIGURES (Continued)

LIST OF FIGURES (Continued)

FIGURE Page

CHAPTER I

INTRODUCTION

Meteorological analysis over data sparse areas relies on remotely sensed data. Unfortunately, results from data gathered by satellite often are smoothed heavily and lack sufficient spatial resolution to be of use in synoptic analysis or forecasting. Temporal resolution usually is adequate.

Satellite sensor technology is not likely to improve the situation significantly in the near future. The most practical source of improved satellite data information and resolution is refined processing and analysis techniques which use currently available data. Fortunately, remote sensing of the atmosphere is most effective where it is needed most, over oceans where land surface effects are non-existent or greatly minimized.

The oceans are genesis regions for synoptic scale weather systems and yet are nearly devoid of meteorological measurements. For example, over the tropical eastern Pacific Ocean, there are only about 8 upper air reporting stations in the area bounded by 180° to 110°W and 30°N to 10°S. Stations are separated by an average of over 2200 km; in contrast, spacing of stations taking upper air observations over the continental U.S. is about 400 km. Even under the best of conditions, upper air observations are taken only every 12 h.

Synoptic scale weather systems are on the order of 200 to 2000 km in space and a few hours to a few days in time (Atkinson, 1981). Weather systems develop in areas where observations are sparse spatially and may be

---

The style is that of the *Monthly Weather Review*.

analyzed poorly or escape detection entirely. Even if such systems are observed, the 12-h interval of surface-based upper air measurements is long enough to lose meaningful synoptic detail.

The current operational method of satellite information retrieval inverts the radiative transfer equation (RTE) to produce atmospheric temperature profiles from satellite radiance data. Mathematically, inversion of the RTE is an ill-posed problem and requires supplemental closure information; the quality of atmospheric temperatures is no better than the quality of the supplemental information. The inversion method employed by NOAA/NESDIS uses a climatologically correct first guess atmospheric sounding which requires knowledge of the season and region under study.

Methods to improve the quality of the first guess constantly are being sought, but until synoptic information is extracted from the satellite observations without conversion to conventional data, little improvement in synoptic analysis using remotely sensed data is anticipated. Despite the success of conventional retrieval methods, additional unused information has been shown to be present in the satellite channel data (Anderson, 1986).

McGuirk et al. (1985), McGuirk et al. (1986) and Anderson (1986) have used empirical orthogonal function (EOF) analysis to explore structural detail of atmospheric data. They found that, in satellite data, individual channel brightness temperatures may be preferable to reconstructed temperature and moisture profiles because the reconstructions are smoothed both horizontally and vertically.

The present research uses advanced multivariate statistical methods which reveal details of synoptic structure in conventional satellite data. This research emphasizes technique development. Synthetic data are used (1) to

minimize interference from cloud and other contamination, (2) to allow study of any synoptic feature(s), and (3) to minimize the statistically undesirable effect of missing data. Emphasis is placed on finding and quantifying the signatures of synoptic features directly in satellite observations.

CHAPTER II

RESEARCH OBJECTIVES AND APPROACH

A. Research objectives

Synoptic features, which have been observed in balloon soundings for many decades and used by operational forecasters, are not observed in satellite data. The primary goals of this research are to identify and quantify synoptic scale meteorological features in satellite channel brightness temperature data. It is hypothesized that this recognition and quantification can be accomplished by: (1) establishing relationships between known atmospheric soundings and corresponding satellite observations; and, (2) applying statistical methods and a fundamental knowledge of the region and season under study. It is further hypothesized that these objectives can be achieved directly from the satellite observations without assistance of a sounding retrieval algorithm. A systematic approach requires several tasks, namely:

1. To prepare a radiative transfer model (RTM) capable of producing satellite channel brightness temperatures and weighting functions (which describe the vertical distribution of atmospheric radiation reaching the satellite sensor) from surface and upper air sounding data;
2. To develop a set of satellite channel brightness temperature distributions which represent distinct synoptic features routinely depicted in atmospheric soundings; and
3. To analyze the origin and distribution of variance in satellite brightness temperature data. This analysis requires three sub-tasks:

a. To identify the synoptic feature resulting in a satellite observation;

b. To estimate parameters which quantify the synoptic feature, such as height and strength of an inversion;

c. To study the spatial coherence of a synoptic feature as a function of horizontal distance away from the parent feature.

Accomplishment of these tasks results in a methodology to infer synoptic structure in certain situations and in regions nearly devoid of balloon-borne soundings.

B. Overview

A primary goal of satellite meteorology is to produce an atmospheric sounding from satellite sensor data. Unfortunately, it is impossible to identify a unique atmospheric sounding from mathematical inversion of the radiative transfer equation; the same satellite channel data can originate from many different atmospheric conditions. The task is to decide which of many atmospheric soundings is the most likely source. The appropriate approach to analysis of uncertain events is statistical.

1. Radiative transfer model (RTM)

This research required a large collection of collocated satellite observations and upper air data depicting specific synoptic features. However, since this inquiry also focused on the development of analytical techniques, the merger of atmospheric soundings and synthetic satellite brightness temperature data produced by a model provided a simplified and more direct approach. This combination posed two distinct advantages: first, it allowed the flexibility to

study any synoptic feature for which atmospheric soundings could be drawn, regardless of the ready existence of collocated satellite and radiosonde observations; and, second, the complex signals found in real satellite observations were eliminated.

The RTM was developed at, and provided by, NASA Space Flight Center's Goddard Laboratory for the Atmospheres and is documented by Susskind et al. (1982). It directly calculates satellite channel brightness temperatures from radiances that would have been measured by sensors on board the TIROS N satellite had they viewed the atmosphere under study. As described by Susskind and co-workers, the RTM "...can reproduce the (spectral) line-by-line calculations of the transmittances, including their dependence on the important (atmospheric) variables, the temperature-humidity-ozone profile and zenith angle of observation." The RTM supports 22 of the 27 channels on board the satellite.

2. Sounding collection

A collection of atmospheric soundings was assembled to represent distinct synoptic regimes that exist in the tropics. The RTM was used to create satellite channel brightness temperatures corresponding to the atmospheric soundings. Although clouds accompanied many of the sounding conditions, the soundings were input to the RTM as cloud-free. Nine sounding classes were identified as:

a. Four types of inversions: frontal, radiation, turbulence, and trade-wind (subsidence);

b. A warm, humid tropical cyclone sounding;

c. Two observed island soundings containing an aggregate of

typical conditions;

d. A warm anticyclone sounding containing a subsidence inversion; and

e. The US Standard Atmosphere to provide a baseline.

While not inclusive, these soundings represent conditions typically found over the tropical eastern Pacific Ocean, the area for which this inquiry was intended.

Each of the single "seed" soundings was augmented by perturbing the temperature and moisture values at each of 66 layers required by the RTM. This random perturbation increased the sample size to one that is statistically meaningful in the framework of 22 supported satellite channels and still preserved the basic feature of the synoptic class. The perturbations in each sounding were introduced as white noise, highly correlated in the vertical, to better simulate real atmospheric variability.

3. Origin and distribution of variance

Satellite multichannel data were shown by Anderson (1986) to have interpretable and physically based variance. In other words, the variance arising from satellite channel data has structure. The structural variance can be partitioned through a two-tier procedure: (1) the satellite brightness temperature data are separated into synoptic regimes; and, (2) the variability within each regime is used to quantify the primary synoptic feature of that regime.

To separate satellite data into synoptic regimes, three classification methods were employed. The methods start with satellite brightness temperature data from known synoptic regimes and lead to distinctly different

procedures to classify features in unknown satellite observations. Two procedures identify correlations between the various satellite channel brightness temperatures for each regime; they specify rules which permit regime classification from the correlations. The third technique is graphical; it converts the individual channel brightness temperatures into facial features on a caricature of a face.[1] Many brightness temperatures may be viewed simultaneously; thus, characteristics of the data, such as synoptic regimes, are identified as different facial expressions. This technique is primarily exploratory; however, it can be used by inexperienced analysts to classify data.

After classification of satellite observations into synoptic regimes, the observations making up a regime may be quantified. The observations within a regime, by definition, are relatively homogeneous, but there is sufficient variance structure to partition the observations once again. The purpose is to measure such features as, for example, height and strength of an inversion. Numerical values are assigned to physical features, and discrete rather than continuous models are developed which predict the characteristics of synoptic features directly in satellite observations.

A synoptic feature may be identified easily at one location but be more difficult to resolve at another where the feature is weaker or contaminated by other synoptic structure. Since synoptic features vary smoothly in space, it is useful to be able to make inferences about a synoptic feature some horizontal distance away from a position where the feature can be quantified accurately. Two vertical cross sections of the atmosphere provided data for this analysis.

---

[1] This technique, not heretofore used in the atmospheric sciences, has demonstrated ability and gained credibility in other physical and social sciences (Wang, 1978; H. Chernoff, Department of Statistics, Harvard University; personal communication).

The same techniques which are used to quantify synoptic features are used to infer spatial coherence of synoptic features.

CHAPTER III

STATUS OF SATELLITE INFORMATION RETRIEVAL

Satellite information retrieval addresses the question: what atmospheric sounding of temperature and dewpoint temperature produces a given set of observed satellite radiances or brightness temperatures? Direct retrieval of important meteorological features from satellite observations has not been achieved, because the equation governing retrieval, the radiative transfer equation (RTE), cannot be inverted unambiguously. Further, a relatively small number of sensor channels are used to sample the atmosphere from the surface to 5 hPa; the number, spectral range, and bandwidth of sensor channels on board the satellite limit the independent information received relative to the large vertical extent over which measurements are made (Rodgers, 1976). Therefore, the need for supplemental information to estimate meteorological features is inherent in satellite system design. The quality and method of introduction of this supplemental information determine the accuracy of retrieved atmospheric soundings. Several procedures are developed in this research which (1) identify the synoptic origin of satellite observations and (2) extract synoptic details that currently are not captured by conventional satellite retrieval algorithms.

This chapter outlines the radiative transfer equation, describes current operational and proposed retrieval methods, and contrasts the new retrieval procedures described herein with current operational strategies.

A. The radiative transfer equation (RTE)

Susskind et al. (1982) cite the form of the radiative transfer equation used by the NASA/Goddard Laboratory for the Atmospheres physical inversion method as

$$R(i) = \epsilon_i B_i\{T_s\}\tau_i(P_s) + (1-\epsilon_i)R_i\,\tau_i(P_s)$$

$$+ p_i' H_i\,\tau_i'(P_s) + \int_{\ln P_s}^{\ln P_t} B_i\{T(P)\}(d\tau/d\ln P)\,d\ln P, \qquad (1)$$

"...where R(i) is the clear column radiance for channel i, ϵ_i is the surface emissivity averaged over sounding channel i, B_i {T} is the mean Planck blackbody function at temperature T, $\tau_i(P)$ is the mean atmospheric transmittance from pressure P to the top of the atmosphere, R_i is an effective atmospheric emission downward flux, p_i' is the directional reflectance of the solar radiation, H_i is the channel averaged solar radiance striking the top of the atmosphere, and $\tau_i'(P_s)$ is an effective atmospheric transmittance of radiation from the sun, reflected from the earth's surface to the satellite. The subscript s refers to the earth surface. The integral, taken from the surface to the satellite pressure P_t, represents the upwelling atmospheric emitted radiation, which is a mean value of the black-body function of atmospheric temperature weighted by the channel weighting function $d\tau/d\ln P$." The RTE provides radiances from specified atmospheric structure; the structure is specified through the temperature distribution, T(P), and the distribution of radiatively active constituents (H_2O, CO_2, NO_2, O_3 and others) through $\tau_i(P)$.

B. Current operational retrieval strategies

The RTE produces radiances from atmospheric structure; the converse is not possible directly. When the RTE is applied to multiple layers in the atmosphere by finite differencing, there are more unknown variables than equations, and the system is not closed.

Houghton et al. (1984) summarized three closure methods used to supply supplementary information. In the first, a climatologically and spatially smoothed sounding is assumed and taken as a first guess solution to the RTE. In the second method, categories of all possible solutions are characterized using a probability density function. Some property of the assumed distribution, the mean or mode, for example, is taken as a solution. By choosing the property and its distribution, the likelihood of a sounding category is specified, and a constraint is imposed. The third approach assumes that some physical property of the unknown sounding, such as an inversion height, is known; the probability density function specifies the occurrence of the feature, and a constraint is imposed (Westwater and Strand, 1968; Westwater et al., 1983). In each approach, the resulting sounding is substituted back into the RTE which is solved iteratively and compared with observations until no reduction in linear least squares difference between observations and estimates is obtained. This method is stable mathematically, but the resulting accuracy is dependent on the quality of the first guess sounding, and it produces soundings in which important meteorological features are lost to smoothing.

Most operational retrieval techniques use some form of a climatological first guess (the first guess method); however, this method always introduces into retrieved soundings vertical structure not measured directly by the satellite, and, as a result, vertical resolution is not well defined. The method of

retrieval by linear regression, that currently is in use by NOAA/NESDIS to define vertical temperature profiles, is a form of the third method (Smith and Woolf, 1976; McMillin, 1988).

Methods to improve retrieval accuracy generally fall into two categories, primarily physical and primarily statistical. Primarily physical methods are derived from the physical model of the radiative transfer equation (1). For example, Fleming et al. (1986, 1988) and Goldberg et al. (1988) presented a minimum variance simultaneous retrieval system which uses a nonlinear operator and tuning data sets and has the advantage of being more computationally efficient than purely statistical methods. Fleming et al. (1988) reported a ten-fold improvement in computation speed; Goldberg et al. (1988) described an improvement in first guess sounding profile.

In spite of the interest of Fleming and co-workers in primarily physical retrieval, recent emphasis appears to be on primarily statistical methods. These methods rely on properties of the data rather than an exact mathematical solution to governing equations. Most statistical approaches limit the possible atmospheric soundings that could produce a set of radiances by partitioning data variance using classification and discrimination techniques.

Uddstrom and Wark (1985) and Thompson et al. (1985) investigated multivariate statistical approaches to improve first guess soundings. Uddstrom and Wark used generated data to specify typical shape functions of 15 μm temperature profiles. While their technique is innovative and exploits data structure, it is limited to temperature retrieval improvement and uses only a portion of the TOVS channels. Thompson and co-workers used pattern recognition techniques to establish temperature pattern libraries from which

first guess information could be obtained. Moisture was not considered. McMillin (1986 and 1988) evaluated classification approaches based on actual measurements. Thompson et al. (1986) suggested that multiple atmospheric soundings which produce a given set of radiances are rare, because the multiple soundings include such features as superadiabatic or otherwise physically unlikely layers; their work lends support to classification methods. Lipton et al. (1986) used classification methods to improve water vapor vertical profile retrieval. They concluded that classes of distinct water vapor profiles could be recognized in infrared spectral radiances from satellites. Moine et al. (1986) used clustering algorithms to recognize air mass characteristics which lead to an improved initial guess retrieval procedure.

C. Advantages of discrete classification

We present a two-tiered discrete method of classification and quantification of synoptic features. There are two pathways for classification one is subjective, and the other is objective. Classification by either method is followed by quantification of the synoptic feature present. This overall approach offers advantages over conventional retrieval and other classification methods.

The technique developed in this research is a discrete method. It is a modification and combination of the first and second methods described by Houghton et al. (1984). Instead of specifying the probability of encountering all possible synoptic conditions as in the first method, or assuming some known physical property of the unknown sounding as in the second, a manageable number of discrete soundings is constructed which represents the possible synoptic regimes expected in the region and season under study. Statistical

techniques which emphasize discrete classes rather than a continuous distribution of variance are used to partition the covariance matrix of individual channel brightness temperatures; the characteristics of a satellite sounding normally will fall into one of the discrete sounding groups (Johnson and Wichern, 1982). The new technique avoids the overwhelming computations of the first technique without imposing the required restrictions of the second. Two steps are involved: classification into one of the discrete classes; and quantification of details within each class.

CHAPTER IV

RADIATIVE TRANSFER MODEL

The upwelling radiation exiting the top of the atmosphere and sensed by satellite sensors is modelled well by the radiative transfer equation (1). This calculation is straightforward and often is referred to as the direct or forward problem of radiative transfer: Namely, if the vertical distribution of temperature and atmospheric absorbers is known, what is the nature of the upwelling radiation?

The usual approach to radiative transfer modeling (RTM) is to divide the atmosphere into multiple horizontal layers, each having well-defined absorbing, emitting and transmitting properties. As radiation passes from the earth surface to the top of the atmosphere, the behavior of the radiation in each layer is computed, and a simulated satellite observation results.

The RTM must emulate not only the atmospheric transmission of radiation but the satellite response to radiation as well. Each channel has a unique sensitivity of radiance observed in a certain spectral interval; this sensitivity depends on local variation in atmospheric temperature, water vapor and ozone. The response is measured by the vertical resolution of the radiance observed within each individual channel and is seen as the amount of radiation emitted from each layer that actually reaches the satellite. This response can be plotted vs. height, and the resulting weighting function curve gives the channel sensitivity to atmospheric structure. The shape and peak height of the weighting function curves graphically depict channel vertical resolution. A channel whose weighting function curve is broad yields little information, because atmospheric structure of small vertical extent affects only a small

portion of the weighting function. A sharp curve represents information over only a very thin atmospheric layer. Weighting functions can vary greatly as atmospheric structure and composition vary.

The ideal RTM for satellite data simulation should possess several characteristics. First, the model should be flexible enough to allow any reasonable atmospheric sounding to be studied without extensive revision of the source code. Second, the model should simulate the sounders on board an operational satellite and provide a radiance or equivalent brightness temperature value for each of the satellite sensors. Third, it should be possible to calculate weighting function curves for each channel. Fourth, data input to and output from the RTM should be convenient. With a minor exception, all attributes were found in a simulation model developed at NASA Space Flight Center's Goddard Laboratory for the Atmospheres (NASA/GLA). The RTM simulates the TIROS N Operational Vertical Sounder (TOVS) and is documented by Susskind et al. (1982), hereafter, Susskind.

A. The TIROS N Operational Vertical Sounder (TOVS)

The radiometer system on board a satellite is a compromise of space, power requirements, and weight, all balanced against information returned. The TOVS evolved with three instruments: (1) the High Resolution Infrared Radiation Sounder, version 2, (HIRS/2); (2) the Microwave Sounding Unit (MSU); and (3) the Stratospheric Sounding Unit (SSU). Information normally provided by the SSU is not modelled by the RTM and is not a part of this research.

The HIRS/2 and MSU spectral properties of the TOVS channels are described in Table 4.1, and the individual channel responses to observed

radiance with respect to variation in atmospheric temperature, moisture and ozone are shown in a series of weighting function curves in Fig. 4.1 (Smith et al., 1979; hereafter, Smith); these regular shaped curves are valid for climatological values of atmospheric gases and the smooth, uncomplicated temperature and moisture profiles of the U.S. Standard Atmosphere. The "real" atmosphere is more complex; vagaries of water vapor and ozone, and, to some extent, atmospheric temperature and zenith angle, add complexity to weighting function curves of natural soundings.

The role of the RTM is to model the TOVS response to the natural atmosphere. The individual channel radiances (or equivalent brightness temperatures) and the shape and peak height of the weighting function curves provide data to measure the RTM's capabilities.

B. Model description

The NASA/GLA RTM is a 66 layer rapid transmission algorithm which directly calculates brightness temperatures (or radiances) for 22 of the 27 TOVS channels. HIRS channels 17 and 20 and the three SSU channels were omitted by the authors because they contain no relevant information for the intended use of the RTM. In addition to the channels omitted by the RTM (17, 20 and the SSU channels), our results frequently omit channels 1, 2, 9, 21 and 24. Channels 1 and 2 fall into the same category as channel 17; their peak height contributions are too high to be useful for mainly tropospheric studies. Channel 9 is an ozone concentration measure and is not relevant. Channel 21 measures surface microwave emissivity and provides little useful information for temperature and moisture sounding. The peak height contribution of channel 24 is too high to be useful. MSU channels 1 - 4 were renumbered

Table 4.1. Characteristics of TOVS sounding channels.

TOVS Channel number	Channel central wavenumber	Central wavelength (μm)	Principal absorbing constituents	Level of peak energy contribution	Purpose of the radiance observation
1	668	15.00	CO_2	30 mb	*Temperature sounding.* The 15-μm band channels provide better sensitivity to the temperature of relatively cold regions of the atmosphere than can be achieved with the 4.3-μm band channels. Radiances in Channels 5, 6, and 7 are also used to calculate the heights and amounts of cloud within the HIRS field of view.
2	679	14.70	CO_2	60 mb	
3	691	14.50	CO_2	100 mb	
4	704	14.20	CO_2	400 mb	
5	716	14.00	CO_2	600 mb	
6	732	13.70	CO_2/H_2O	800 mb	
7	748	13.40	CO_2/H_2O	900 mb	
8	898	11.10	Window	Surface	*Surface temperature* and cloud detection.
9	1 028	9.70	O_3	25 mb	*Total ozone* concentration.
10	1 217	8.30	H_2O	900 mb	*Water vapor sounding.* Provides water vapor corrections for CO_2 and window channels. The 6.7-μm channel is also used to detect thin cirrus cloud.
11	1 364	7.30	H_2O	700 mb	
12	1 484	6.70	H_2O	500 mb	
13	2 190	4.57	N_2O	1 000 mb	*Temperature sounding.* The 4.3-μm band channels provide better sensitivity to the temperature of relatively warm regions of the atmosphere than can be achieved with the 15-μm band channels. Also, the short-wavelength radiances are less sensitive to clouds than those for the 15-μm region.
14	2 213	4.52	N_2O	950 mb	
15	2 240	4.46	CO_2/N_2O	700 mb	
16	2 276	4.40	CO_2/N_2O	400 mb	
17	2 361	4.24	CO_2	5 mb	
18	2 512	4.00	Window	Surface	*Surface temperature.* Much less sensitive to clouds and H_2O than the 11-μm window. Used with 11-μm channel to detect cloud contamination and derive surface temperature under partly cloudy sky conditions. Simultaneous 3.7- and 4.0-μm data enable reflected solar contribution to be eliminated from observations.
19	2 671	3.70	Window	Surface	
20	14 367	0.70	Window	Cloud	*Cloud detection.* Used during the day with 4.0- and 11-μm window channels to define clear fields of view.

	Frequency (GHz)	Principal absorbing constituents	Level of peak energy contribution	Purpose of the radiance observation
21	50.31	Window	Surface	*Surface emissivity* and *cloud attenuation* determination.
22	53.73	O_2	700 mb	*Temperature sounding.* The microwave channels probe through clouds and can be used to alleviate the influence of clouds on the 4.3- and 15-μm sounding channels.
23	54.96	O_2	300 mb	
24	57.95	O_2	90 mb	

(After Smith et al., 1979.)

21 - 24 for convenience in this research.

The model requires as input at each layer the following meteorological variables: temperature, dewpoint and ozone concentration. In addition, the model requires certain geophysical parameters: the latitude and longitude of the measurement; whether the measurement is made over land or water; whether day or night; the sun and satellite zenith angles; and an estimate of surface microwave emissivity. The model returns individual channel radiances and equivalent brightness temperature values for each evaluated atmospheric sounding.

C. Modification

As received from NASA/GLA, the RTM was designed to process a predetermined number -- usually thousands -- of soundings, and input/output steps were unwieldy for our purposes. The model assumed meteorological information had been pre-processed and would be available at specific levels. Weighting functions were not available.

A number of modifications were made to the input/output structure. Preprocessing steps were added to allow any number of soundings to be evaluated Additionally, a scheme was developed to interpolate temperatures and dewpoint depressions between given pressure levels and to compute those required for the 66 layer model. Weighting function calculations were extracted from the layer transmission values, and the output format was changed to be compatible with data sets used for statistical analysis. Through supplementary graphics applications, model output was customized to create logarithmic pressure vs. temperature plots depicting each processed sounding. Finally, weighting function data output and plots were added.

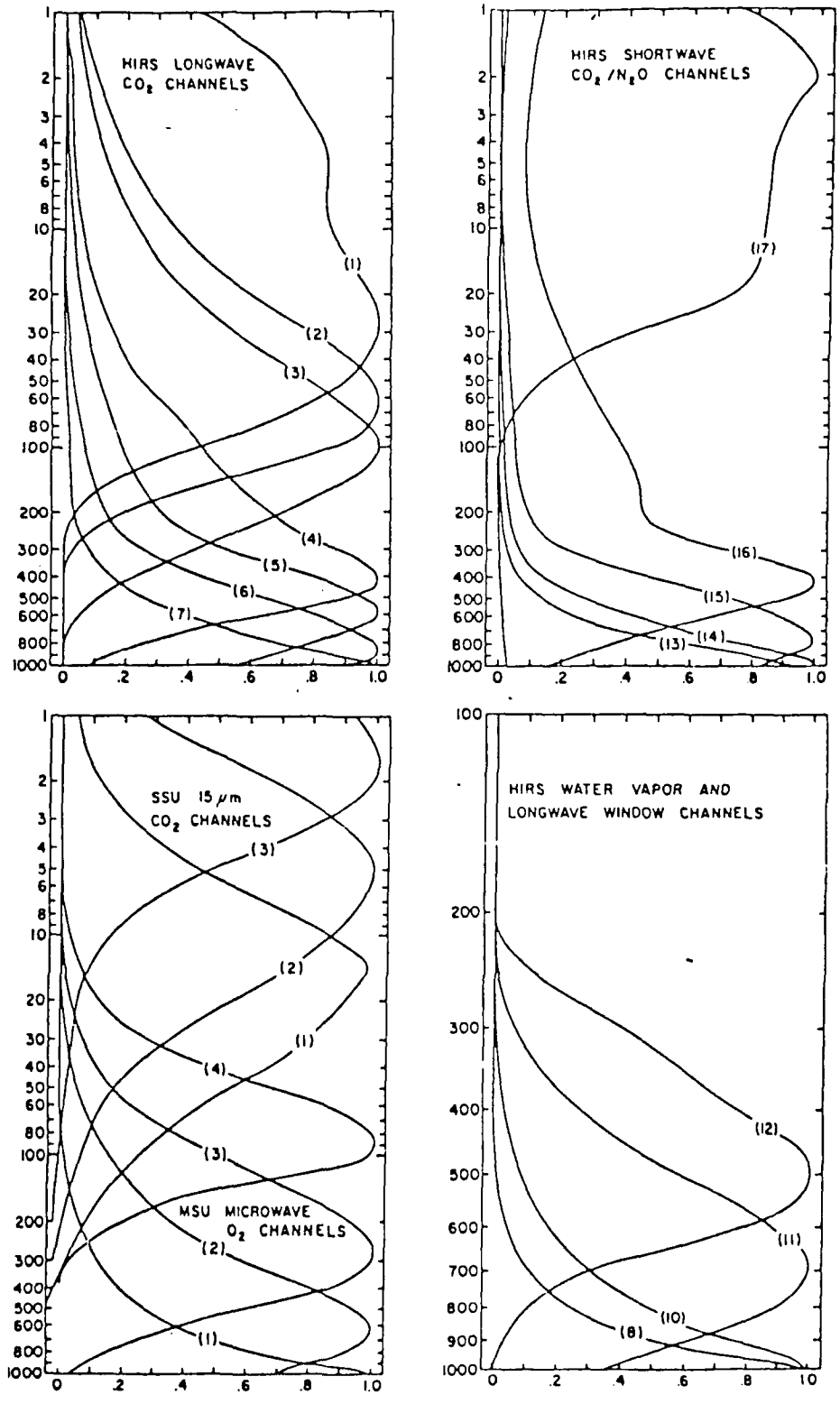

Figure 4.1. Normalized TOVS weighting functions. See text for description. After Smith et al., 1979.

D. Verification

Verification was accomplished first by Susskind before the model was released for export and later as a part of this work. Susskind compared (1) reconstructed atmospheric soundings based on RTM output with collocated radiosondes and (2) RTM output with a more sophisticated line spectral model. Our verification compared (1) RTM output with satellite observations using collocated radiosonde observations as RTM input and (2) calculated weighting function curves with those specified by TOVS designers (Smith).

1. Published verification by Susskind

Brightness temperatures calculated by the RTM were compared with a series of oceanic radiosonde sites chosen (1) to emulate those stations to be studied and (2) to minimize land surface effects on the computed radiances One group of sites is tropical; the other is mid-latitudinal.

Under clear conditions, Susskind found overall agreement in the HIRS channels between 1° and 2°C and between 2° and 3°C in the MSU channels (Susskind et al., 1982; Susskind et al., 1984). Fig. 4.2 summarizes the channel-by-channel brightness temperature differences for the tropical and mid-latitude sounding groups. Susskind also compared the layer model (the RTM) with a more sophisticated and slower line-by-line spectral model which was used in the RTM development. Susskind and co-workers gave no benchmark times, but they suggested that the significant tradeoff in speed and convenience of the layer model (the RTM) proved to be worth the small decrease in accuracy. The channel-by-channel brightness temperature deviation between the RTM and the line by line model is shown in Fig. 4.3. In general, the agreement between RTM and the more precise radiative model is better

than between the RTM and observed data.

2. Verification for this research

Two aspects of the exported model and its modifications were tested: brightness temperature accuracy and weighting function reproduction. First, ten satellite soundings were selected which are similar to the tropical soundings created for the climatology in this research and for which collocated radiosonde observations are available from the 1979 FGGE period. The radiosonde soundings were evaluated by the RTM, and the resulting brightness temperatures were compared with the satellite observations. As with Susskind's results, the greatest deviation was found in the water vapor channels. The overall channel-by-channel brightness temperature deviations compare favorably with those of Susskind (Fig. 4.4); in fact, the two are almost indistinguishable.

Channel radiances for the US Standard Atmosphere were generated by the RTM, and weighting functions (Fig. 4.5) were produced. There generally is good agreement between the RTM weighting functions and the corresponding weighting functions shown by Smith (Fig. 4.1). The only exceptions occur in the 4.3 μm temperature sounding group (HIRS shortwave CO_2 and N_2O channels 13-16) in which significant departure of the level of peak energy contribution was found in channels 14-16. Our results agreed closely with Susskind's for most channels (Fig. 4.6). The greatest departure is in HIRS channel 6, which, according to Smith, should peak at 800 hPa. Our result is approximate; channel 6 peaks near the ground, and a clear maximum is not apparent. The differences in weighting function peak height between the RTM and Smith's results are shown in Fig. 4.7.

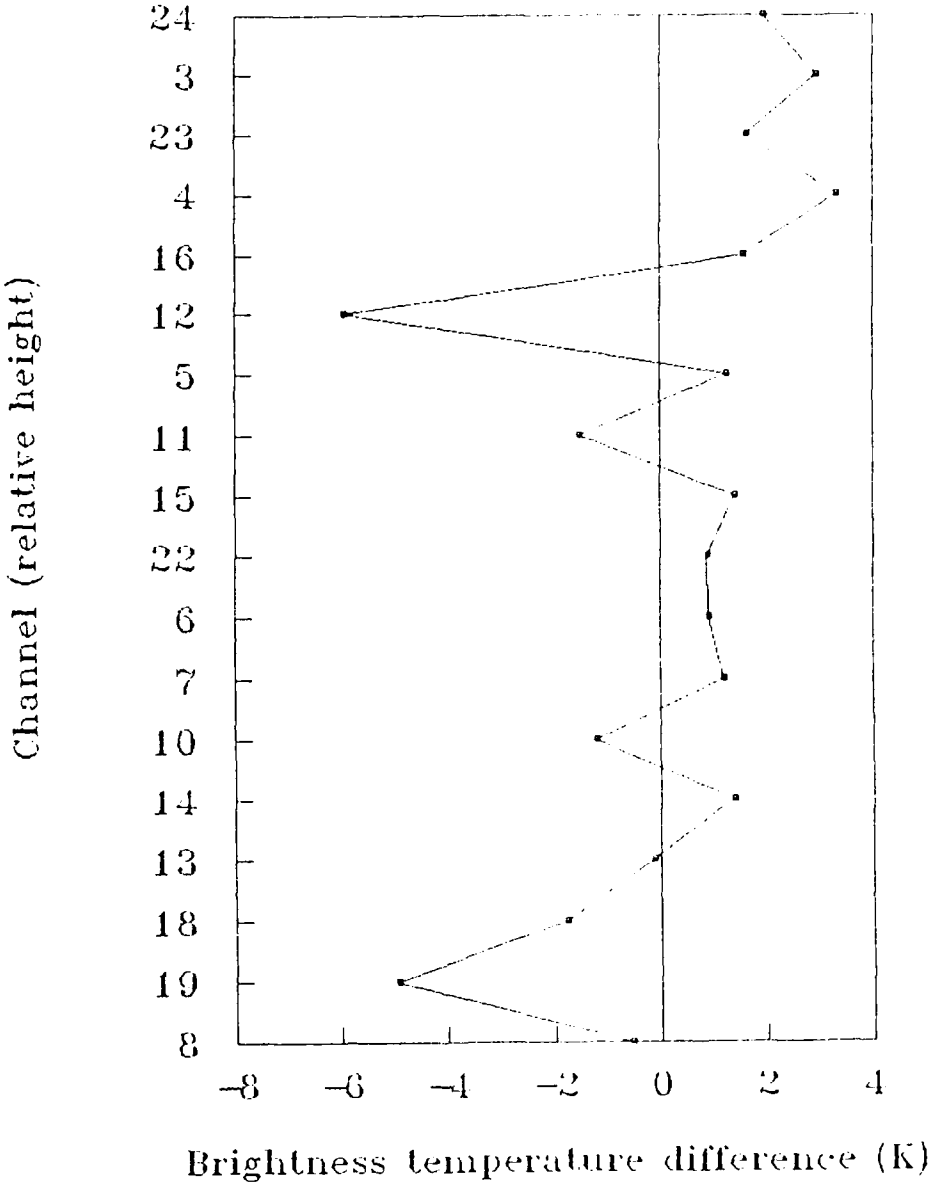

Figure 4.2a. TOVS channel brightness temperature differences between RTM output and satellite observation, tropical profile. After Susskind et al., 1982.

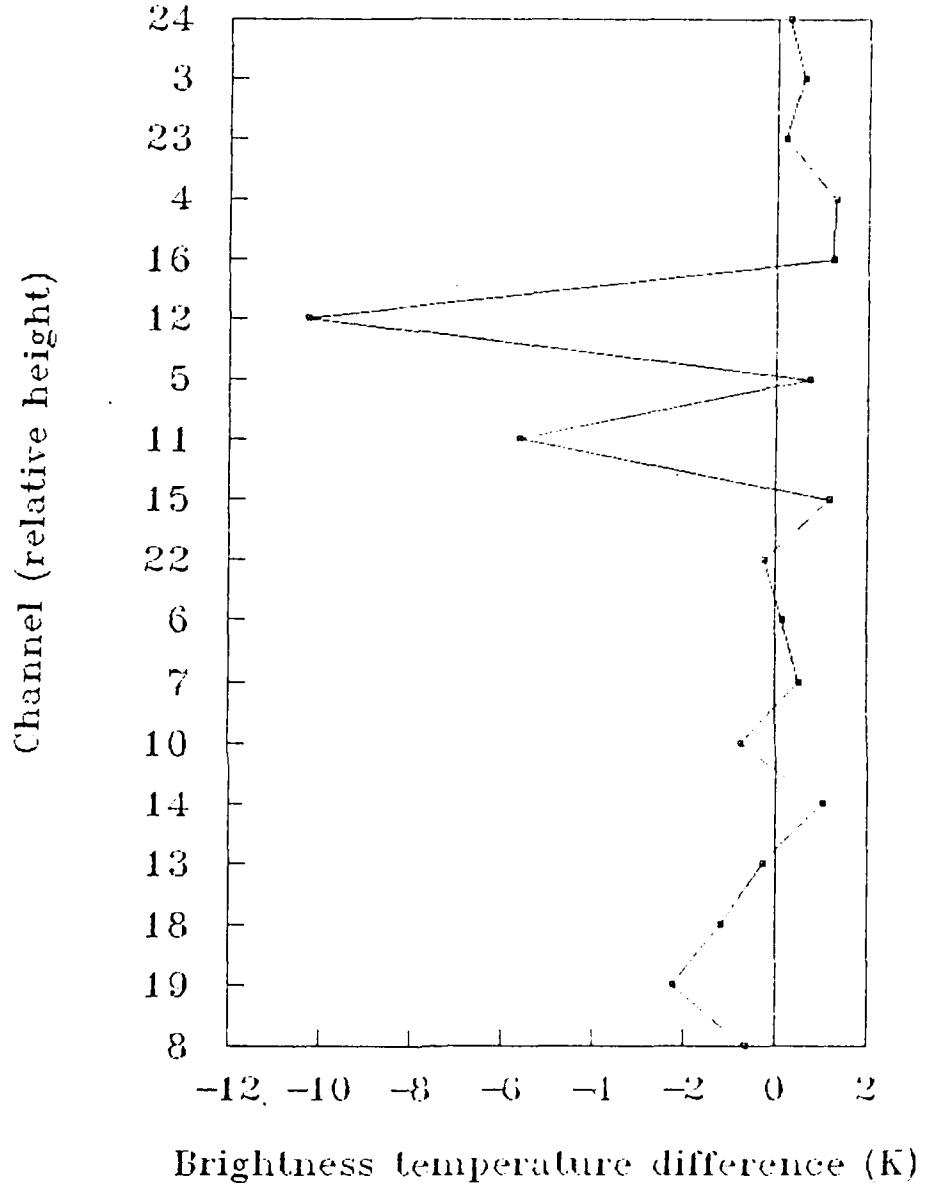

Figure 4.2b. As in Fig. 4.2a, except for mid-latitude profile. After Susskind et al., 1982.

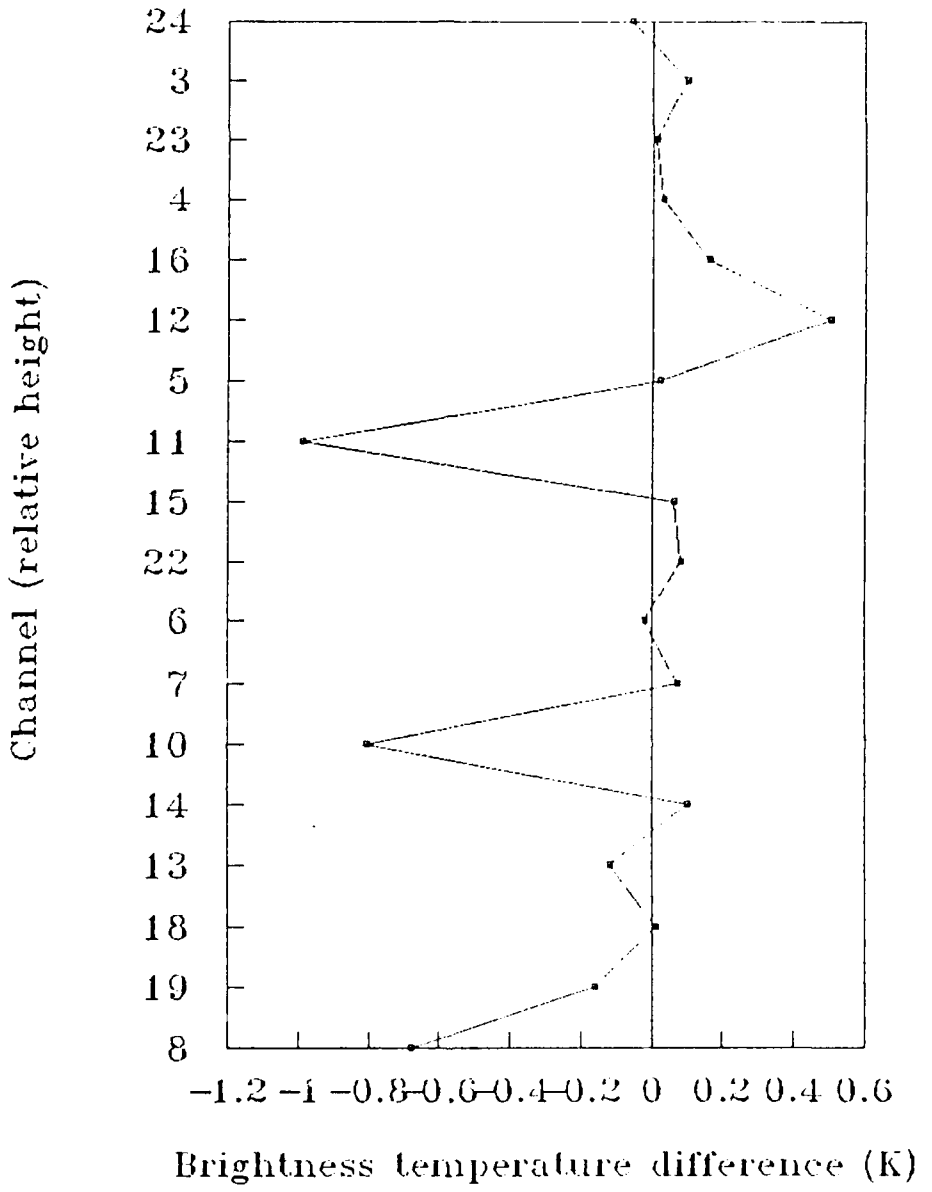

Figure 4.3a. TOVS channel brightness temperature differences between RTM output and more sophisticated line-by-line spectral model, tropical profile. After Susskind et al., 1982.

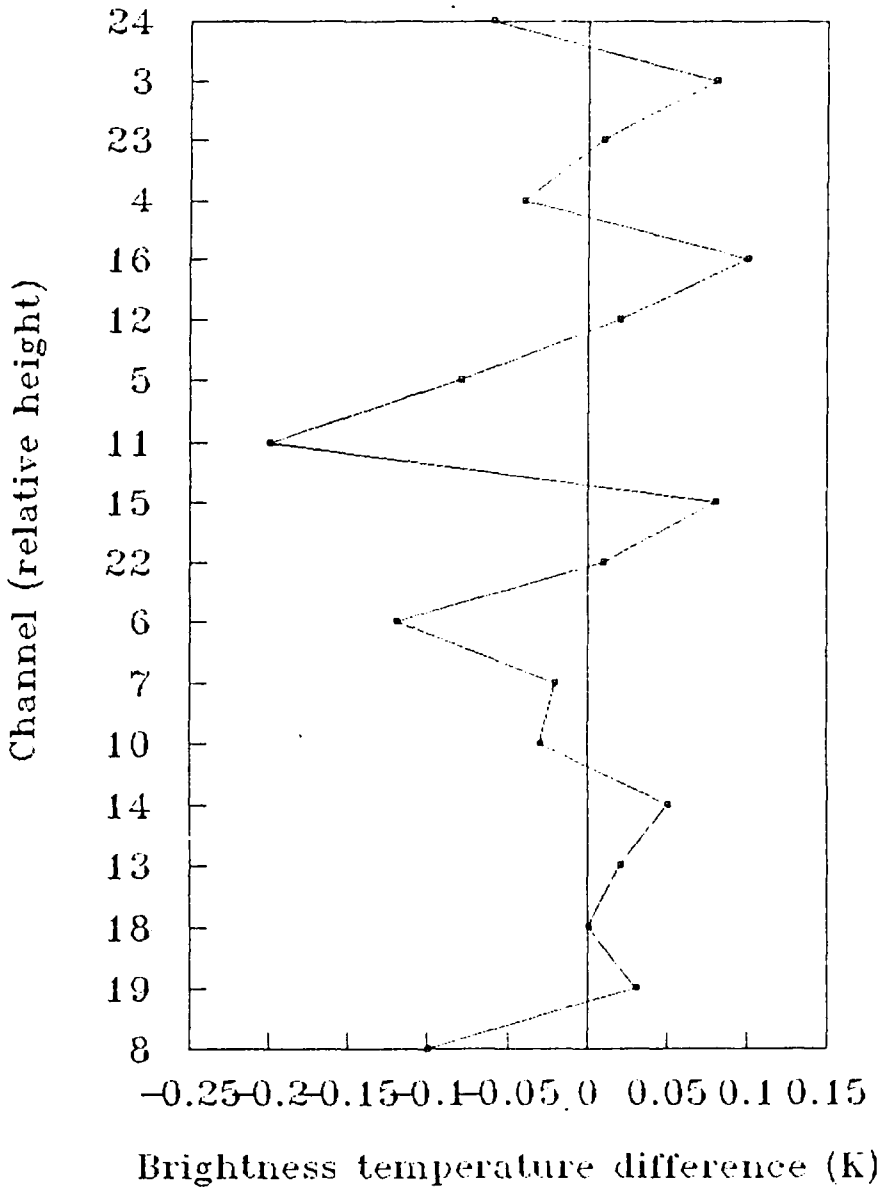

Figure 4.3b. As in Fig. 4.3a, except for mid-latitude profile. After Susskind et al., 1982.

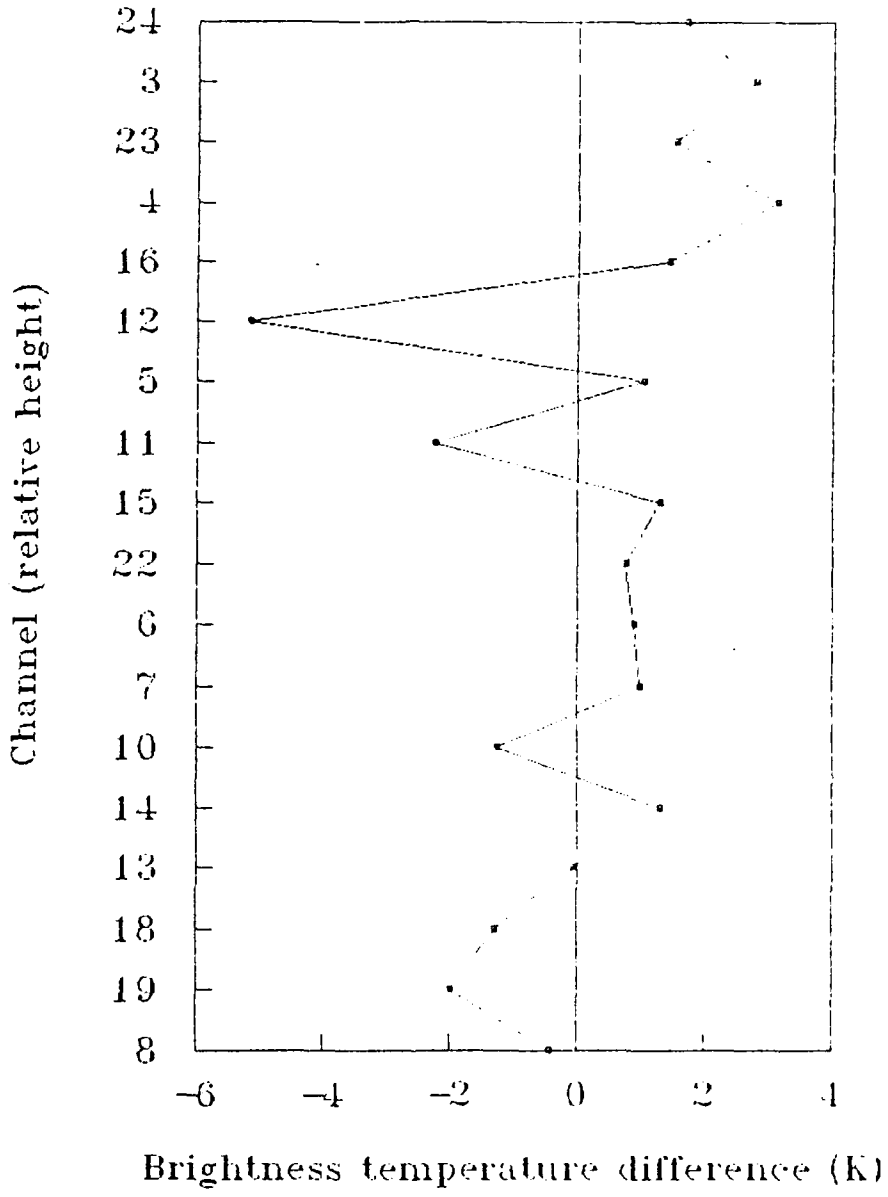

Figure 4.4. TOVS channel brightness temperature differences between RTM and FGGE soundings. See text for details.

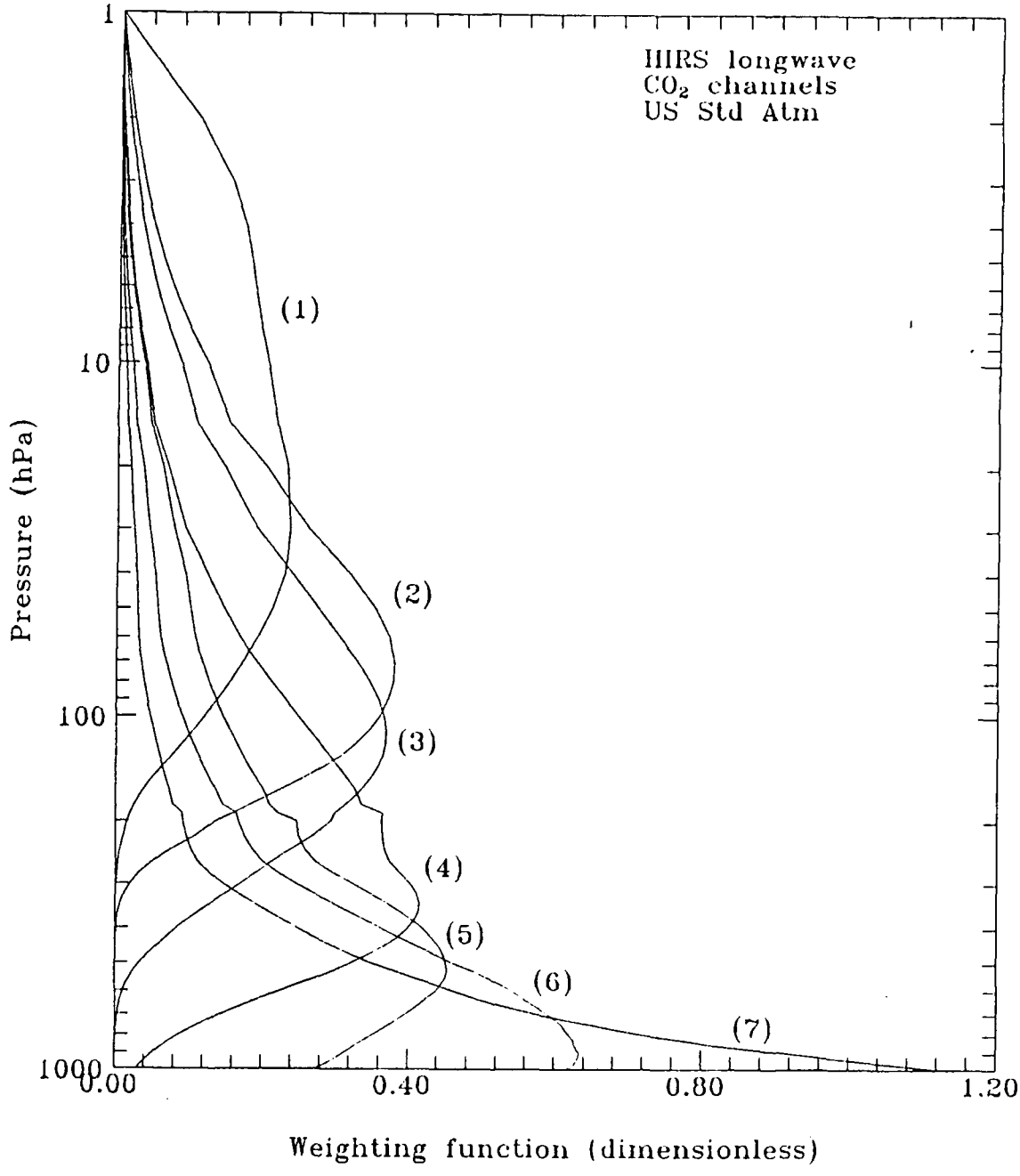

Figure 4.5a. Weighting functions (non-normalized) produced by RTM. TOVS channels 1-7. US Standard Atmosphere evaluated.

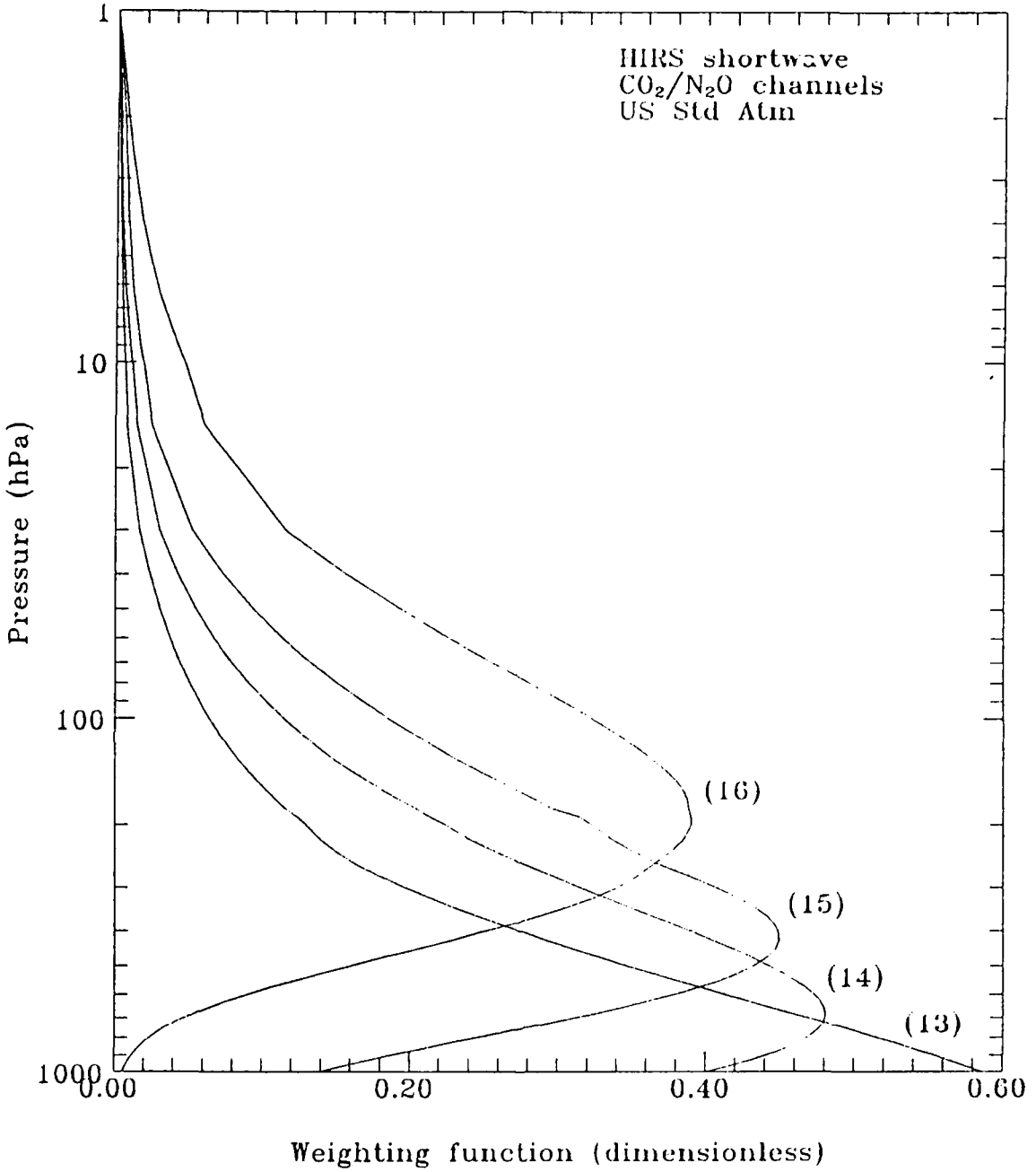

Figure 4.5b. As in Fig. 4.5a, except for TOVS channels 13-16.

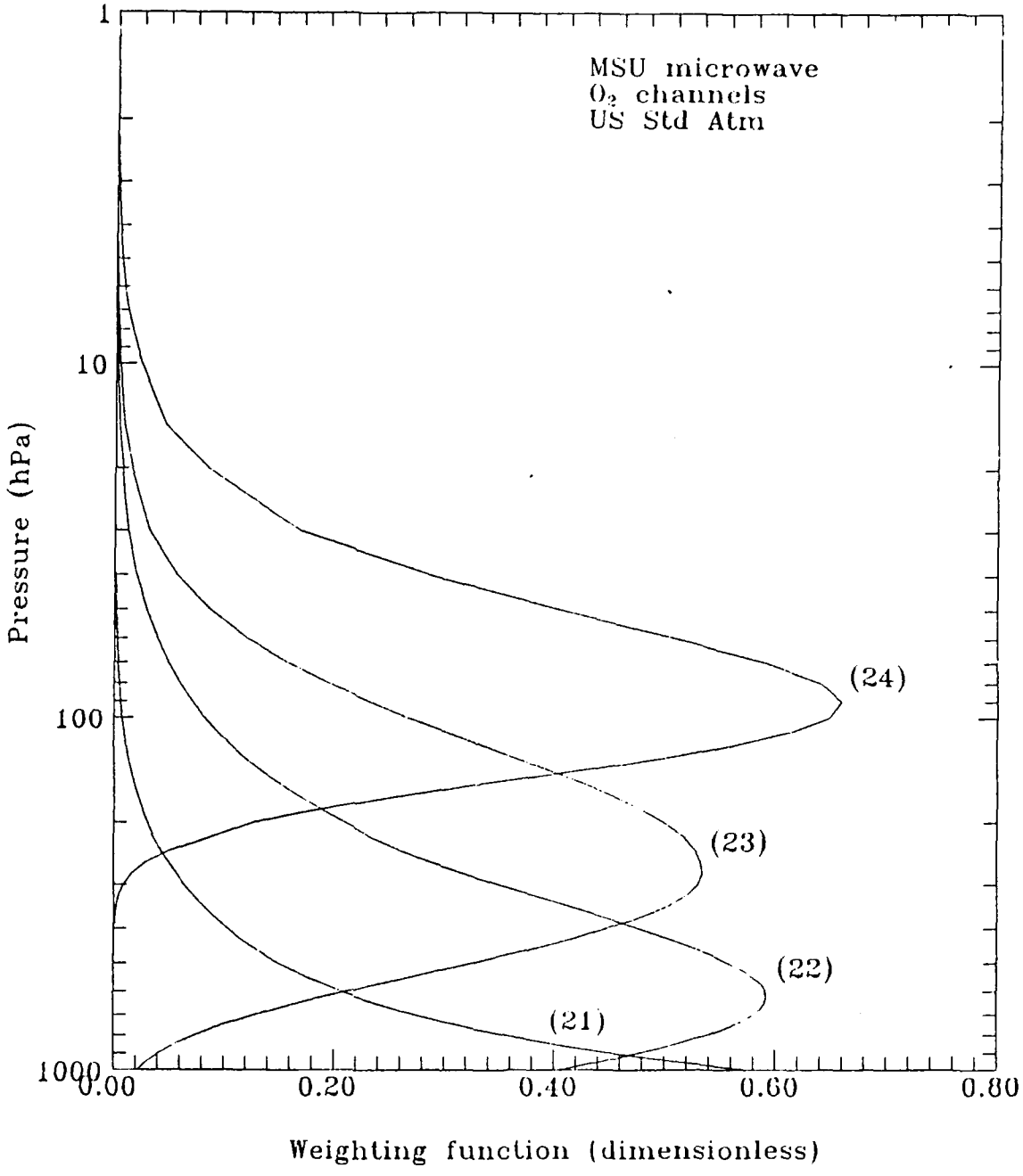

Figure 4.5c. As in Fig. 4.5a, except for TOVS MSU channels 1-4 (renumbered 21-24 for convenience.)

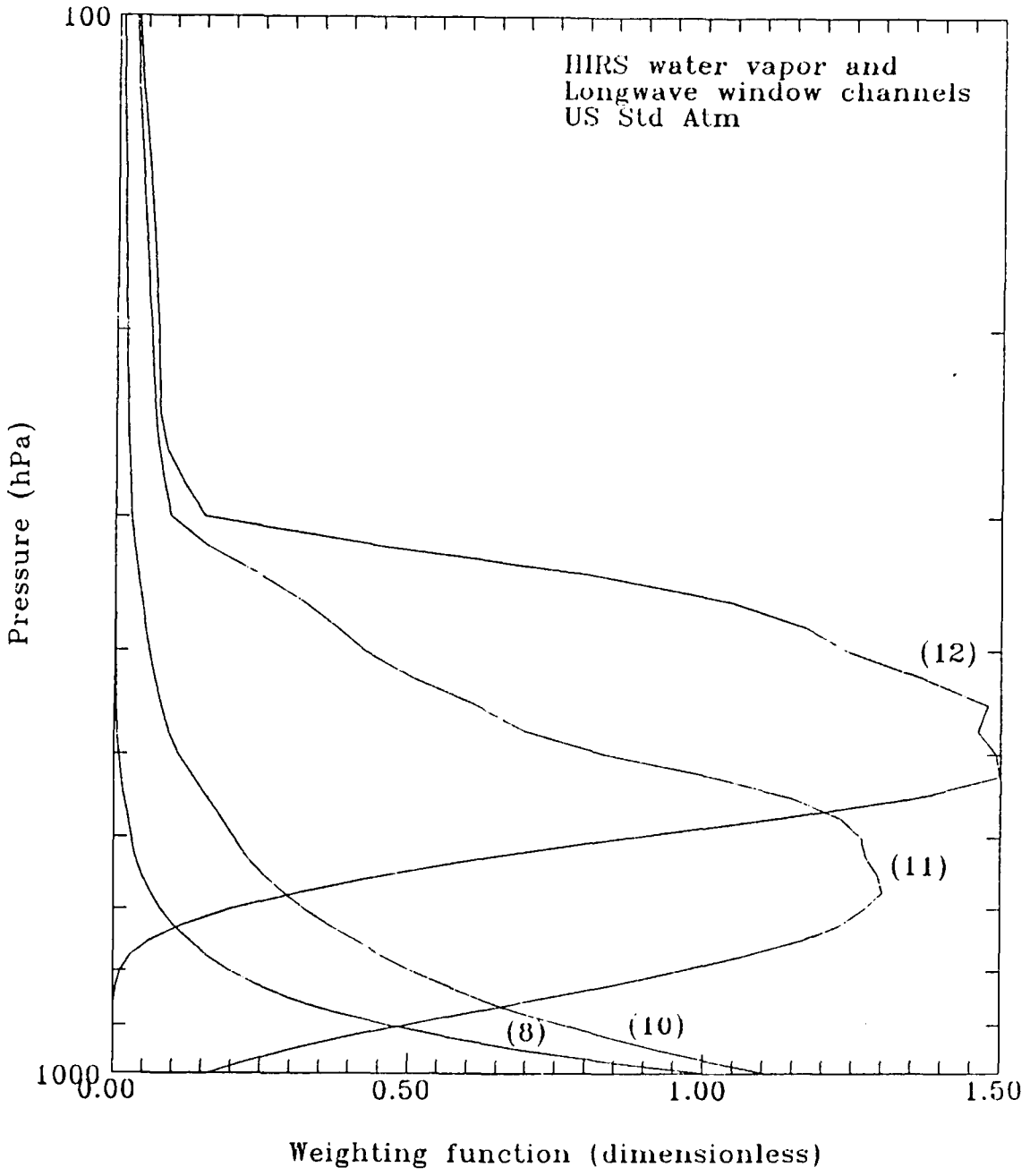

Figure 4.5d. As in Fig. 4.5a, except for TOVS channels 8, 10-12.

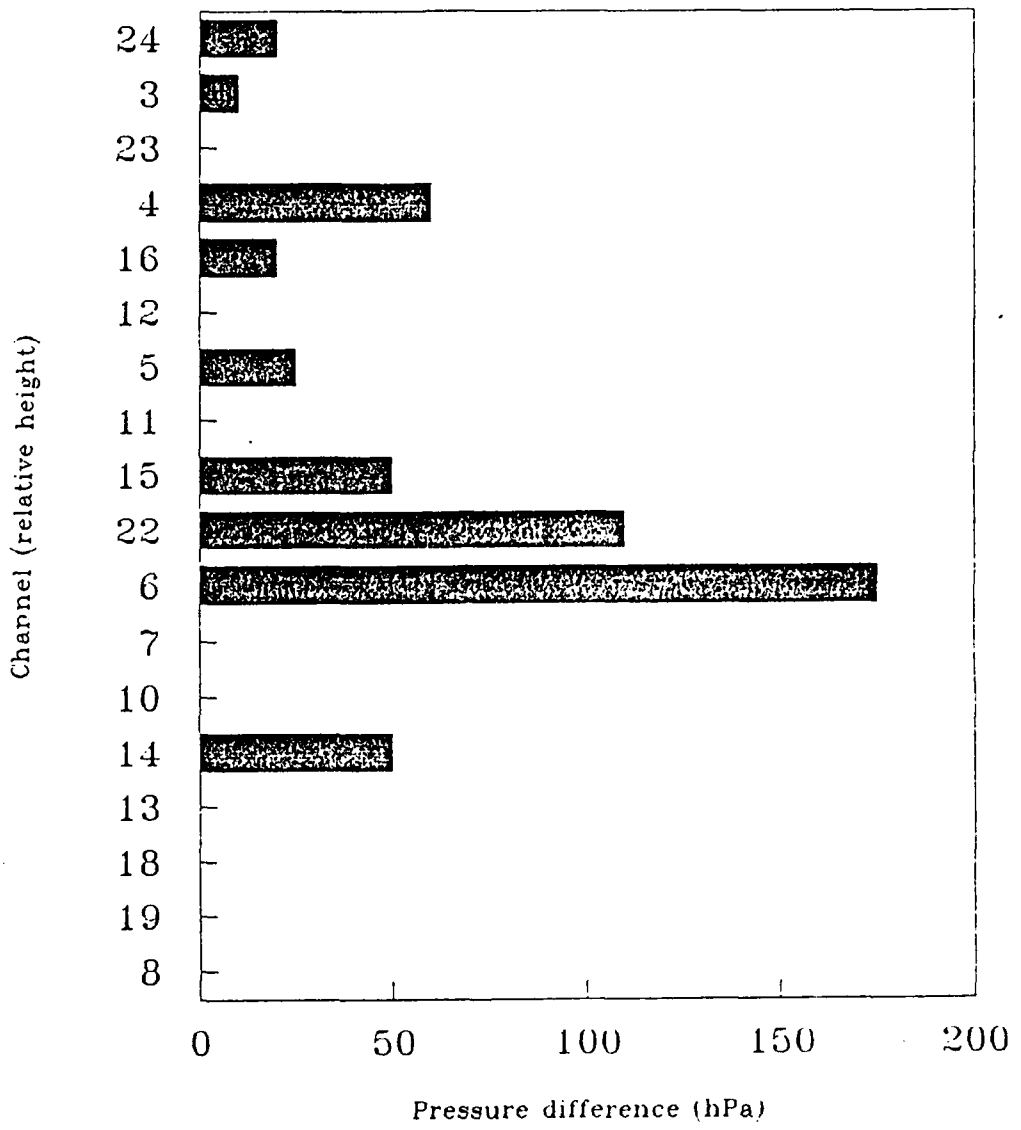

Figure 4.6. TOVS weighting function peak height contributions. Results achieved by RTM authors compared with this research. For US Standard Atmosphere.

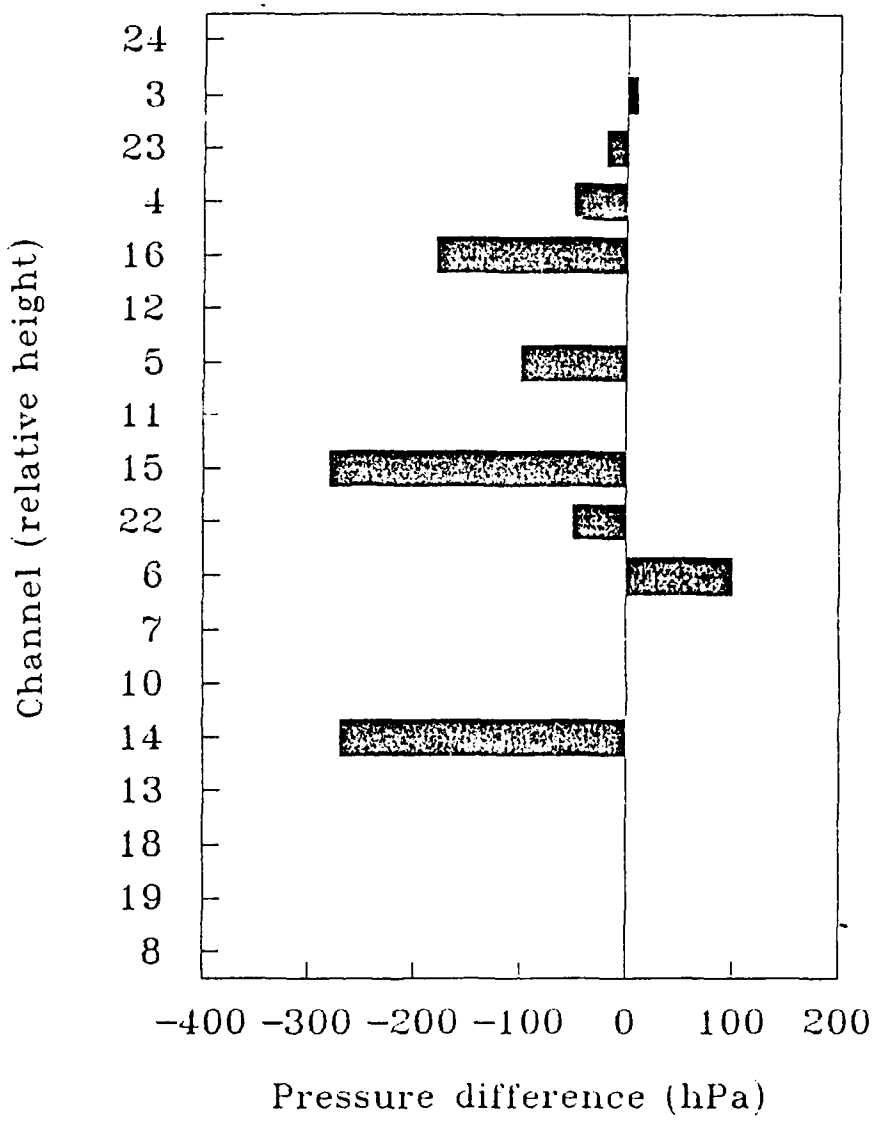

Figure 4.7. TOVS weighting function peak height contributions. Results of Smith et al., 1979 compared with RTM. For US Standard Atmosphere.

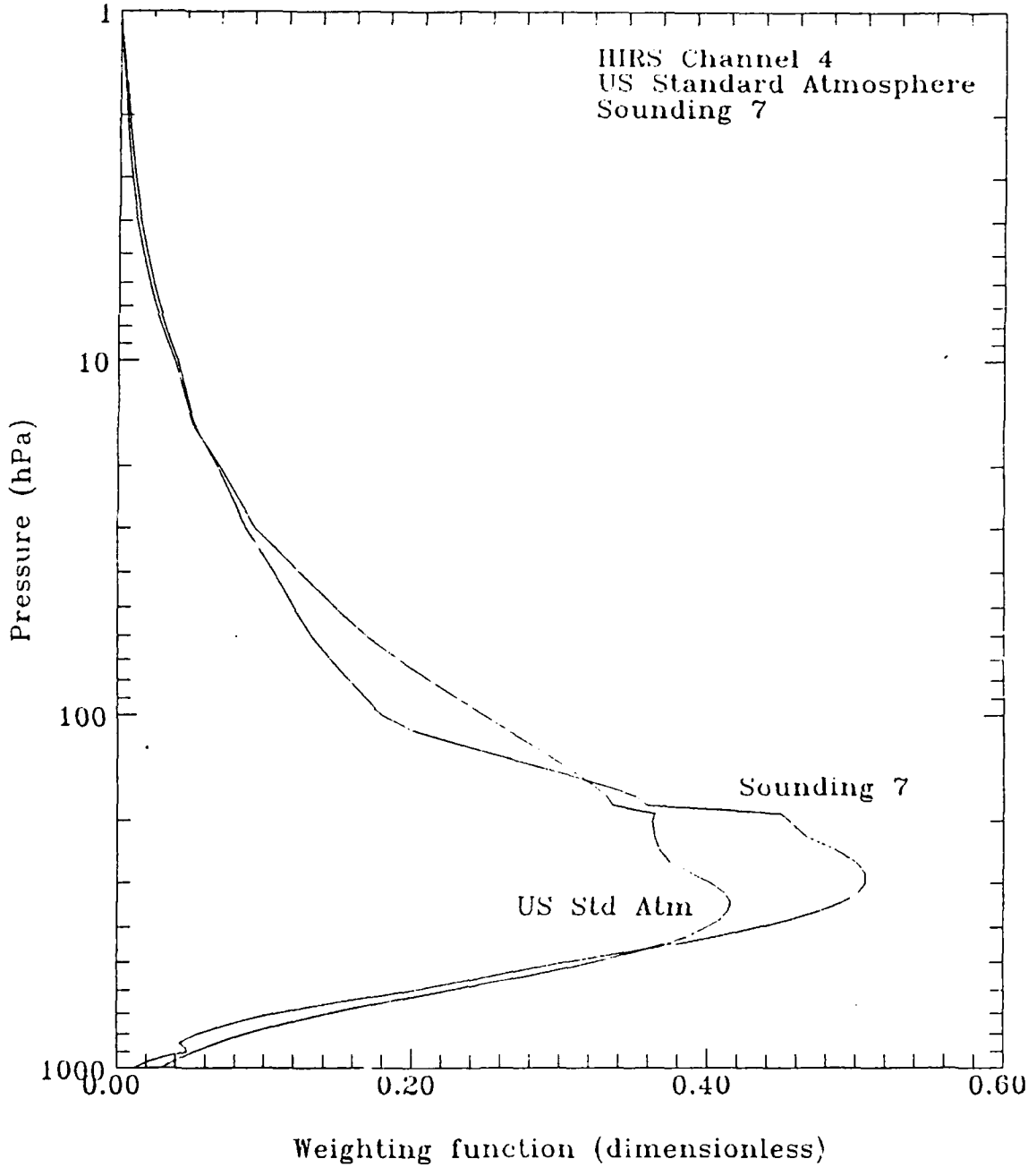

Figure 4.8a. Non-normalized weighting functions calculated by RTM. US standard atmosphere compared with subsidence inversion sounding. 15 μm temperature sounding group represented by HIRS channel 4.

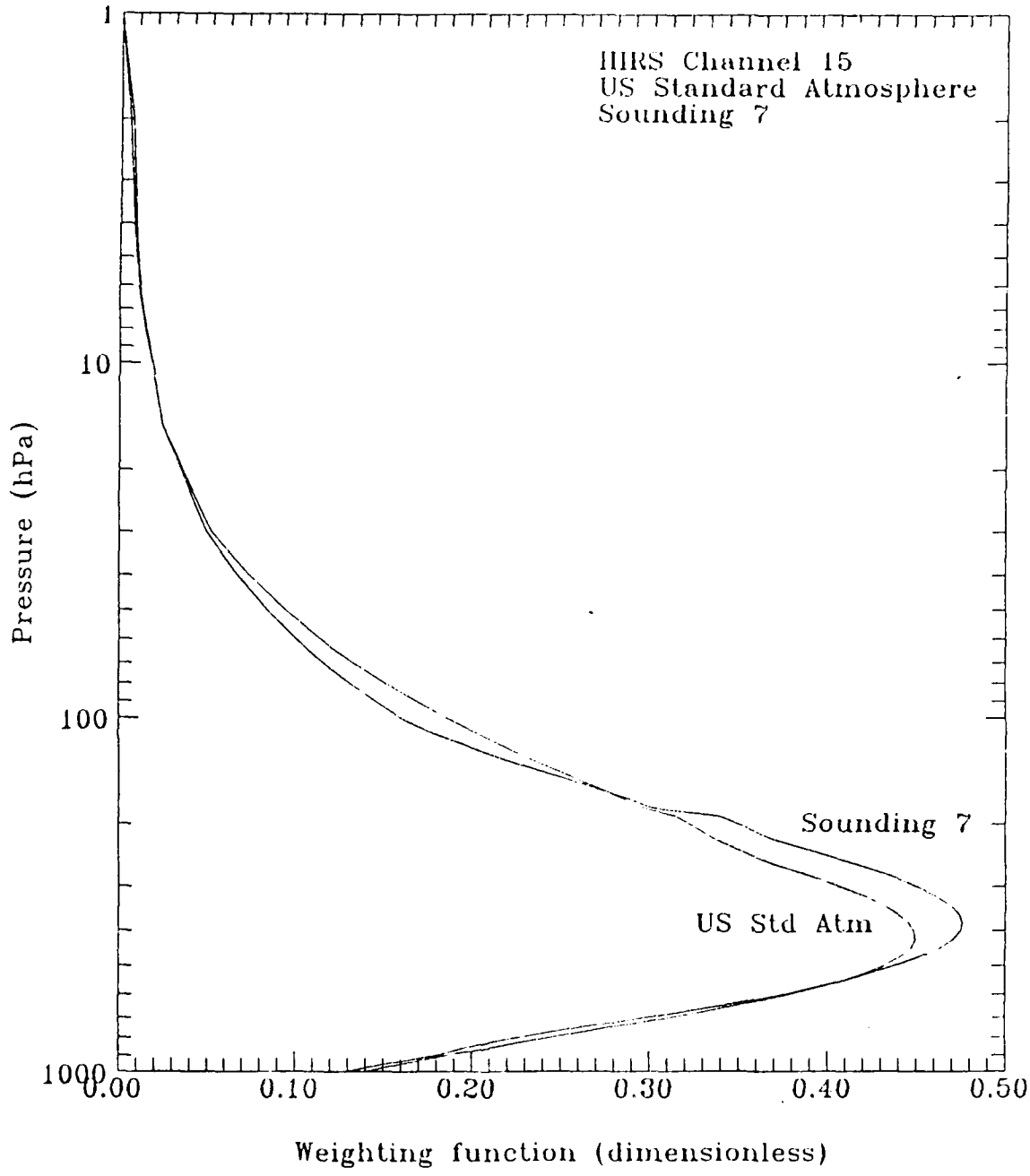

Figure 4.8b. As in Fig. 4.8a, except 4.3 μm temperature sounding group represented by HIRS channel 15.

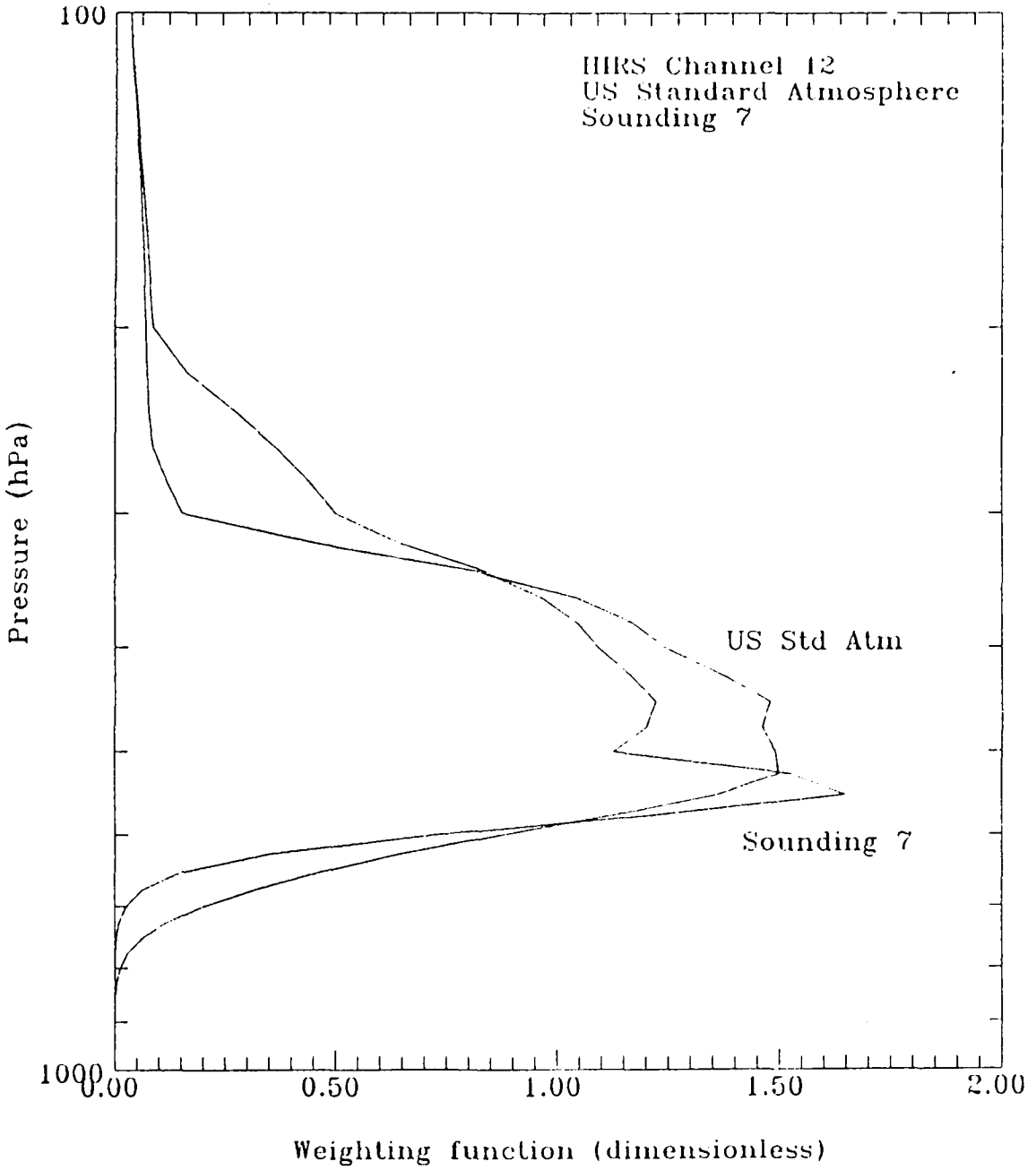

Figure 4.8c. As in Fig. 4.8a, except water vapor sounding group represented by HIRS channel 12.

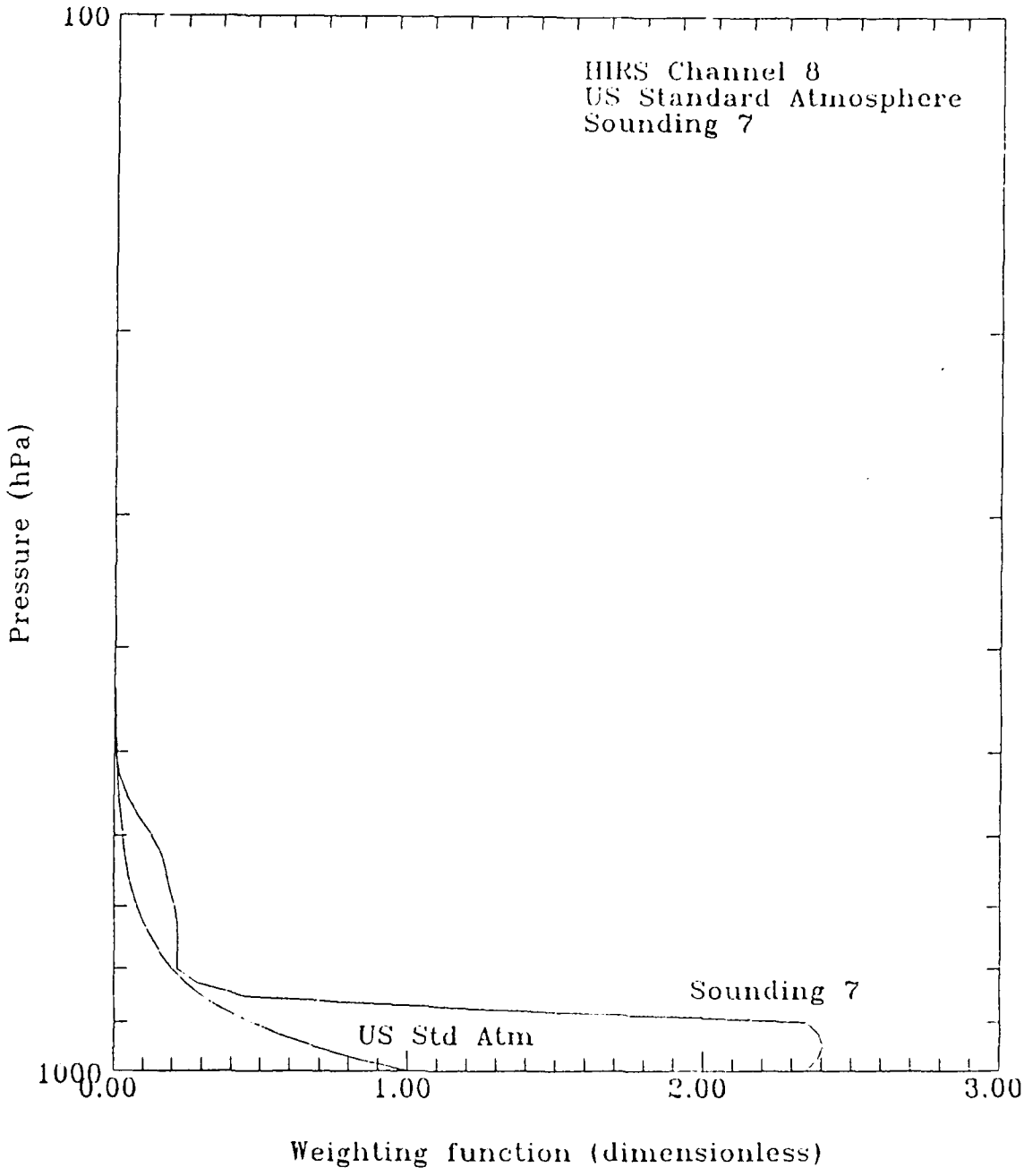

Figure 4.8d. As in Fig. 4.8a, except surface (window) temperature group represented by HIRS channel 8.

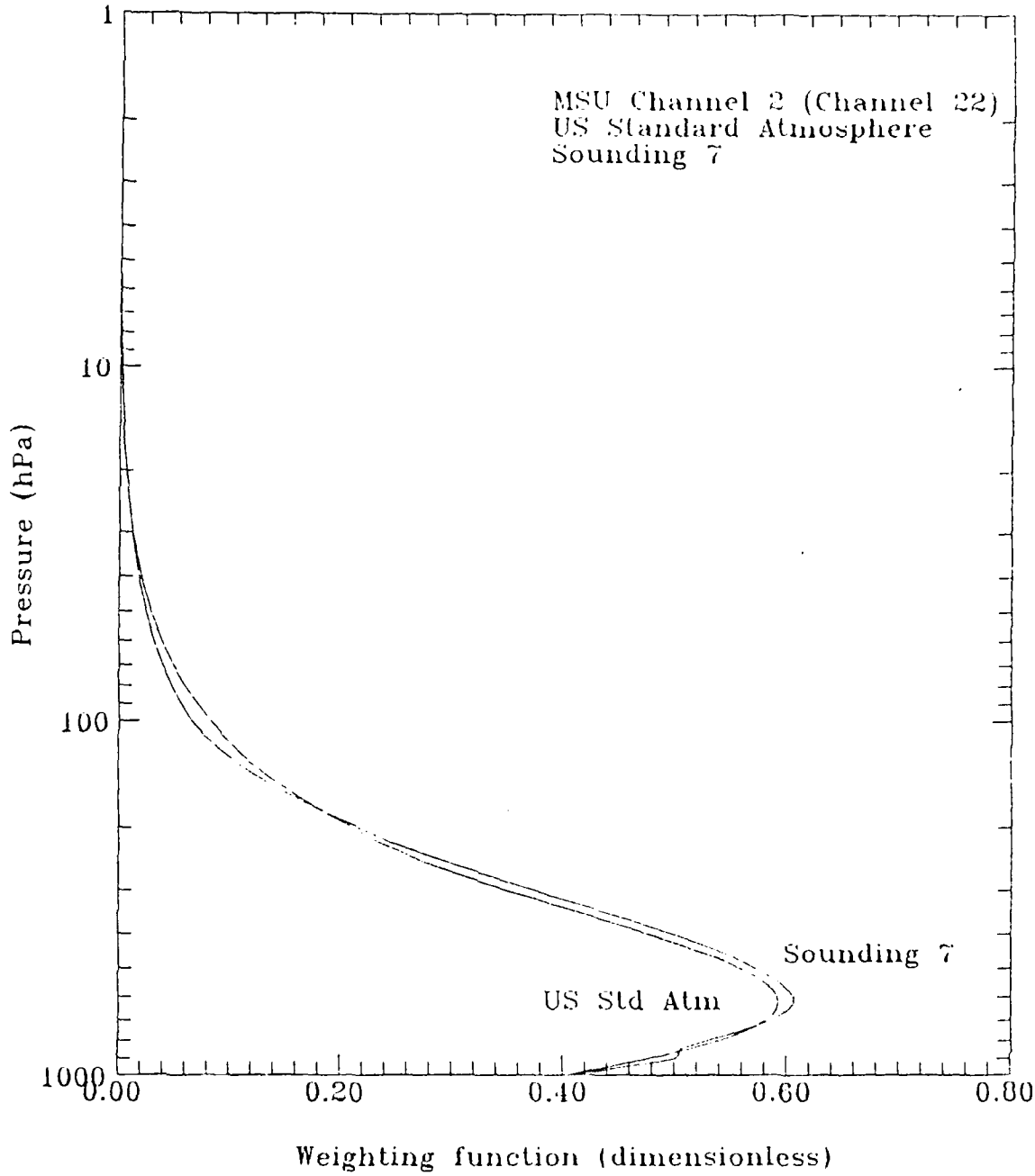

Figure 4.8e. As in Fig. 4.8a, except MSU temperature sounding group represented by MSU channel 2 (renumbered channel 22).

The methods developed herein to analyze satellite data require unbiased RTM response to a variety of atmospheric conditions; namely, satellite data variance should arise only from differences in atmospheric soundings evaluated by the RTM. In the last verification step, comparison weighting function curves were plotted to illustrate the response of the RTM to the training data seed soundings. Two seed soundings are used for illustration: the US Standard Atmosphere and sounding #7, the subsidence inversion. Figure 4.8 shows RTM-computed weighting function curves for these two soundings from each of the major sounding groups. The 15 μm temperature sounding group is represented by HIRS channel 4 (Fig. 4.8a); the 4.3 μm temperature sounding group is represented by HIRS channel 15 (Fig. 4.8b); the water vapor sounding group is represented by HIRS channel 12 (Fig. 4.8c); the surface window channels are represented by HIRS channel 8 (Fig. 4.8d); and the MSU channels are represented by MSU channel 2 (renumbered as channel 22) (Fig. 4.8e). The curves are plotted without normalization to portray relative magnitude. The height of the peak energy contribution was found to be consistent among the training data soundings.

The intent of verification was to ensure that the present employment of the RTM is without procedural error: results demonstrate that the RTM performs as intended.

CHAPTER V

DATA

This chapter describes the types of data used in this research: (1) developmental atmospheric temperature and dewpoint soundings; (2) sets of developmental synthetic TIROS operational vertical sounder (TOVS) satellite channel brightness temperatures; (3) radiative transfer model (RTM) physical and geophysical parameters; (4) collections of verification soundings for sensitivity studies; and, (5) vertical cross sections of verification soundings.

For use in technique development, eight different atmospheric soundings were created, each representing a specific synoptic feature. (The US Standard Atmosphere is included as the ninth sounding. It contains no specific features; it is used for reference.) Each of these initial "seed soundings" was perturbed to create 50 similar, but different, soundings; a synthetic data base of 450 temperature and dewpoint temperature soundings resulted, each of which was evaluated by the RTM. This process produced 450 synthetic satellite observations, each estimating 22 channels of what the TOVS would have seen had the sounding actually occurred in nature. In operation, the TOVS carries 27 channels. The RTM does not support HIRS channels 17 or 20 or the three stratospheric sounder channels. Further, for the purposes of this research, HIRS channels 1, 2 and 9 and MSU channels 1 and 4 (renumbered 21 and 24) are not useful and are excluded from most statistical computations. The 450 atmospheric soundings and corresponding synthetic satellite observations representing nine synoptic regimes comprises the developmental data base.

All data were selected to represent typical conditions occurring over the tropical eastern Pacific Ocean. It is not the intent of this research to expand

the data to include all possible synoptic conditions or beyond that which is required to demonstrate the potential of the techniques.

The first part of this chapter describes, in more detail, the construction of this data base. The latter part, Sections D, E and F, describes additional atmospheric and satellite soundings generated for verification and sensitivity studies.

A. Atmospheric soundings

Nine atmospheric temperature and moisture soundings were chosen to represent synoptic features normally found over the study area (for example, see Riehl, 1979). The profiles selected are: four types of inversions (frontal, radiation, turbulence, and trade-wind); a warm humid tropical sounding without cloud; two island-influenced soundings; a warm anticyclone containing a subsidence inversion; and the US Standard Atmosphere which is included as a baseline. Most of the profiles are fabricated based on observed conditions; this procedure provides the advantage of generality without the disadvantage of smoothing found in climatological data. In fact, if climatological data were used, the smoothing inherent in such data would eliminate the very synoptic features to be studied.

The relevant synoptic features of interest typically occur below 500 hPa. All profiles except one are identical above 500 hPa and resemble a tropical mean sounding. The transition is smooth from the synoptic feature to the upper portion of the sounding. The upper troposphere was assumed dry although this is commonly not the case (Blackwell, 1987).

1. Description of the soundings

The temperatures and dewpoint depressions for all nine vertical profiles are reproduced as Table 5.1 and shown in Fig. 5.1. The US Standard Atmosphere temperature profile is shown as a heavy line for reference in each sounding.

a. The frontal inversion (Sounding #1; Fig. 5.1a) is cool and moderately dry at the surface. A mild inversion (1°C/100 hPa) extends from 900 to 800 hPa. Above the inversion and upwards to 600 hPa, the dewpoint depression is small.

b. Sounding #2 is a radiation inversion (Fig. 5.1b). The inversion strength is 5°C from the surface to 900 hPa. It is moist at the surface (5°C dewpoint depression). From the top of the inversion upwards to 500 hPa, the dewpoint depression is maintained between 10° and 13°C.

c. The turbulence inversion (Sounding #3; Fig. 5.1c) itself is shallow, only 50 hPa thick. The profile is adiabatic and of constant mixing ratio below the inversion. Between the inversion and 500 hPa, the dewpoint depression is constant at 30°C.

d. The trade wind inversion in sounding #4 (Fig. 5.1d) is moist between the surface and 800 hPa, at the base of the inversion. The inversion is dry and shallow; the top is reached at 750 hPa. The 700 to 600 hPa layer is not excessively dry; this feature, though common, does not typify all of the trade wind regime.

e. Sounding #5 is a warm humid tropical profile (Fig. 5.1e) which ordinarily would contain cloud. Clouds are not considered in this research and are eliminated from all profiles. This sounding is

moist and nearly isothermal from the surface to 600 hPa. Above 800 hPa, there is gradual drying, and a nearly constant dewpoint depression of approximately 15°C is maintained from 700 to 500 hPa. Overall, the profile is 10 to 20°C warmer than the Standard Atmosphere.

f. Sounding #6 typifies effects that might be observed over tropical islands (Fig. 5.1f). There are two moist layers, one at the surface and the other at 600 hPa with a drier layer in between.

g. The typical warm subsidence inversion of the oceanic anticyclone is represented in sounding #7 (Fig. 5.1g). There is a strong temperature inversion and moisture gradient between 900 and 800 hPa.

h. The US Standard Atmosphere as supplied by Hayden[1] is shown as sounding #8 (Fig. 5.1h). There are minor variations between sounding #8 and that given by the US Standard Atmosphere (1966).

i. A second island-influenced sounding is shown as sounding #9 (Fig. 5.1i). There is a shallow layer of humid air near the surface overlain by a near constant dewpoint depression to 500 hPa.

To illustrate the significant overlap of synoptic features, all nine soundings are shown in Fig. 5.2. The identity of the plotting symbols is not important; they are used to differentiate the individual profiles.

---

[1] C.M. Hayden, NOAA/NESDIS, Madison, WI; personal communication.

Table 5.1. Seed sounding temperature and dewpoint depression data.

Sounding #1. Frontal inversion.

Pressure (hPa)	Temperature (°C)	Dewpoint depression (°C)
1000.0	10.0	10.0
900.0	9.0	19.0
800.0	10.0	12.0
700.0	5.0	8.0
600.0	-2.0	13.0
500.0	-5.0	30.0
400.0	-15.0	30.0
300.0	-30.0	30.0
200.0	-50.0	30.0
100.0	-80.0	30.0
1.0	1.0	30.0

Sounding #2. Radiation inversion.

Pressure (hPa)	Temperature (°C)	Dewpoint depression (°C)
1000.0	15.0	5.0
900.0	20.0	10.0
800.0	14.0	11.0
700.0	7.0	12.0
600.0	-2.0	13.0
500.0	-5.0	30.0
400.0	-15.0	30.0
300.0	-30.0	30.0
200.0	-50.0	30.0
100.0	-80.0	30.0
1.0	1.0	30.0

Table 5.1. (continued)

Sounding #3. Turbulence inversion.

Pressure (hPa)	Temperature (°C)	Dewpoint depression (°C)
1000.0	24.0	16.0
850.0	10.0	4.0
800.0	10.0	10.0
600.0	-2.0	13.0
500.0	-5.0	30.0
400.0	-15.0	30.0
300.0	-30.0	30.0
200.0	-50.0	30.0
100.0	-80.0	30.0
1.0	1.0	30.0

Sounding #4. Trade wind inversion.

Pressure (hPa)	Temperature (°C)	Dewpoint depression (°C)
1000.0	22.0	2.0
900.0	16.0	6.0
800.0	10.0	3.0
750.0	13.0	38.0
700.0	8.0	20.0
600.0	-2.0	13.0
500.0	-5.0	30.0
400.0	-15.0	30.0
300.0	-30.0	30.0
200.0	-50.0	30.0
100.0	-80.0	30.0
1.0	1.0	30.0

Table 5.1. (continued)

Sounding #5. Warm, humid tropical profile.

Pressure (hPa)	Temperature (°C)	Dewpoint depression (°C)
1000.0	25.0	3.0
900.0	25.0	3.0
850.0	23.0	1.0
840.0	22.0	0.0
800.0	24.0	4.0
730.0	27.0	12.0
700.0	25.0	14.0
680.0	24.0	17.0
630.0	25.0	20.0
600.0	23.0	20.0
500.0	-5.0	30.0
400.0	-15.0	30.0
300.0	-30.0	30.0
200.0	-50.0	30.0
100.0	-80.0	30.0
1.0	1.0	30.0

Sounding #6. Island I--two moist layers.

Pressure (hPa)	Temperature (°C)	Dewpoint depression (°C)
1000.0	28.0	8.0
850.0	17.0	3.0
700.0	9.0	21.0
600.0	3.0	4.0
500.0	-5.0	30.0
400.0	-15.0	30.0
300.0	-30.0	30.0
200.0	-50.0	30.0
100.0	-80.0	30.0
1.0	1.0	30.0

Table 5.1. (continued)

Sounding #7. Warm subsidence inversion.

Pressure (hPa)	Temperature (°C)	Dewpoint depression (°C)
1000.0	25.0	4.0
920.0	20.0	2.0
870.0	18.0	2.0
850.0	20.0	16.0
820.0	22.0	22.0
800.0	19.0	23.0
700.0	9.0	14.0
600.0	3.0	11.0
500.0	-5.0	30.0
400.0	-15.0	30.0
300.0	-30.0	30.0
200.0	-50.0	30.0
100.0	-80.0	30.0
1.0	1.0	30.0

Table 5.1. (continued)

Sounding #8. U.S. Standard Atmosphere as supplied by Hayden (1986).

Pressure (hPa)	Temperature (°C)	Dewpoint depression (°C)
1000.0	14.2	4.5
950.0	11.5	5.5
920.0	9.8	6.1
850.0	5.5	7.2
780.0	1.0	8.1
700.0	-4.5	8.9
670.0	-6.8	9.1
620.0	-10.7	10.0
570.0	-14.8	9.4
500.0	-21.1	11.0
475.0	-23.7	13.0
430.0	-28.3	13.0
400.0	-31.7	14.3
350.0	-37.8	13.8
300.0	-44.5	30.0
250.0	-52.5	30.0
200.0	-52.5	30.0
150.0	-52.5	30.0
135.0	-52.5	30.0
115.0	-52.5	30.0
100.0	-52.5	30.0
85.0	-52.5	30.0
70.0	-52.5	30.0
60.0	-52.5	30.0
50.0	-52.5	30.0
30.0	-52.5	30.0
25.0	-52.5	30.0
20.0	-52.5	30.0
15.0	-52.5	30.0
10.0	-52.5	30.0
7.0	-52.5	30.0
5.0	-52.5	30.0
4.0	-52.5	30.0
3.0	-52.5	30.0
2.0	-52.5	30.0
1.0	-52.5	30.0

Table 5.1. (continued)

Sounding #9. Island II--moist surface layer.		
Pressure (hPa)	Temperature (°C)	Dewpoint depression (°C)
1000.0	23.0	2.0
850.0	19.5	13.0
700.0	10.0	16.0
500.0	-8.0	8.0
400.0	-18.0	9.0
300.0	-30.0	12.0
250.0	-41.0	30.0
200.0	-54.0	30.0

2. Expansion of the seed soundings

Section 1 describes nine specific synoptic conditions. A number of soundings representative of these features and normal atmospheric variability around them is required to satisfy the multivariate statistical methods applied to this synthetic data set. If there are n variables in each sounding, there must be at least $2n$ soundings for the technique to be statistically meaningful. Since the output of the RTM contains 22 satellite channel brightness temperatures, an input data set must contain at least 44 observations. At the time the research was begun it was not known that HIRS channels 1, 2, 9, 17 and 20 and MSU channels 1 and 4 (renumbered 21 and 24) would not yield useful information. In the beginning, 50 observations were generated for convenience; that practice was continued throughout the research.

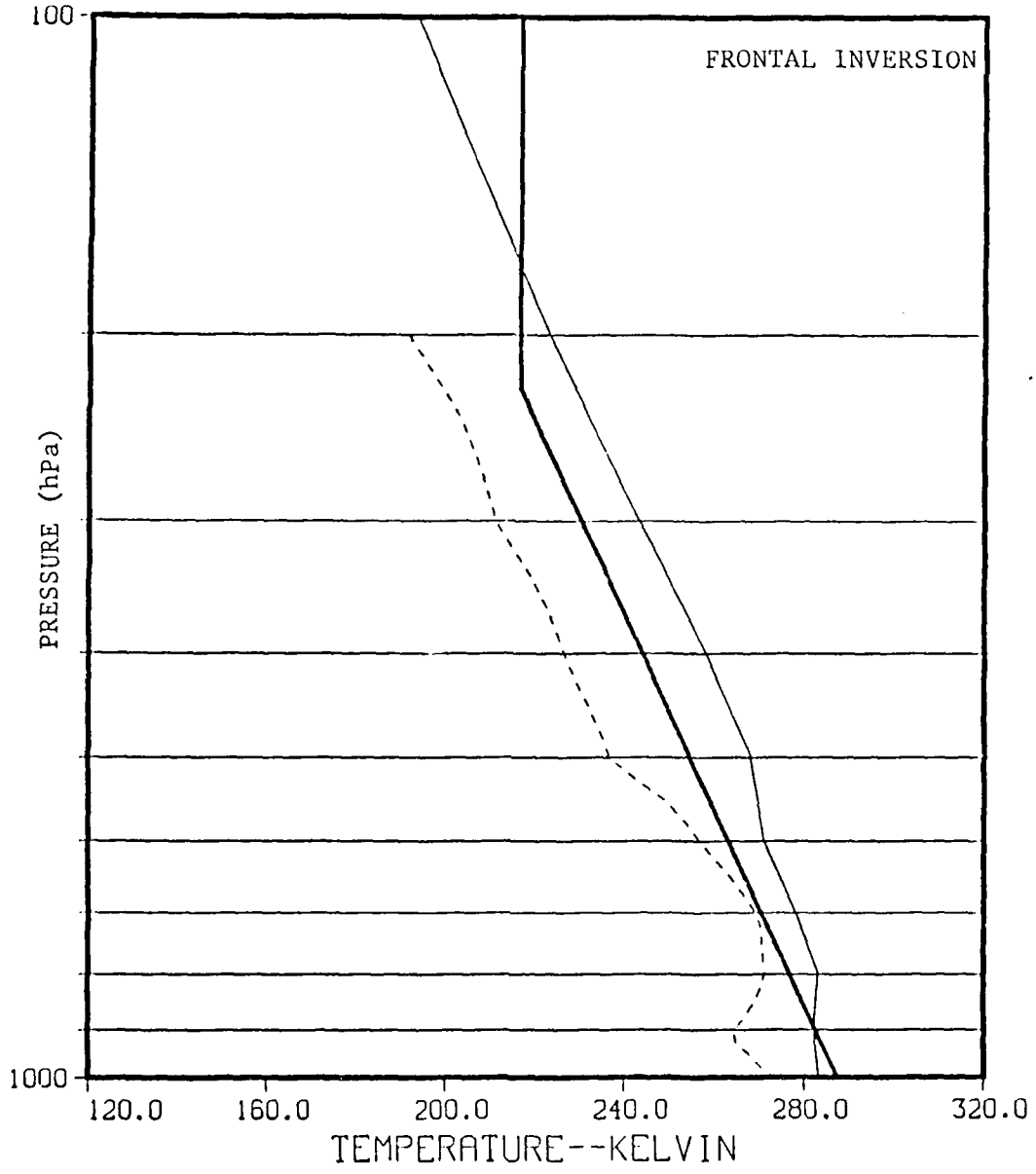

Figure 5.1a. Seed sounding #1, frontal inversion.

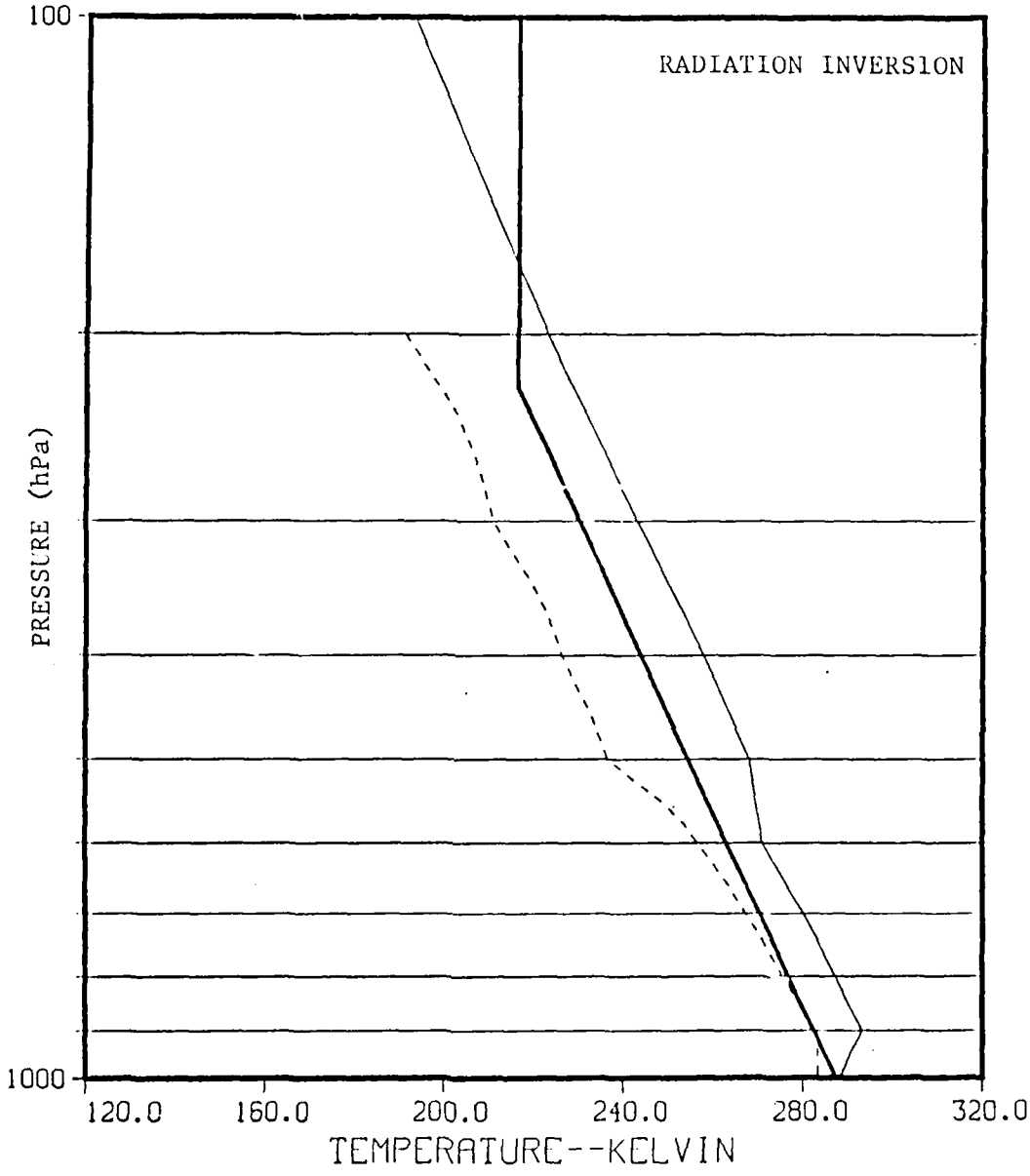

Figure 5.1b. As in Fig. 5.1a, except for seed sounding #2, radiation inversion.

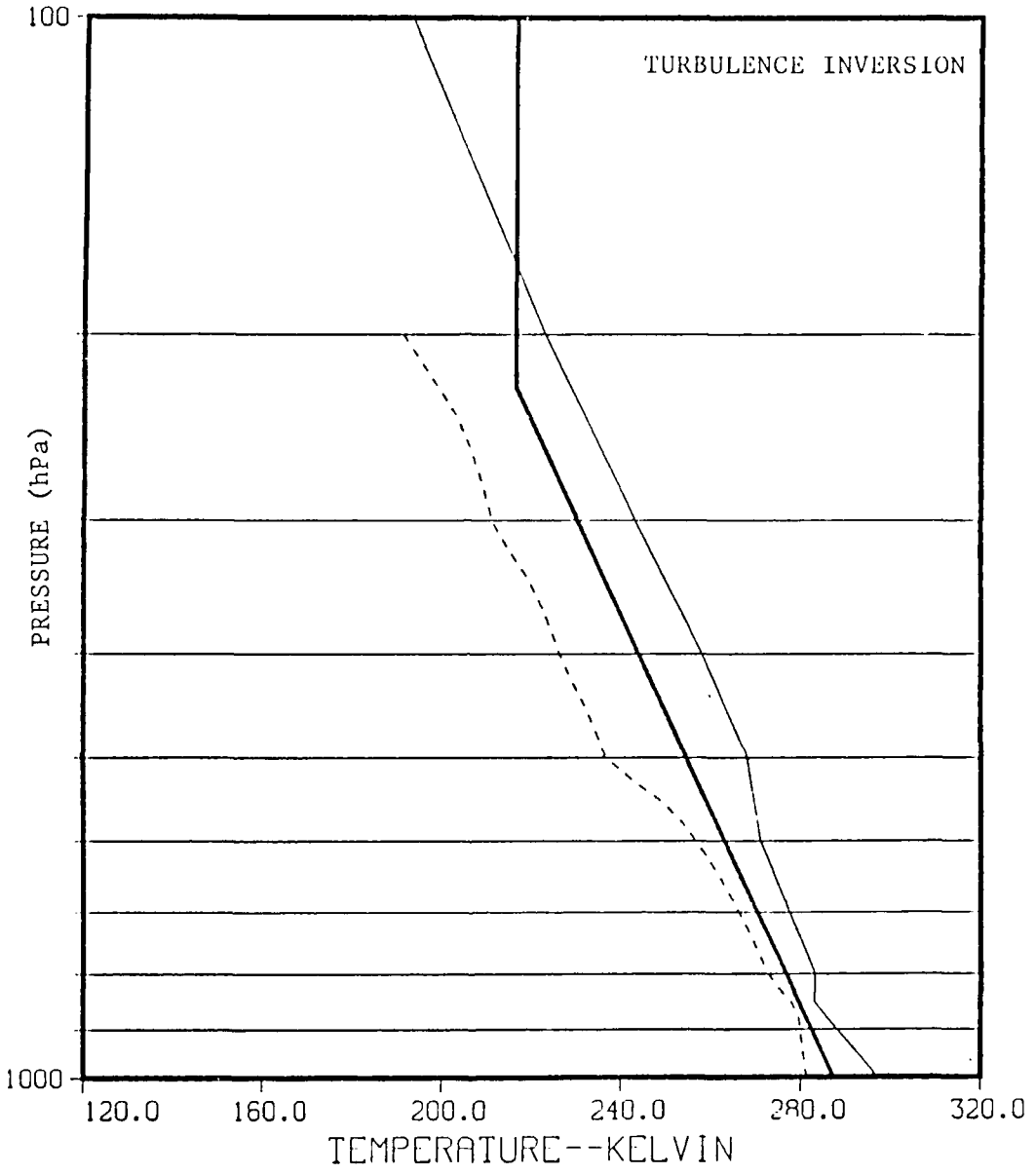

Figure 5.1c. As in Fig. 5.1a, except for seed sounding #3, turbulence inversion.

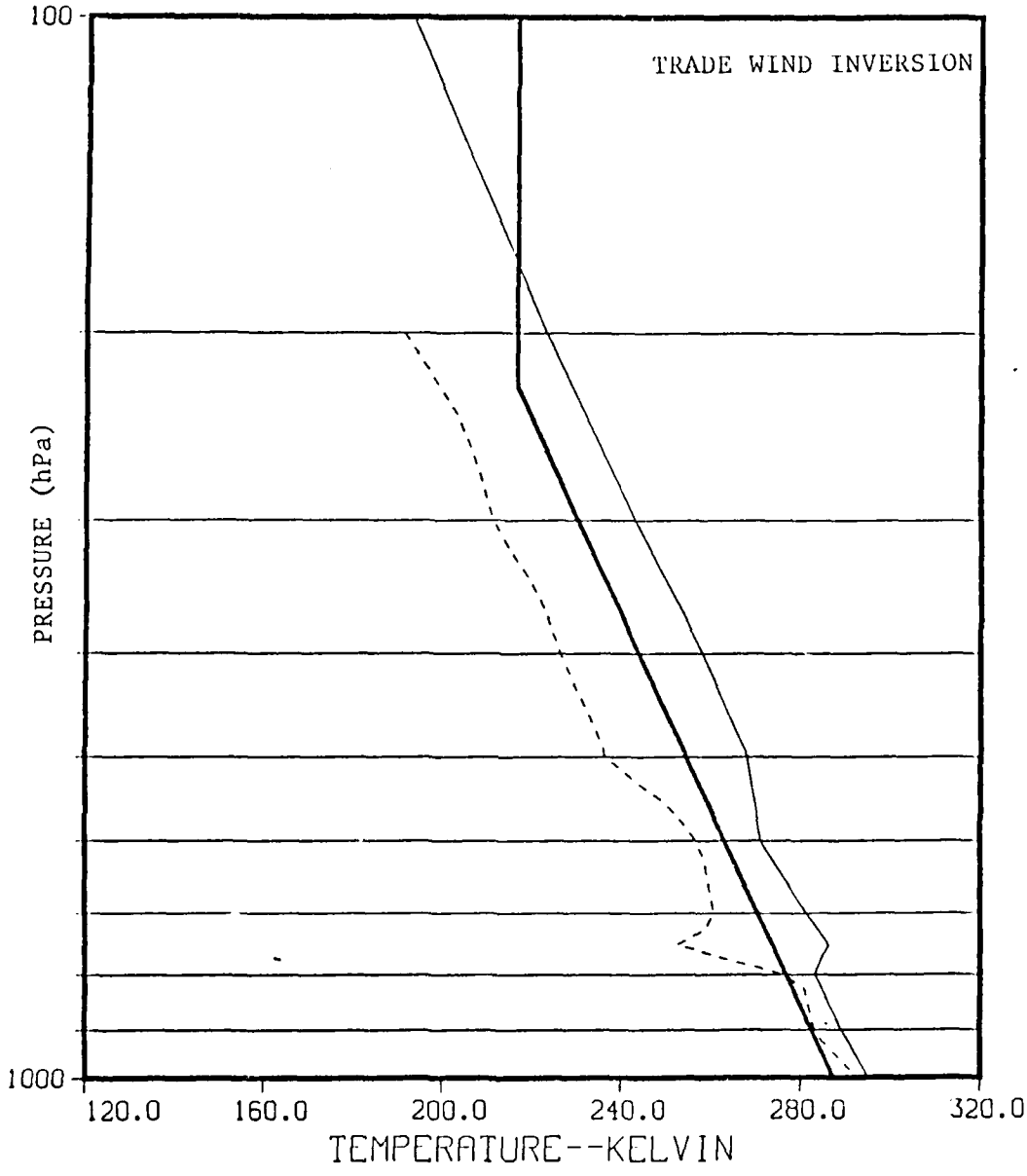

Figure 5.1d. As in Fig. 5.1a, except for seed sounding #4, trade wind inversion.

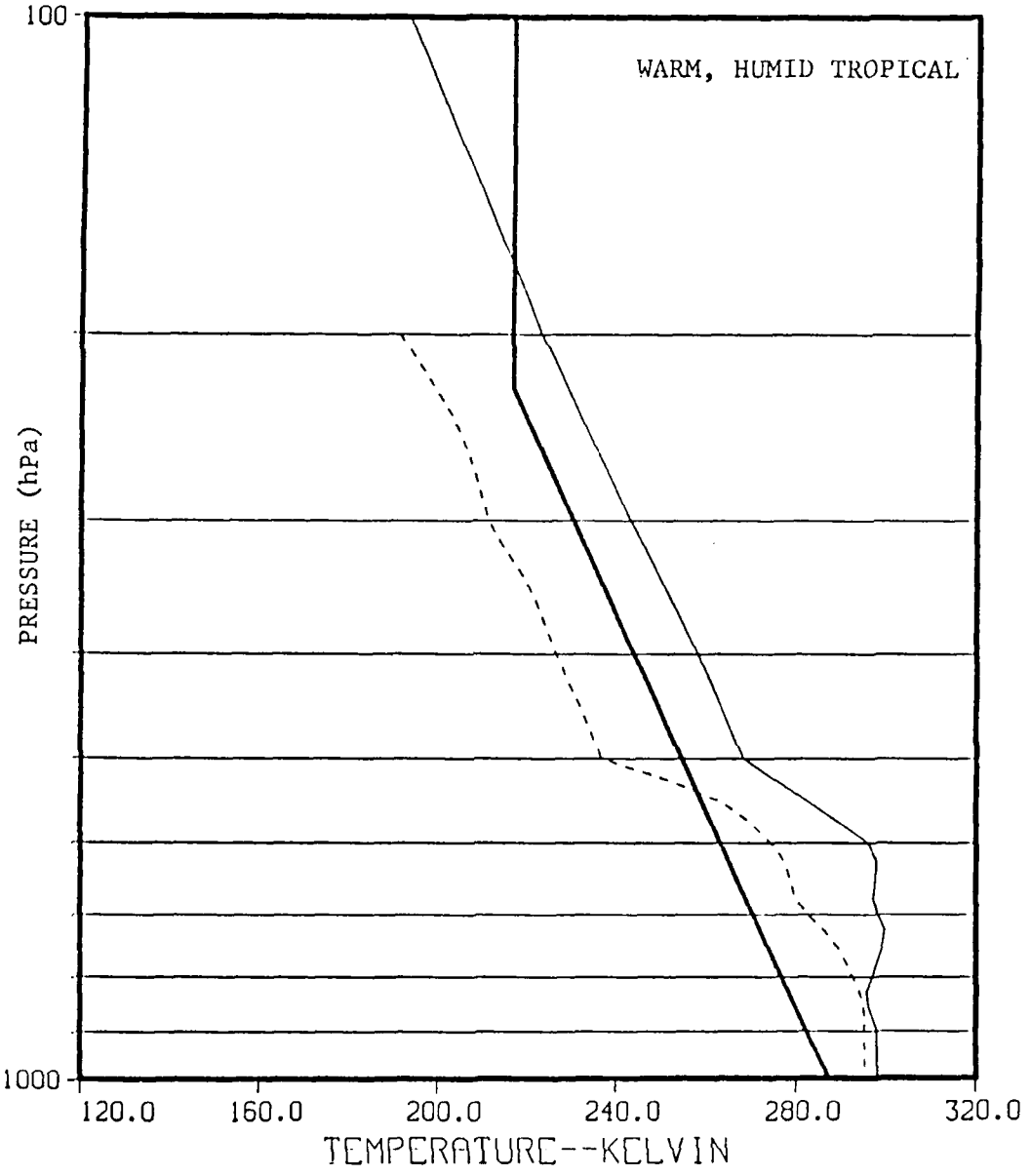

Figure 5.1e. As in Fig. 5.1a, except for seed sounding #5, warm, humid tropical profile.

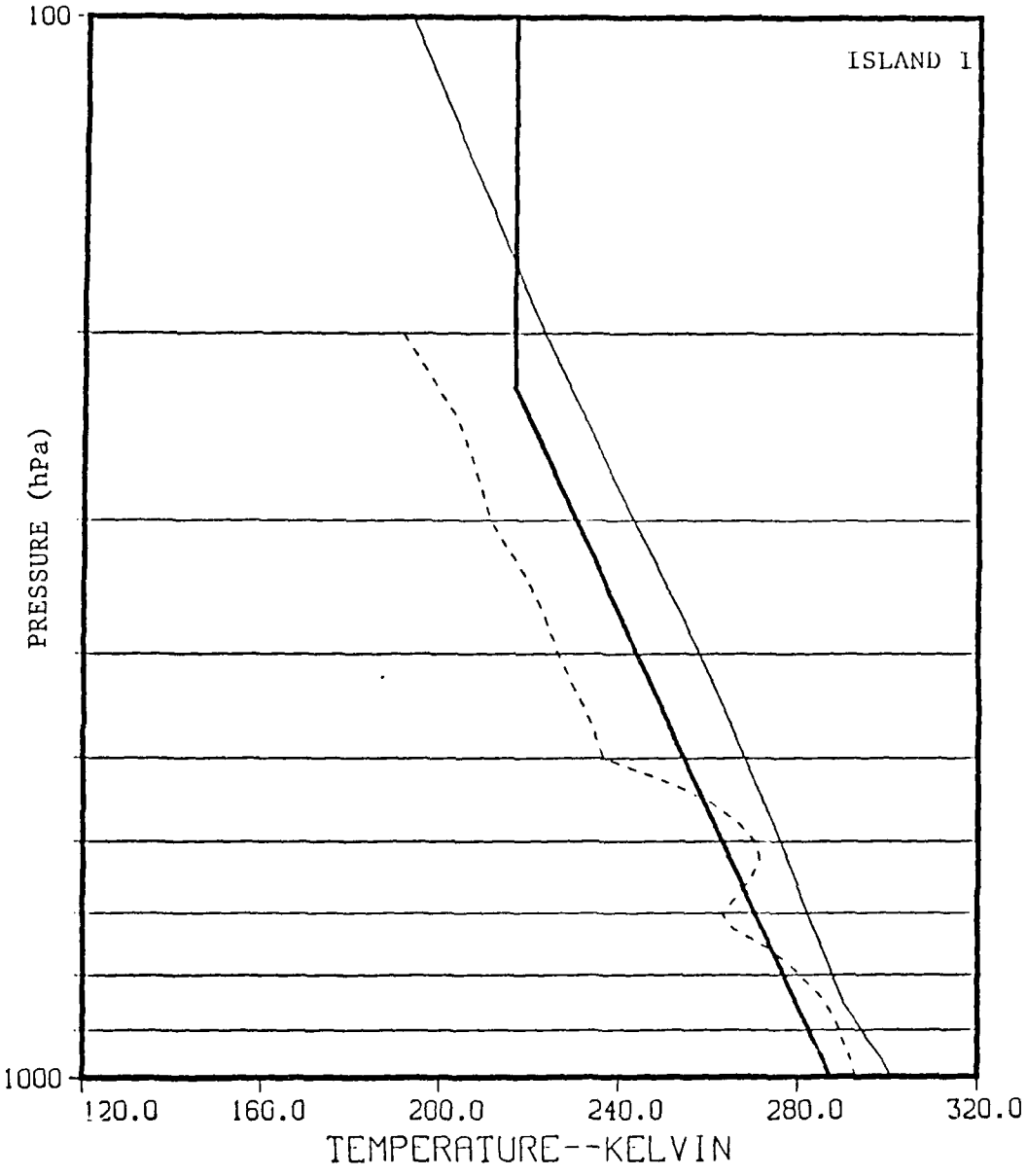

Figure 5.1f. As in Fig. 5.1a, except for seed sounding #6, typical tropical island sounding I.

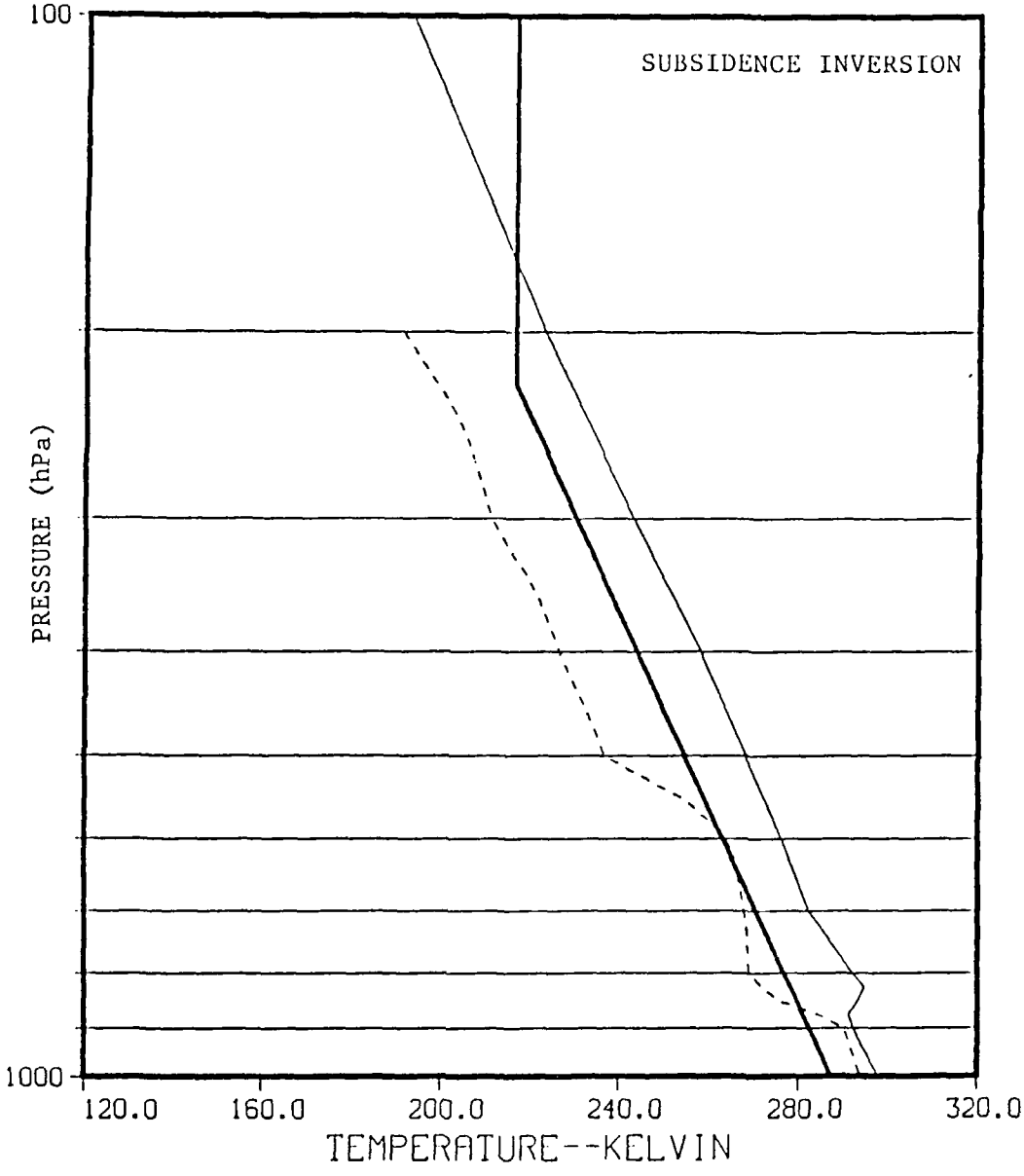

Figure 5.1g. As in Fig. 5.1a, except for seed sounding #7, warm subsidence inversion.

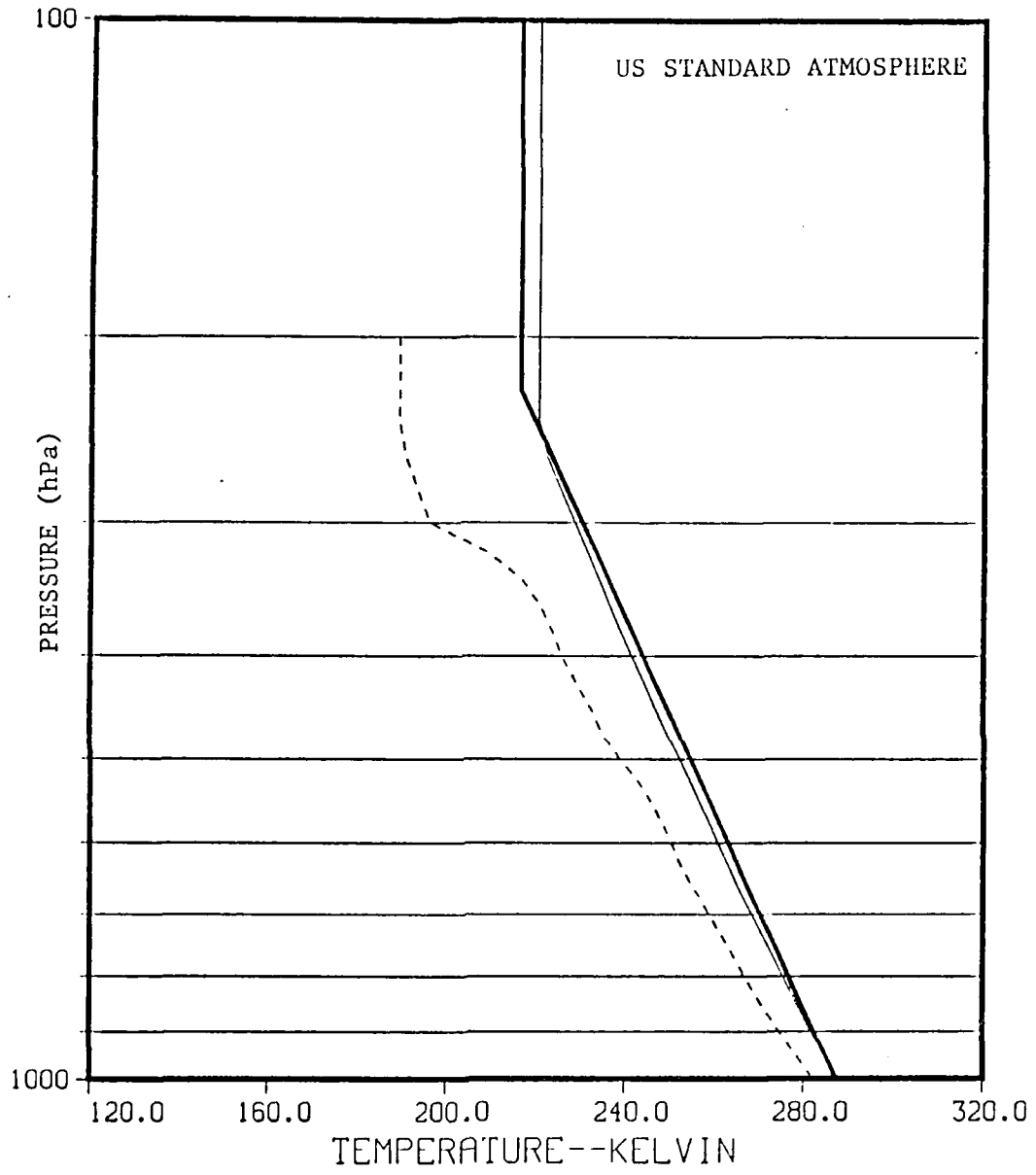

Figure 5.1h. As in Fig. 5.1a, except for seed sounding #8, the US Standard Atmosphere. See text for details.

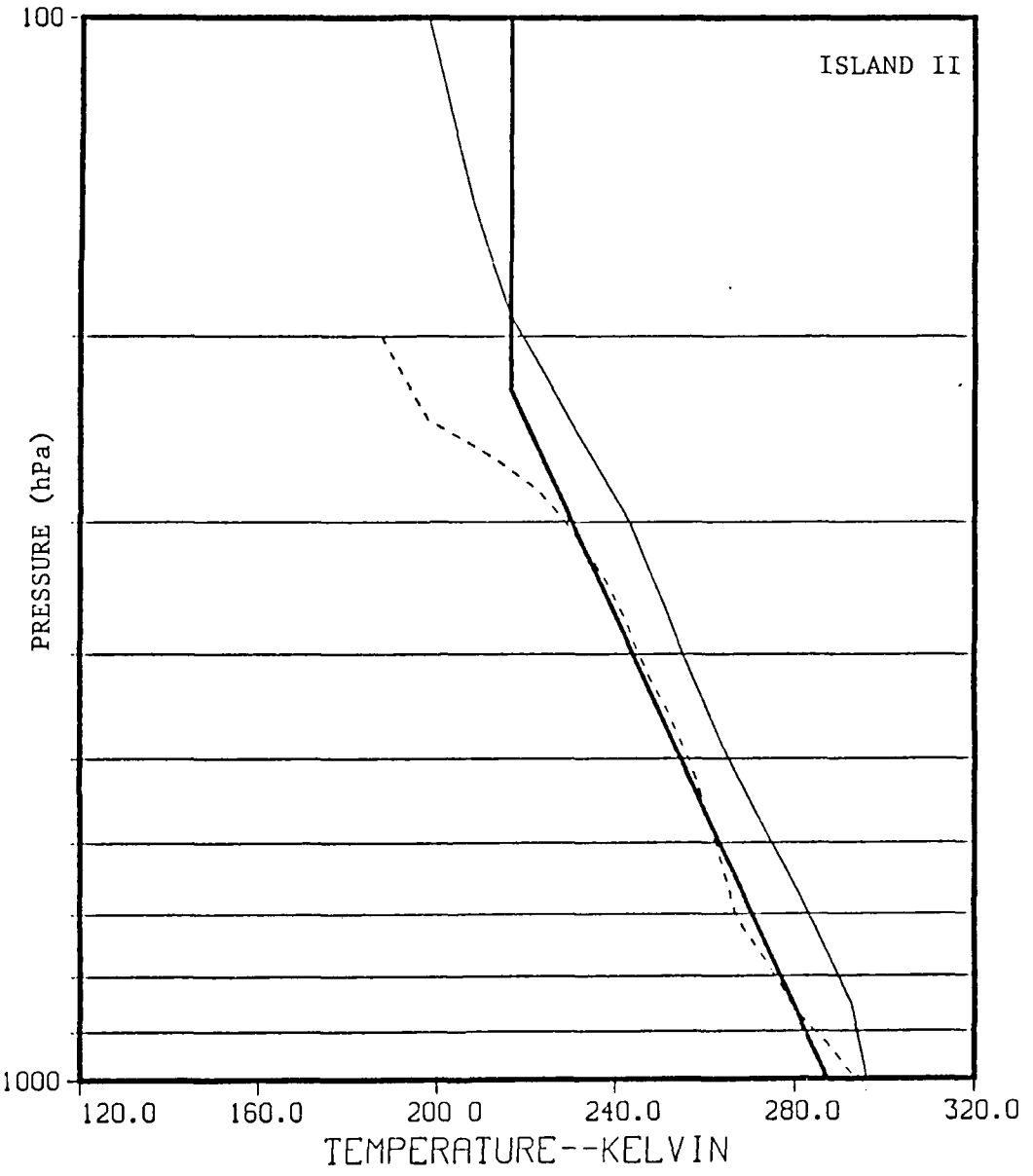

Figure 5.1i. As in Fig. 5.1a, except for seed sounding #9, island-influenced sounding II.

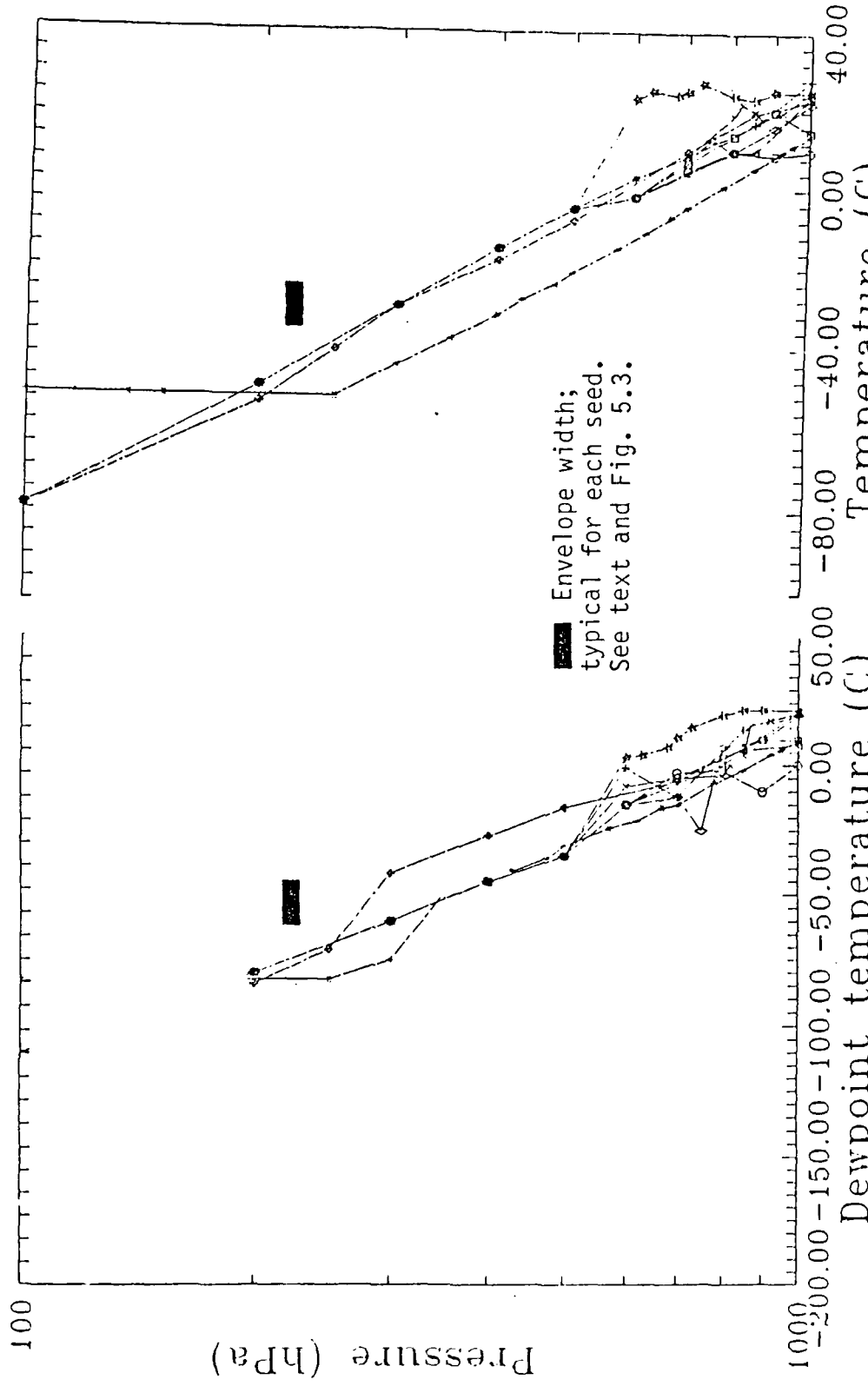

Figure 5.2. A synthesis of all seed soundings portrayed in Fig. 5.1. Moisture soundings have been offset for clarity. Heavy horizontal bars show the approximate envelope width (±4%) for each sounding set. The resulting overlap of each sounding set can be inferred.

Each sounding in Fig. 5.1 was used as a "seed" to construct 50 statistically similar, but different, soundings, which were interpolated to the 66 layers required for input into the RTM. The 50 soundings were generated by adding random perturbations to the seed values at each of the 66 layers. The specific character of the seed was preserved by restricting the perturbations to lie within prescribed limits. Temperature profiles in the atmosphere typically are correlated highly in the vertical. Therefore, the perturbation was treated as a modified, first-order autoregressive process (Chatfield, 1984), using the equation:

$$X_t = aX_{t-1} + \epsilon, \tag{2}$$

where X_t is either temperature or dewpoint depression at layer t; t-1 denotes the layer immediately below t; a is a correlation coefficient between adjacent layers, and ϵ is a random perturbation, introduced as white noise.

Brightness temperatures produced by the RTM depend on atmospheric vertical structure; essentially, the RTM smoothes by integrating the RTE over 66 layers (see Eqn. 1). There are two extremes in the vertical structure of a sounding as shown in Fig. 5.3: no vertical correlation, in which the temperature and moisture values at a given level are unrelated to those at adjacent levels; and perfect correlation, in which temperature and moisture values at one level completely determine those at all other levels. It was not clear *a priori*, which behavior masks the synoptic features more severely. Both extremes were examined, and the results are nearly identical. The technique development used the correlated data because the sounding profiles are more physically realistic. For highly correlated data, the vertical correlation

coefficient, a, was set to 0.95, a compromise between the theoretical limit of 1.0 and the estimated observational value of 0.8 to 0.9, depending on channel, as given by Anderson (1986).

The perturbation expansion of each seed sounding appears as an envelope in Fig. 5.4 rather than a single trace of temperature and dewpoint temperature as in Fig. 5.1. Synoptic information present in the seed sounding is preserved by the shape of the perturbation envelope. Although vertical correlation of temperature and dewpoint temperature produces smooth profiles, the soundings are permitted to wander within the width of the envelope. The width of the envelope is $\pm 4\%$ of the seed temperature and dewpoint temperature (in absolute temperature, K), and even this small variation is enough to create significant overlap in similar seed soundings as shown in Fig. 5.2. To test the ability of the statistical model to discriminate among strongly overlapping sounding classes, the perturbation range was varied to a maximum $\pm 12\%$ (approx. $\pm 25°C$).

B. Synthetic satellite observations

Synthetic satellite observations constitute the second type of data used in the developmental data base. Each of the 450 satellite soundings generated as described above were processed through the RTM to create a set of synthetic satellite observations.

Satellite observations are written as vectors whose elements are individual satellite channel brightness temperatures. For computational purposes, each synthetic satellite observation is represented by a matrix of 3 columns by 22 rows. The first column vector contains the channel number; the second contains the brightness temperatures corresponding to the channel; and the

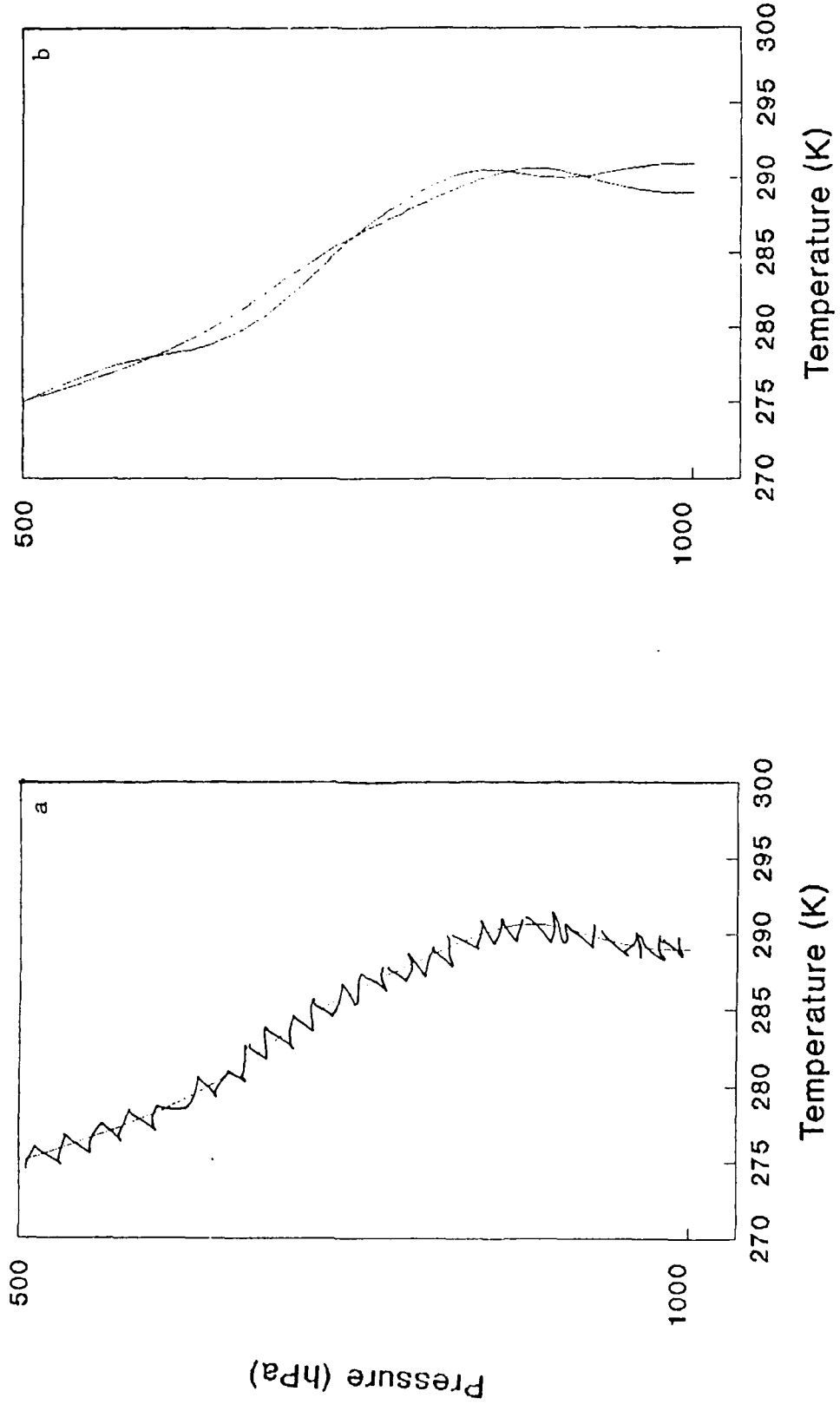

Figure 5.3. Sample perturbed temperature sounding for perturbations less than ±4%. Smooth background line is the seed temperature sounding. Heavy line is a schematic representation of one of fifty generated soundings for (a) vertically uncorrelated ($\alpha = 0$) and (b) vertically correlated ($\alpha = 0.95$) perturbations in temperature structure.

third is a label.

All elements of the label vector for a given sounding have the same value. Initially, the label values are assigned arbitrarily. It is essential to note that the label does not assign a satellite sounding to a given synoptic regime. Rather, it is the synoptic signature present in the brightness temperature vector that determines classification; the label is for identification only. An example satellite observation matrix is given as Table 5.2.

C. Radiative transfer model geophysical parameters

The RTM requires specification of several global parameters (Table 5.3), layer transmission coefficients and ozone climatology. These data are entered once and do not change in a normal computational series; they were fixed in this research to maintain consistent RTM performance. The layer transmission coefficients were determined empirically by Susskind. The ozone climatology for January at 20°N was among many supplied by P. Pirano (NASA, Goddard Laboratory for the Atmospheres, Greenbelt, MD; personal communication).

The RTM requires temperatures and dewpoint temperatures from the surface to 1 hPa at 66 specific layers. Missing intermediate levels are supplied by an interpolation subroutine, and if the profile does not extend to the surface, or more commonly to 1 hPa, these missing data are replaced by climatology. Temperature and moisture climatologies were supplied by Susskind (Table 5.4).

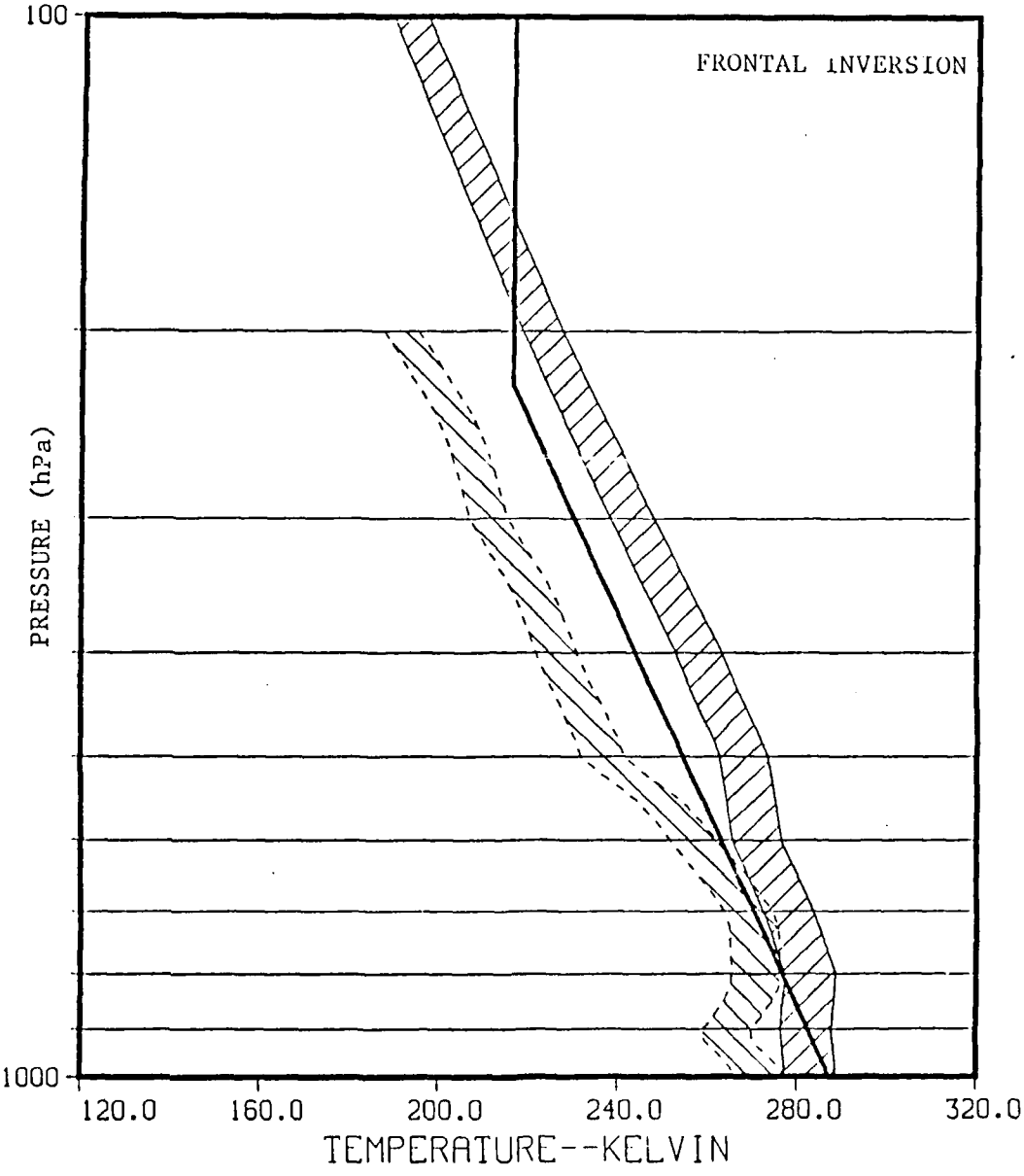

Figure 5.4. Perturbation expansion ($\pm 4\%$) of seed sounding #1. Region bounded by solid lines is the envelope for temperature profiles; area bounded by dashed lines is the envelope for moisture profiles. The character of the synoptic feature is preserved in the shape of the envelope. Heavy line is US Standard Atmosphere temperature profile for reference. See text for details.

Table 5.2. Sample satellite observation, sounding #1.

Channel*	Brightness temperature (K)	Label
1	243.113	1
2	221.832	1
3	224.315	1
4	237.764	1
5	251.919	1
6	262.506	1
7	271.267	1
8	282.439	1
9	267.169	1
10	281.270	1
11	270.411	1
12	259.295	1
13	274.743	1
14	268.564	1
15	258.593	1
16	241.546	1
18	281.769	1
19	282.280	1
21	226.947	1
22	259.616	1
23	234.183	1
24	209.223	1

* Channels 17 and 20 are not supported by the RTM. Microwave sounder unit (MSU) channels 1-4 are renumbered 21-24 for convenience.

D. Verification atmospheric soundings

1. Test atmospheric soundings

The techniques developed in this research for the identification of synoptic regimes were evaluated with seven test soundings denoted A through G. They contain synoptic features similar to, and in some cases, more complex than, those represented in the developmental training data set. The test soundings

Table 5.3. Radiative transfer model fixed parameters.

RTM global parameter	Value, units
Day/night	Day
Land/water	Water
Latitude	20°N
Longitude	140°W
Sun zenith angle	46.9°
Satellite zenith angle	8°
Surface microwave emissivity	0.60
Surface pressure	1000 hPa

are composites of actual tropical soundings and are constructed to fit within the realm of the training data regimes without duplicating them. The test soundings are shown in Fig. 5.5.

2. Fine structure analysis soundings

Fine structure analysis is the second step in the two-tier process of information retrieval. After preliminary identification of synoptic regime, additional information, such as the height or strength of an inversion, is revealed about the fine structure of the satellite sounding. To illustrate the technique, three series of trade wind inversion training data soundings and three series of frontal inversion training data soundings were analyzed. The strength of the trade wind inversions are 2, 5 and 10°C in 50 hPa; the base of the inversions vary in 50 hPa increments from 950 to 600 hPa, and all inversions are 50 hPa thick. The strength of the frontal inversions are 2, 5 and 10°C in 100 hPa; the bases of the inversions vary in 50 hPa increments from

Table 5.4. Temperature and moisture climatologies (from Susskind).

Layer number[a]	Temperature (K)	Moisture (molecules cm^{-2} x 10^{20})[b]
1	269.96	0.00068167
2	263.66	0.00068167
3	254.37	0.00068167
4	247.77	0.00068167
5	242.66	0.00068167
6	239.06	0.00068167
7	236.01	0.00068167
8	233.37	0.00068167
9	231.04	0.00068167
10	228.96	0.00068167
11	225.16	0.0034084
12	222.46	0.0036084
13	219.46	0.0068167
14	214.67	0.0068167
15	210.96	0.0068167
16	205.70	0.0068167
17	201.26	0.0068167
18	200.06	0.0068167
19	199.01	0.0068167
20	198.06	0.0068167
21	200.41	0.014013
22	202.56	0.020582
23	204.53	0.026625
24	206.36	0.032221
25	208.06	0.037430
26	210.30	0.042302
27	212.41	0.046880
28	214.40	0.051195
29	216.28	0.055277
30	218.06	0.059150
31	222.03	0.18819
32	225.66	0.30640
33	229.30	0.42644
34	232.95	0.56028
35	236.36	0.69586
36	239.70	0.86779
37	242.84	1.0745
38	245.80	1.2689
39	248.60	1.4526
40	251.26	1.6265
41	254.36	2.6190
42	257.28	3.5513
43	260.04	4.4318
44	262.66	5.2659

Table 5.4. (continued)

Layer number[a]	Temperature(K)	Moisture(molecules cm^{-2} x 10^{20})[b]
45	265.04	6.8217
46	267.31	9.0679
47	269.47	11.212
48	271.55	13.262
49	273.54	15.227
50	275.45	17.114
51	277.29	18.928
52	279.06	20.674
53	280.22	24.156
54	281.33	29.315
55	282.41	34.303
56	283.46	39.130
57	284.48	43.805
58	285.46	48.339
59	286.71	53.095
60	287.92	58.069
61	289.10	62.905
62	290.25	67.610
63	291.37	72.192
64	292.46	76.656
65	292.46	76.656
66	292.46	76.656

[a] Layer 1 is at the top of the atmosphere; layer 66 is at the surface.

[b] The unit is a measure of volume. In a layer model, the number of molecules in a volume of atmosphere determines the transmission properties within the layer. The measurement is computed for a 1 cm^2 cross section with height specified by layer thickness.

950 to 600 hPa, and all inversions are 100 hPa thick. Fig. 5.6 shows examples of three soundings with trade wind inversions at 850 hPa, each with a different strength. The frontal inversion training data set was constructed in a similar manner. The test soundings containing inversions were evaluated by the RTM, and a set of brightness temperature vectors was produced.

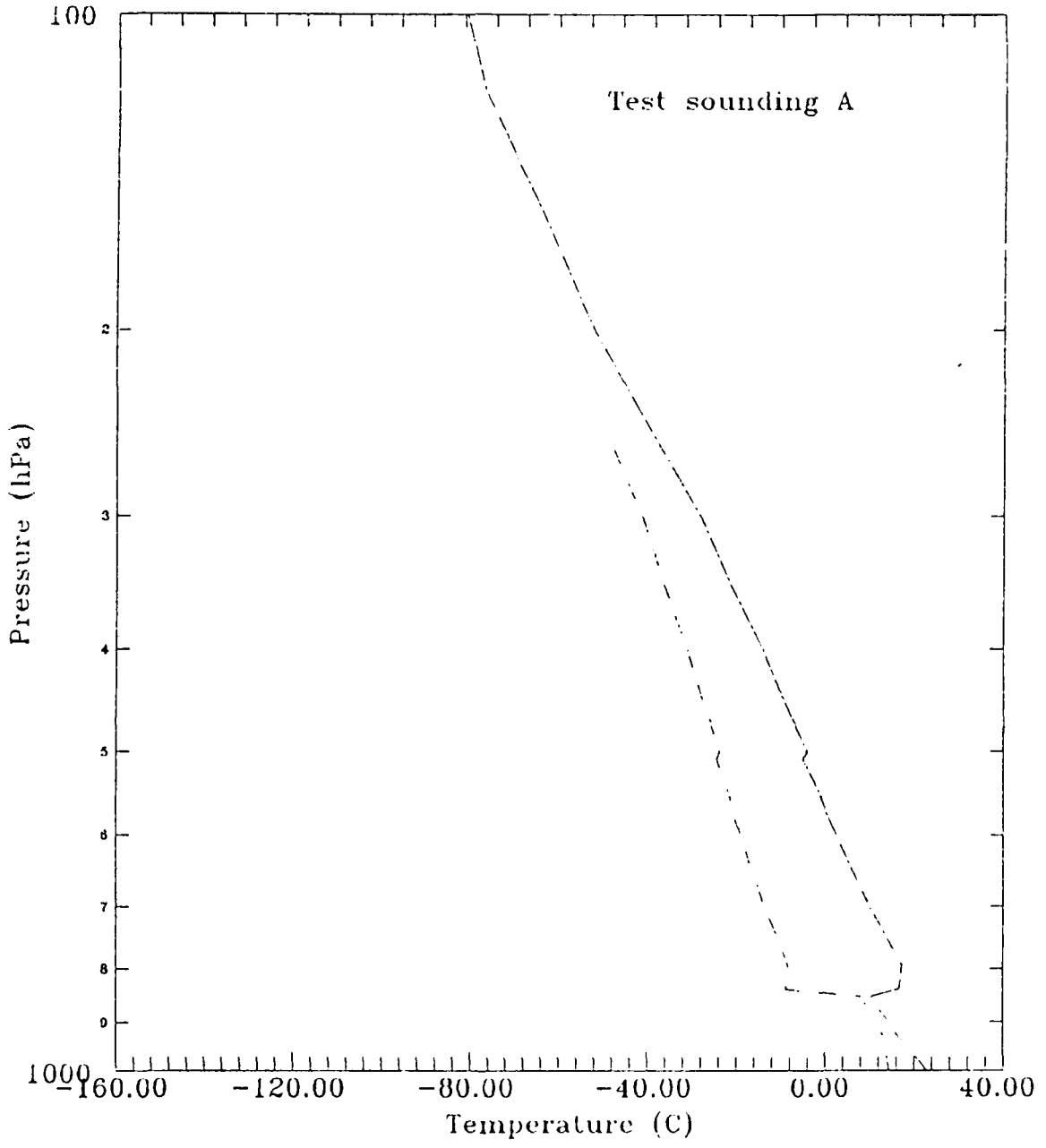

Figure 5.5a. Test sounding A. See text for details.

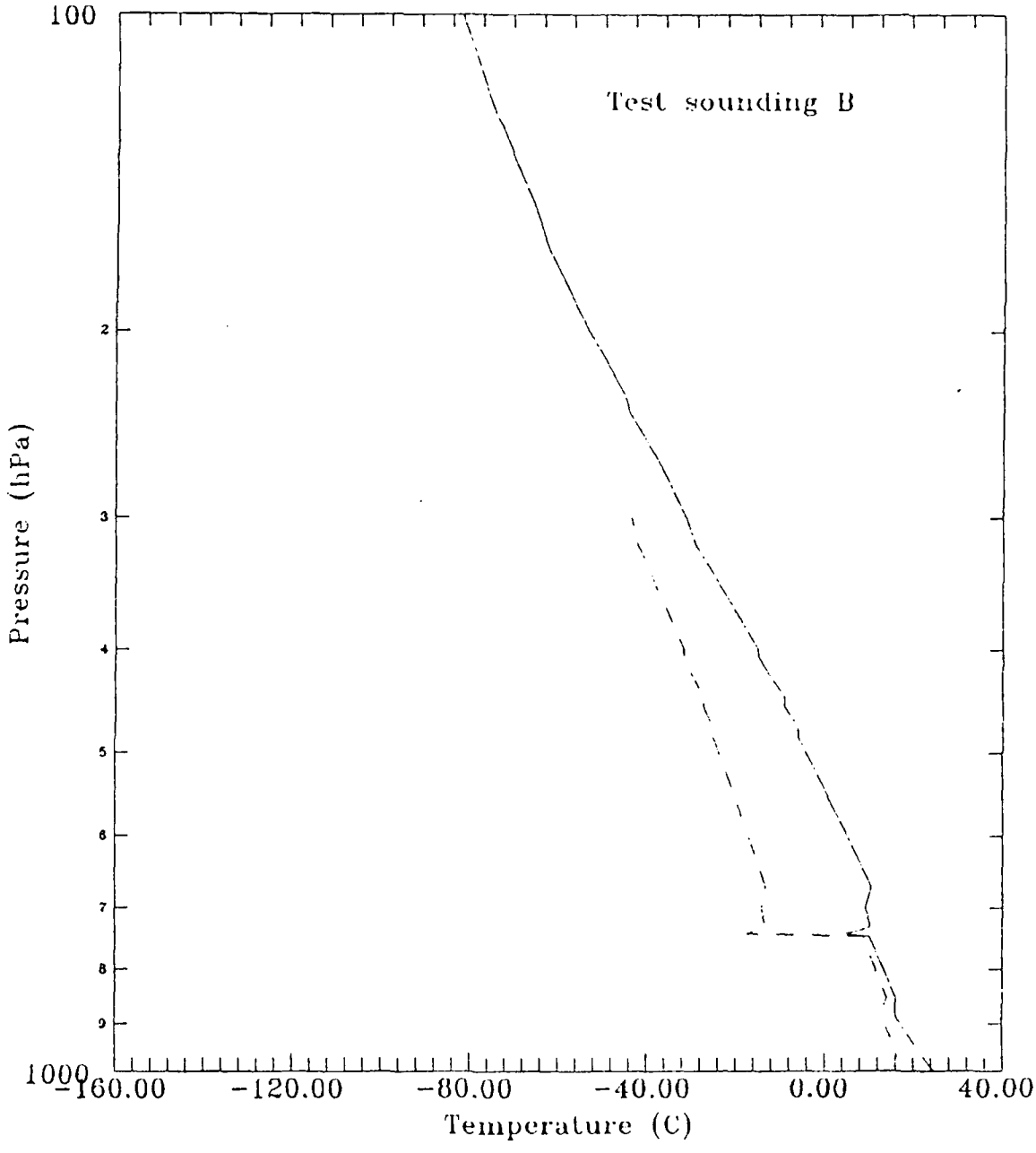

Figure 5.5b. As in Fig. 5.5a, except for test sounding B.

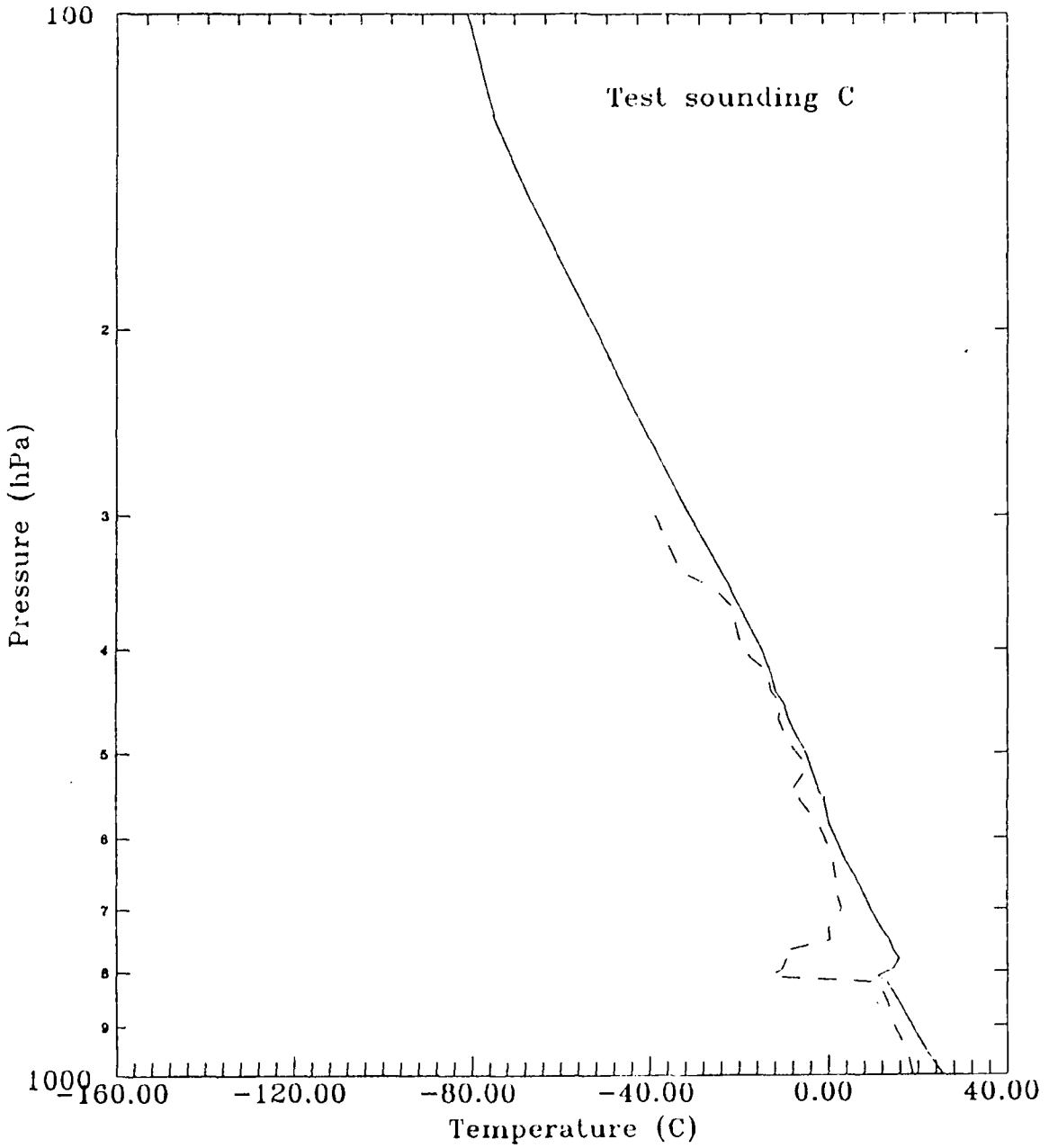

Figure 5.5c. As in Fig. 5.5a, except for test sounding C.

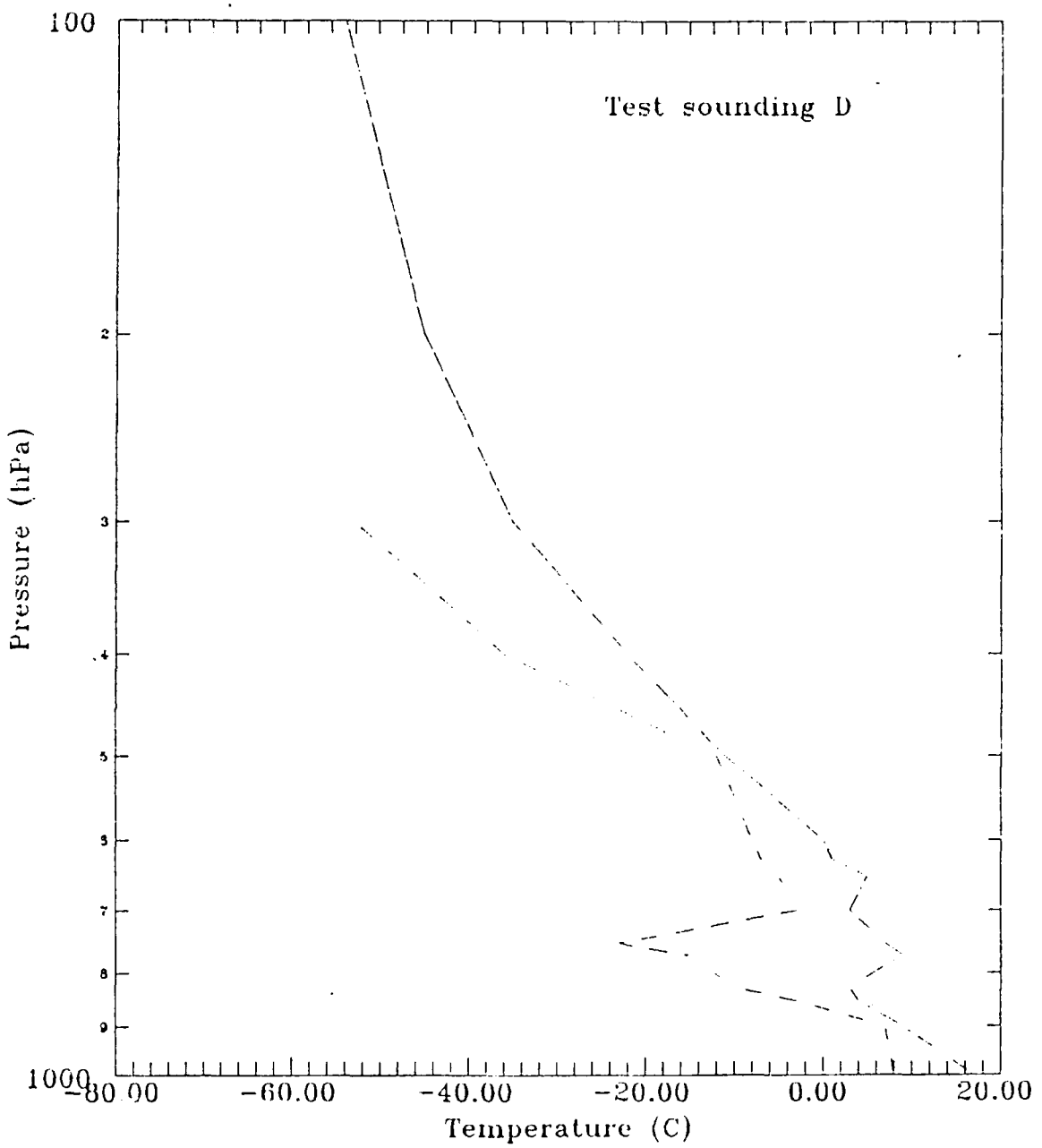

Figure 5.5d. As in Fig. 5.5a, except for test sounding D.

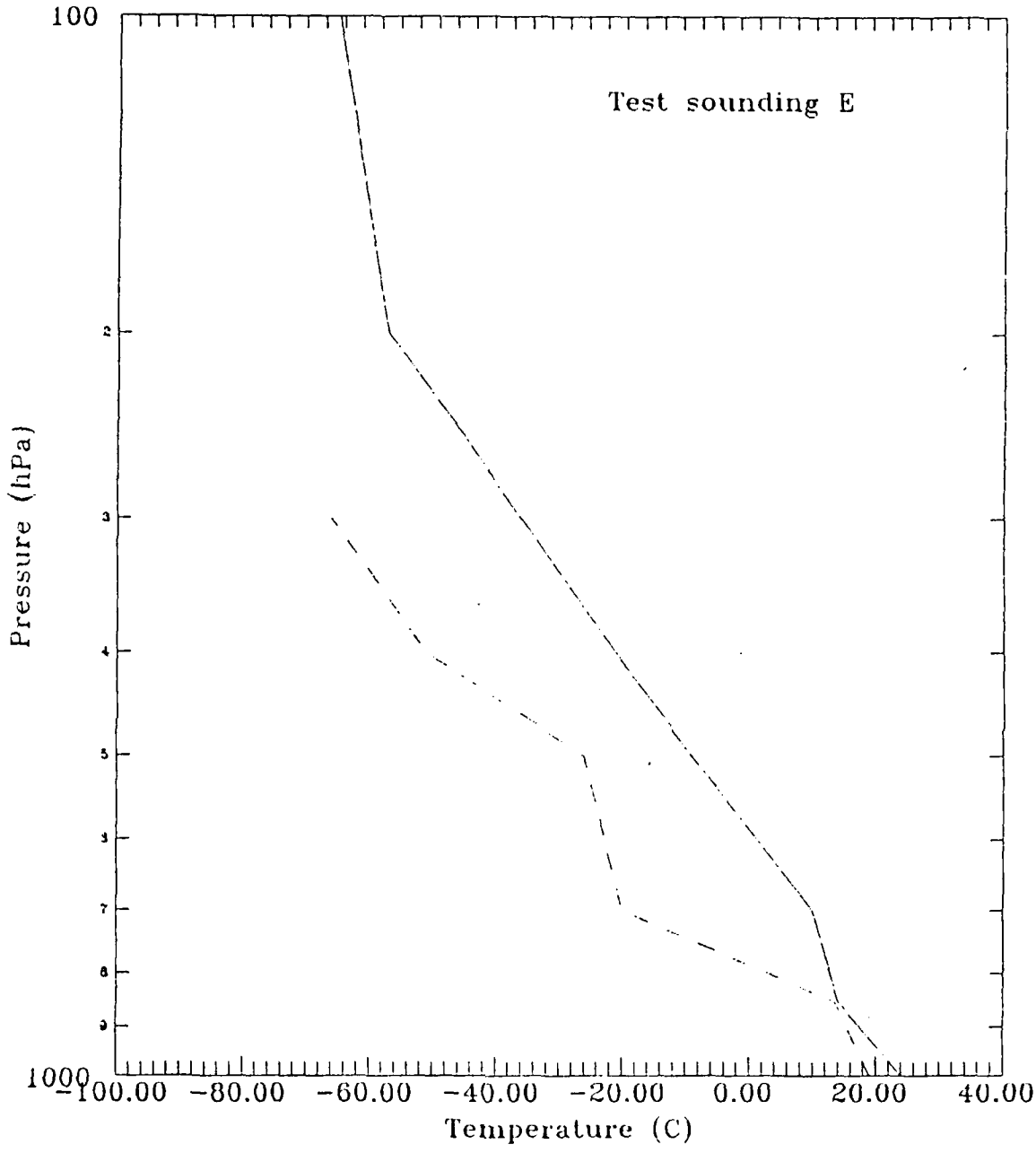

Figure 5.5e. As in Fig. 5.5a, except for test sounding E.

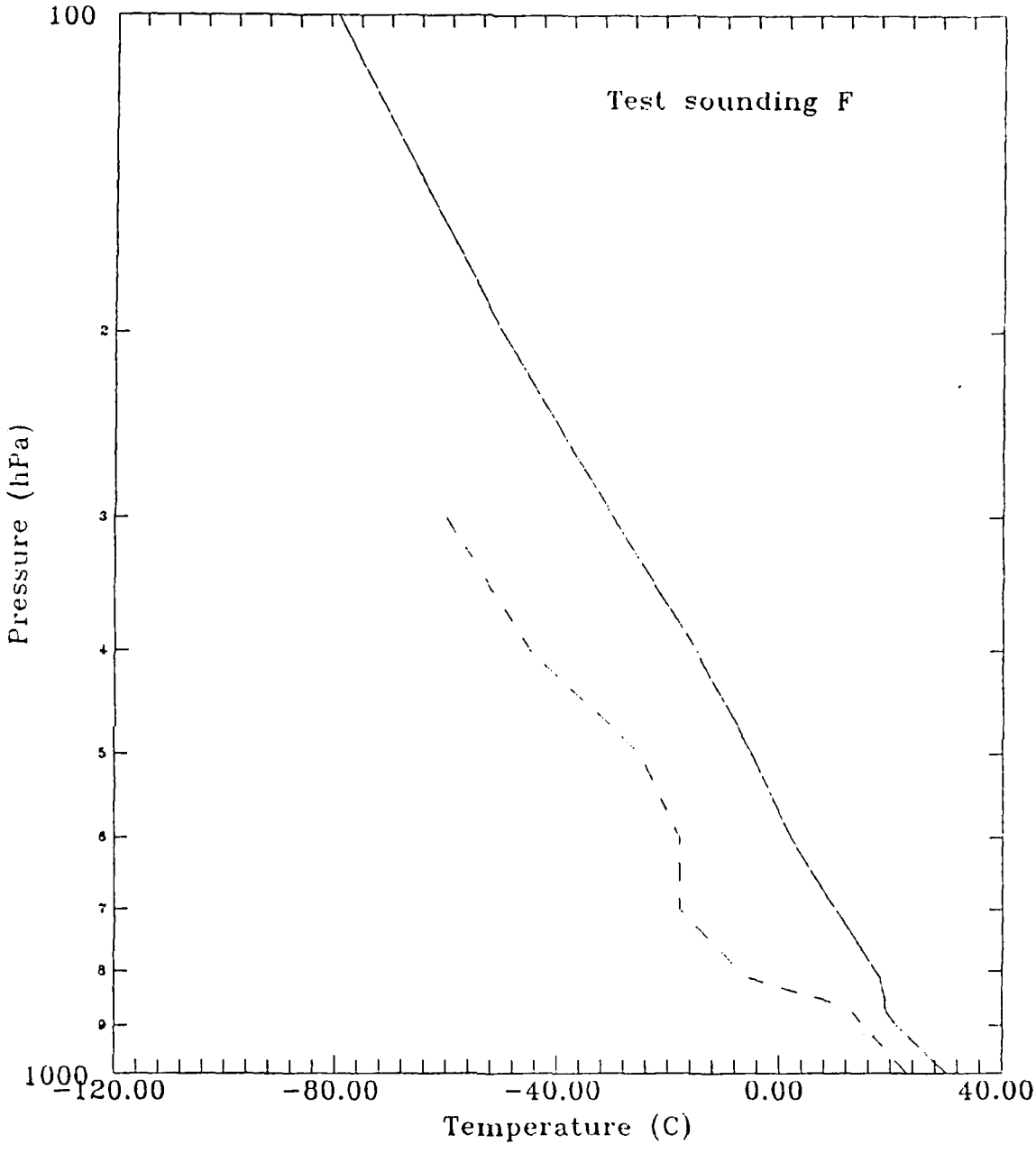

Figure 5.5f. As in Fig. 5.5a, except for test sounding F.

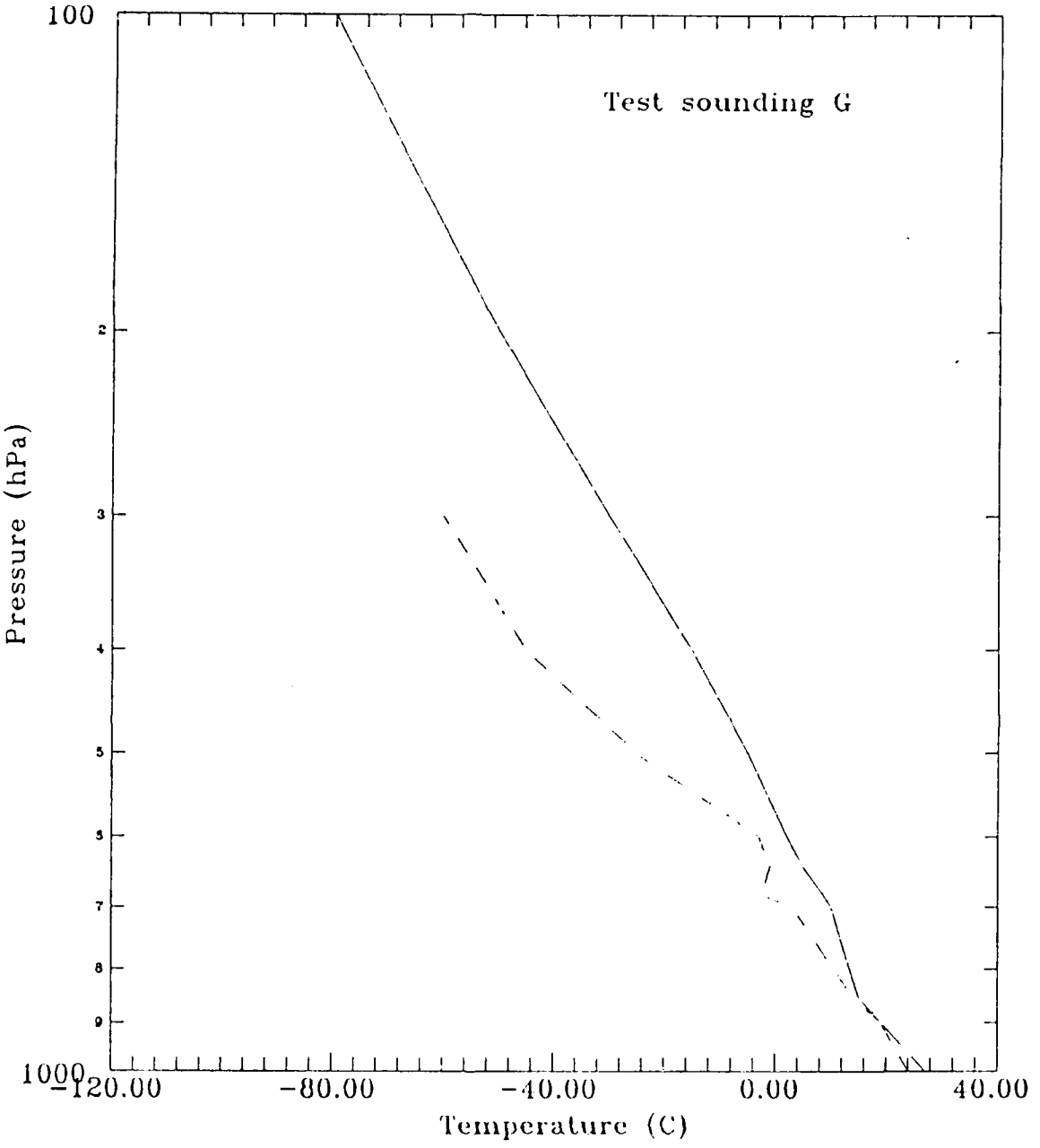

Figure 5.5g. As in Fig. 5.5a, except for test sounding G.

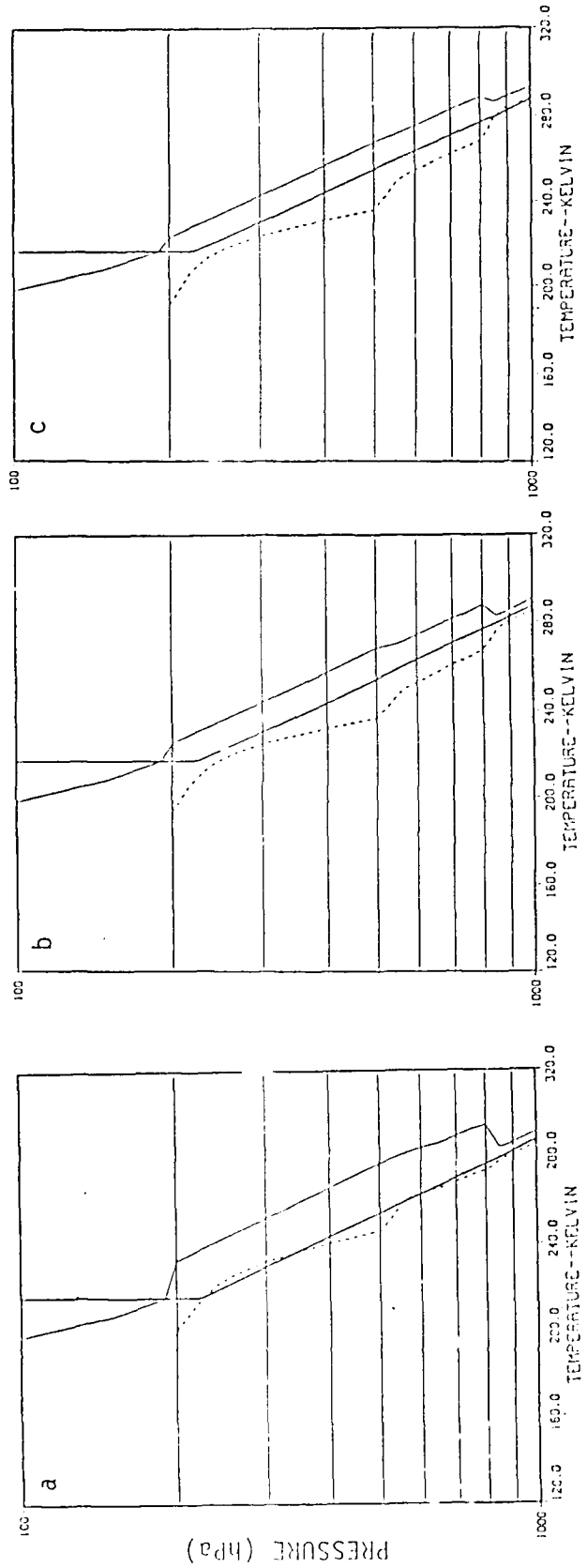

Figure 5.6. Example of trade wind inversion training data set. Each sounding depicts trade wind inversion with base at 850 hPa. Inversion strength is 10°C in 50 hPa in (a), 5°C in 50 hPa in (b), and 2°C in 50 hPa in (c).

3. Spatial coherence

After a synoptic feature, such as a trade wind or frontal inversion has been identified in a satellite sounding, the synoptic scale spatial coherence of that feature is examined. This analysis was accomplished using two cross sections taken across frontal boundaries. Cross section A (Fig. 5.7) ranges from 161°W, 39°N eastward to 125°W, 28°N and is represented by six soundings; cross section B (Fig. 5.8) ranges from 100°W, 45°N eastward to 84°W, 29°N and contains five soundings. In each section, the central synoptic feature is a frontal boundary which is marked by horizontal lines on the sounding. The soundings comprising the sections were evaluated by the RTM, and a set of brightness temperatures was produced.

E. Summary of data sets

Three different sets of training data were created for this research. They are referenced extensively in Chapter VI and are summarized here: (1) nine seed atmospheric soundings each containing a specific synoptic feature (except the US Standard Atmosphere) and associated soundings created by perturbation; (2) soundings containing the trade wind inversions of varying height and strength; and, (3) soundings containing the frontal inversions of varying height and strength.

Three verification data sets were created: (1) seven test atmospheric soundings containing realistic profiles; (2) vertical cross section A; and, (3) vertical cross section B.

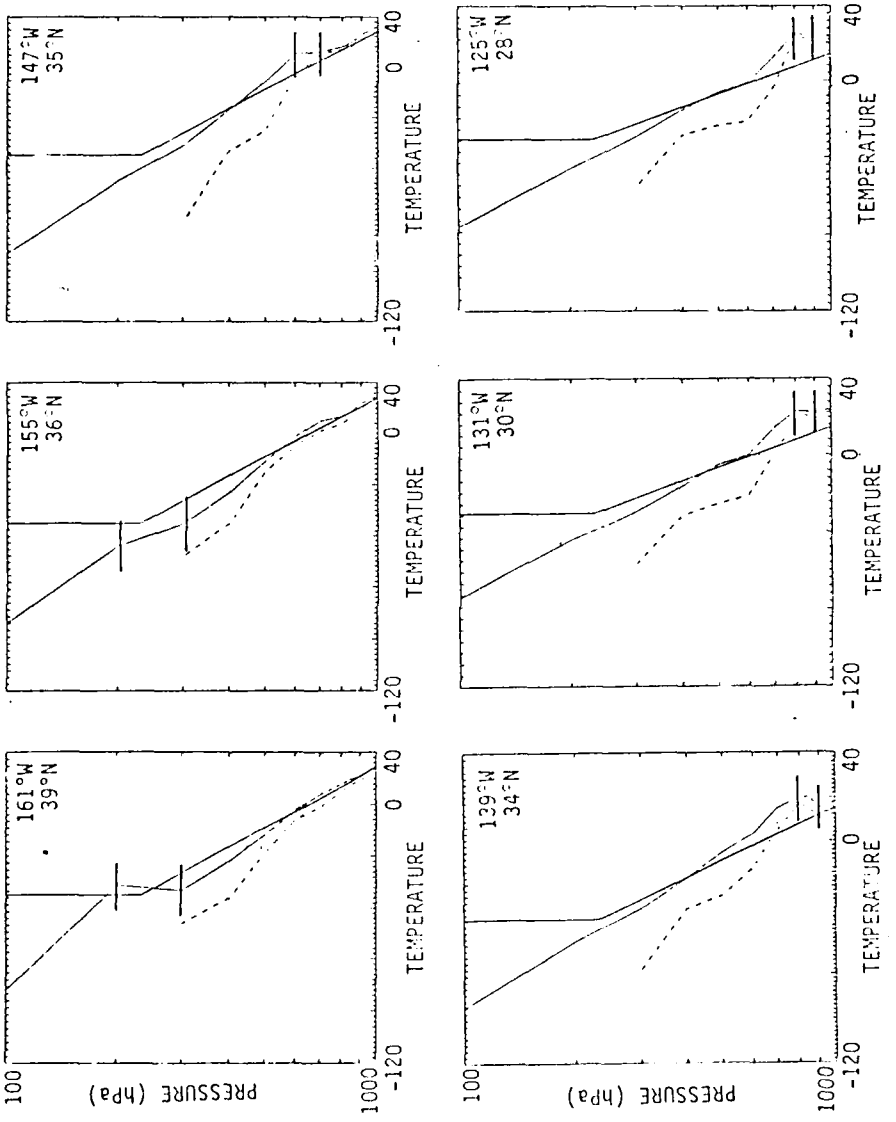

Figure 5.7. Soundings taken through vertical cross section A. Cross section is oriented west to east, 161°W, 39°N to 125°W, 28°N. See text for additional details.

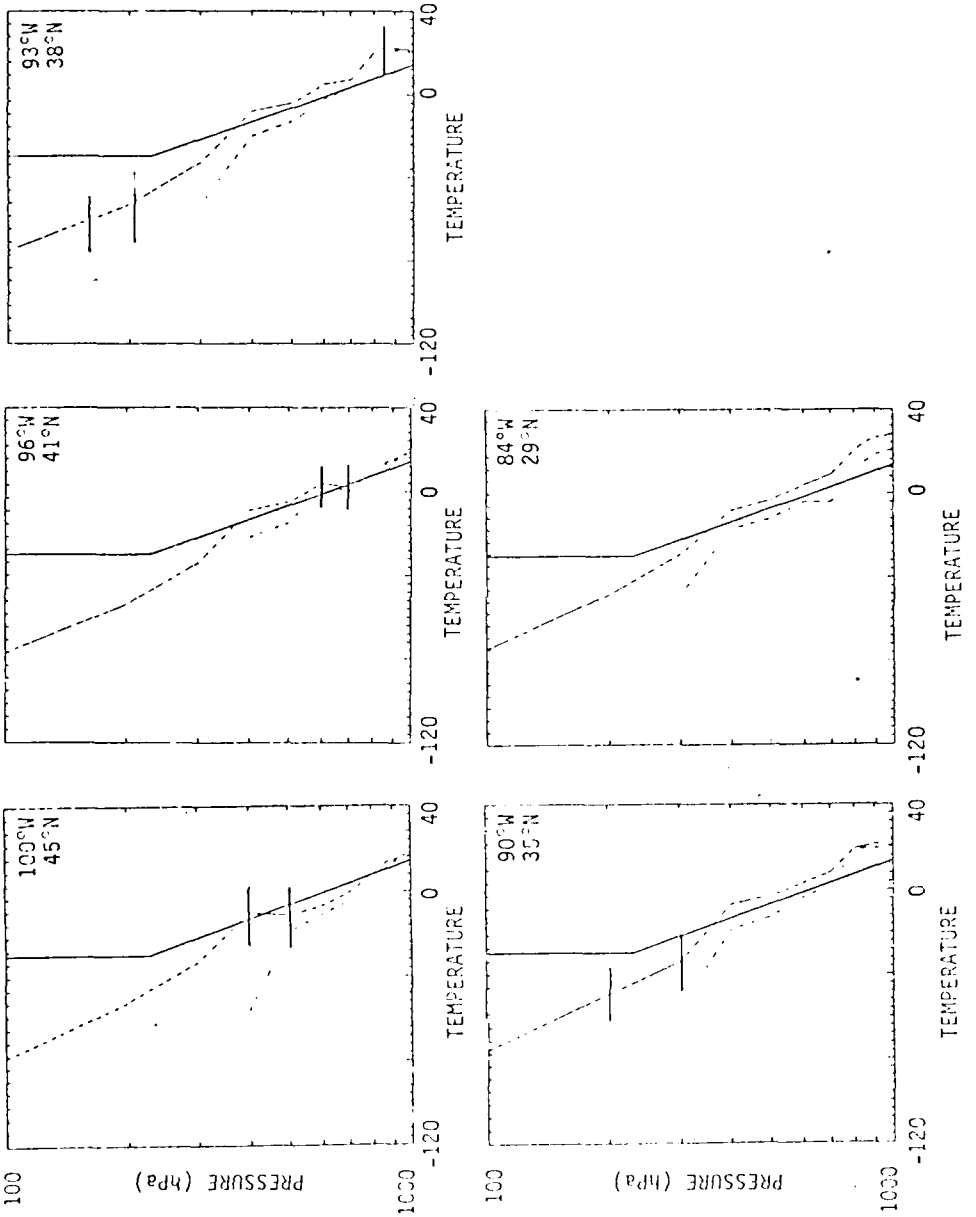

Figure 5.8. As in Fig. 5.7, except for vertical cross section B. Cross section is oriented west to east, 100°W, 45°N to 84°W, 29°N.

CHAPTER VI

ANALYSIS OF SYNOPTIC FEATURES IN SATELLITE CHANNEL BRIGHTNESS TEMPERATURE DATA

A statistical methodology is developed for identifying synoptic features and extracting quantitative synoptic information directly from satellite observations. The techniques evaluate individual satellite channel brightness temperatures. In a preparatory step, a set of synthetic satellite observations is created from a group of atmospheric soundings (see Chapter V). Three remaining steps are described in this chapter. First, the satellite observations are labelled both by *a priori* knowledge of the original atmospheric sounding and by cluster analysis. Second, the satellite soundings are classified into synoptic regimes using three methods: (1) multivariate graphics; (2) canonical discriminant analysis (CDA); (3), and discriminant analysis. Third, quantitative measurements are made of synoptic features within certain regimes.

The terms "groups," "clusters," "regimes" and "classes" are used interchangeably and refer to soundings originating from a given seed, or soundings possessing the same synoptic feature.

Satellite data were shown by Anderson (1986) to have interpretable and physically-based variance structure. Understanding the variance structure leads to methods permitting classification of satellite observations into synoptic regimes based on the variance structure of the observations. If regimes exist, the total variance of the observations can be partitioned into two physically different portions: *Between-class* variance explains the differences among groups of soundings which belong in different synoptic regimes; and, *within-*

class variance yields information about the fine structure of atmospheric soundings that are members of a single regime.

Classification of synoptic regimes and quantification of specific features among these regimes requires evaluation of three training data sets, containing: (1) 450 seed soundings; (2) trade wind inversions; and, (3) frontal inversions (see Chapter V). Classification employs between-class variance; quantification uses within-class variance. This knowledge is transferrable to new unknown soundings, to assign them to synoptic regimes and to infer the fine structure of synoptic features therein.

A. Labelling

The classification techniques require that each satellite brightness temperature matrix contain a numerical label column vector. All elements in the label vector are the same for a given satellite observation. Initially, the label vector is nothing more than a dummy variable which identifies the origin of a given satellite channel brightness temperature matrix. As such, each satellite observation may have a unique, sequential label, or, as an observation is determined to be a member of a specific synoptic regime, the observation may be assigned a label which identifies that regime. The label may be applied through knowledge of the original atmospheric sounding or assigned objectively through cluster analysis (Johnson and Wichern, 1982). Both methods are used.

A priori assignment is accomplished during creation of the seed sounding training data set. After each of nine atmospheric seed soundings was perturbed and evaluated by the radiative transfer model (RTM), a label corresponding to the seed sounding number is appended to the satellite sounding matrix of channel numbers and brightness temperatures. There are

450 brightness temperature observations representing nine synoptic regimes in the training data set; each matrix contained the appropriate label.

Clustering or grouping is another method to assign a numerical label vector to satellite soundings (Johnson and Wichern, 1982; Karson, 1982). In clustering, few assumptions are made about the number of groups or their structure; rather, the data determine the number of groups within bounds set by the analyst. This determination is based on similarities of the brightness temperature vectors as measured from the data structure of each vector. Clustering constructs classes in such a way that vectors within the same class are relatively homogeneous; vectors in different classes are relatively dissimilar. Since the number of possible arrangements is enormous, it is not practical to expect to find the best solution. Rather, clustering finds a solution in which no movement of an observation from one cluster to another will produce clusters in which the observations exhibit smaller least squared distances from the cluster center or a fewer number of clusters. Labels produced by cluster analysis reproduced, identically, the *a priori* labelling.

B. Classification methods

1. Graphical classification

a. Background

Subjective, graphical, multivariate classification techniques can be used to accomplish the same goal as objective, numerical methods. Graphical techniques require analyst training and intervention, but the methods provide supplemental information when analyzing data that: (1) are ambiguous or flawed; (2) are highly correlated; or, (3) contain trends.

Nearly all of the graphical schemes seek to represent n dimensions on a 2-dimensional surface. The strategies rely on pictorial results and often are preceded by simple calculations for normalization or similar preparation. In several schemes, the observations of a multivariate data set are used as coefficients of equations or as terms in mathematical functions. After preliminary calculations, the equations or functions are graphed; data classification is inferred by shapes or features found in the plotted results. These methods make it possible to follow subtle differences in a multivariate data set such as occur when the data represent changing conditions. This is especially revealing when only a few elements of the multivariate data change, and these elements cannot be predicted *a priori*.

Most multivariate graphical techniques are appropriate when the number of observations and dimensions is small; when the number is large, the resulting graphics become complex and difficult to decipher. A successful technique for relatively large multivariate data sets is a heuristic approach, Chernoff faces.

b. Chernoff faces

Chernoff faces, named after its creator (Chernoff, 1973a), is a subjective, multivariate, graphical technique which displays up to 17 variables[1] simultaneously in two dimensions. Normalized values of the variables govern the size, shape and placement of facial features on a caricature of a human face. One face is produced for each satellite observation, and synoptic regimes

---

[1] The number of variables displayed depends on the computer algorithm in use. Chernoff's original algorithm displays 20 variables; the algorithm used in this research displays 17 variables.

are classified subjectively by grouping similar facial expressions. Facial representation provides an insightful preliminary evaluation of multivariate data and is useful to view trends, to detect outliers or questionable data, and to discover subtle relationships among variables. It was designed by Chernoff to take advantage of the innate ability of the human observer to distinguish (and thus classify) subtle differences in facial features.

There are advantages and disadvantages to the use of Chernoff faces. The two primary drawbacks are: (1) faces are not suitable for quantitative analysis; and, (2) their success depends, in part, on the judicious assignment of variables to facial features (Chernoff, 1973a). Regarding (2), some researchers (Johnson and Wichern, 1982) insist on arbitrary, rather than planned, assignment, because blind variable assignment removes analytical bias. In the case of blind variable assignment, several assignments are attempted, and usually one case stands out as most valuable. Alternatively, planned assignment allows foreknowledge of correlated variables to be utilized fully. The main advantages to using Chernoff faces are: (1) faces can reveal complex relationships in large multivariate data sets and detect changes, trends and similarities in data; (2) faces are comprehensive, self-explanatory and remarkably quick to analyze; (3) the dimensionality of even simple faces is high and the ability to detect contrasts is excellent; and, (4) computational resources required to produce Chernoff faces are modest.

Table 6.1 lists the original program variables, and Fig. 6.1 shows the basic features used by Chernoff for creating a face (Wang, 1979). In this example, the face is capable of representing 20 variables. Not all variables are shown because not all were used.

Table 6.1. Program variables employed in constructing a face: example data.

Variable	Description	Symbol[a]
x_1	Distance from origin O to P	h*
x_2	Angle between OP and X-axis	θ
x_3	Half height of face	
x_4	Eccentricity of upper ellipse	
x_5	Eccentricity of lower ellipse	
x_6	Length of nose	
x_7	Position of center of mouth	Y_m
x_8	Curvature of mouth	
x_9	Length of mouth	a_m
x_{10}	Height of centers of eyes	Y_e
x_{11}	Separation of center of eyes	x_e
x_{12}	Slant of eyes	θ
x_{13}	Eccentricity of eyes	
x_{14}	Half-length of eyes	L_e
x_{15}	Position of pupils	
x_{16}	Height of eyebrow center relative to eye	Y_b
x_{17}	Angle of eyebrow	θ**
x_{18}	Length of eyebrow	L_b
x_{19}	Ear diameter	Y_e
x_{20}	Nose width	

[a] Symbols are not assigned to variables not used in the example.

c. *Example of Chernoff faces classification*

Because Chernoff faces likely are unfamiliar to the meteorologist, an example reported by Wang (1979) is presented for illustration.

Thirteen large metropolitan U.S. cities were studied. The aim was to group cities with similar economic situations. Each feature is a quantified element of a city's economic profile. In this example, two groups were classified with three ungrouped outliers (Fig. 6.2). Only seven variables were used, and the remainder of the facial features were fixed. Assignment of variables to

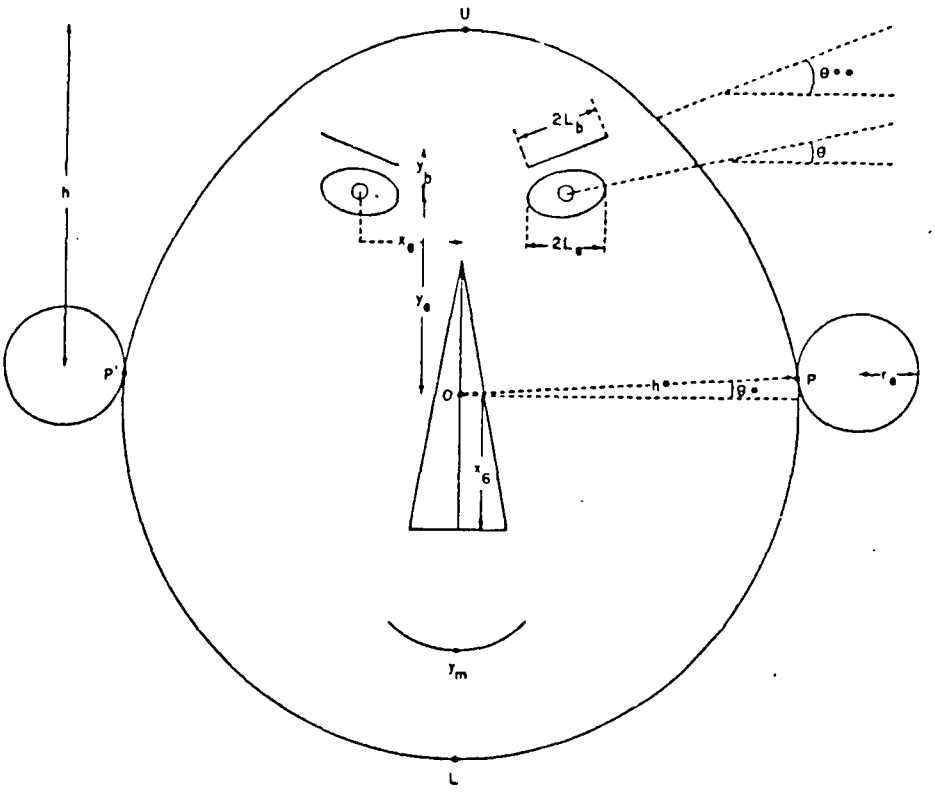

Figure 6.1. Chernoff faces. Basic features in facial construction. After Wang, 1978.

facial features was made arbitrarily. After practicing with a similar training set of faces, analysts arranged the faces subjectively. A verifying objective cluster analysis duplicated the results.

Three important observations are reinforced upon analysis of Fig. 6.2. First, classification by response to faces is subjective. For example, a slightly less discriminating analyst could incorporate group III into group II. Second, thoughtful assignment of variables to facial features provokes emotional reaction to faces and enhances classification accuracy; in contrast, careless variable assignment reduces accuracy. The eyes and mouth evoke the greatest response, and, as a result, Chernoff faces are most effective when important factors in the data are assigned to the eye and mouth variables. Third, conceivably, an analyst could contaminate results by unjustified *a priori* assumptions.

d. Classification of the regime training data set

The brightness temperatures of the regime training data set were classified by the Chernoff faces procedure (BMDP, 1988). The algorithm limits variable selection to 17; in addition to those channels not available from the radiative transfer model (RTM), channels 1, 2, 9, 21, and 24 were eliminated (in this and additional analyses), because they contain little structural variance that contributes to meaningful regime differences (See Chapter V). Facial feature assignments are listed in Table 6.2. Each group of facial features corresponds to a group of physically similar radiance channels; for example, the 15 μm tropospheric temperature indicators are represented by the eye variables. The assignment of TOVS channels to Chernoff facial features is not arbitrary. The number of variables which may be assigned to specific facial features is fixed

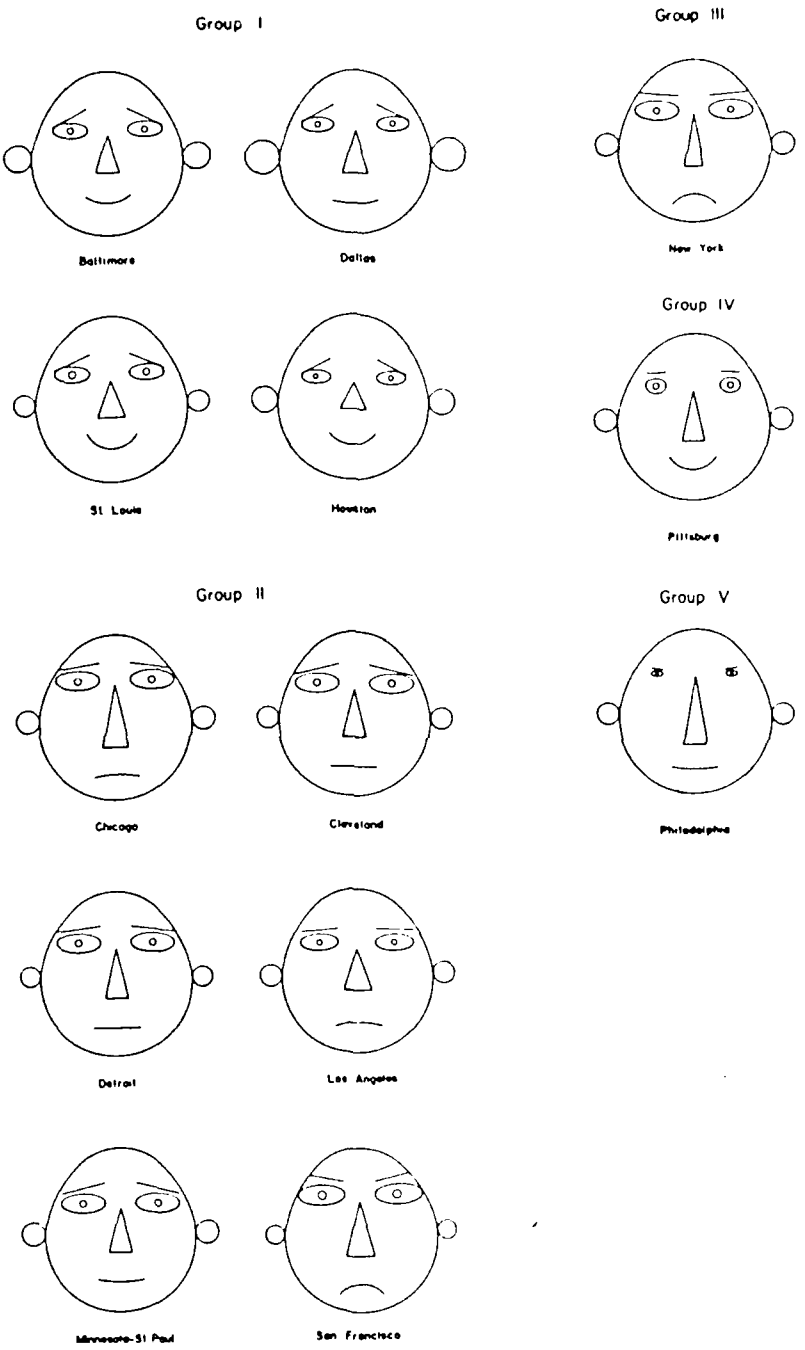

Figure 6.2. Chernoff faces which classify major metropolitan areas. After Wang, 1978.

by the BMDP algorithm. After eliminating irrelevant channels, those remaining group conveniently into the assignments shown. The 15 and 4.3 μm temperature sounding channels control the eye and mouth features respectively; this assignment emphasizes IR temperature response. The Chernoff faces depicting the nine training data regimes are shown in Fig. 6.3. Face numbers correspond to regime numbers.

Table 6.2. Program variables employed in constructing a face: regime training data.

Channel	Peak level (hPa)	Purpose of observation	Facial feature
3	100	Temperature (15 μm)	Eye vert width
4	400	Temperature (15 μm)	Eye hor width
5	600	Temperature (15 μm)	Iris size
6	800	Temperature (15 μm)	Eye spacing
7	900	Temperature (15 μm)	Eye height
22	700	Temperature (MSU)	Nose length
23	300	Temperature (MSU)	Nose width
10	900	Water vapor (8.3 μm)	Brow length
11	700	Water vapor (7.3 μm)	Brow width
12	500	Water vapor (6.7 μm)	Brow slant
8	Window	Surface temperature	Ear width
18	Window	Surface temperature	Ear length
19	Window	Surface temperature	Ear height
13	1000	Temperature (4.3 μm)	Middle mouth length
14	950	Temperature (4.3 μm)	Corner mouth length
15	700	Temperature (4.3 μm)	Mouth open amount
16	400	Temperature (4.3 μm)	Mouth smile

Examination of facial features reveals several important relationships among brightness temperatures resulting from satellite observation of synoptic regimes. The temperatures and dewpoint temperatures of the seed soundings

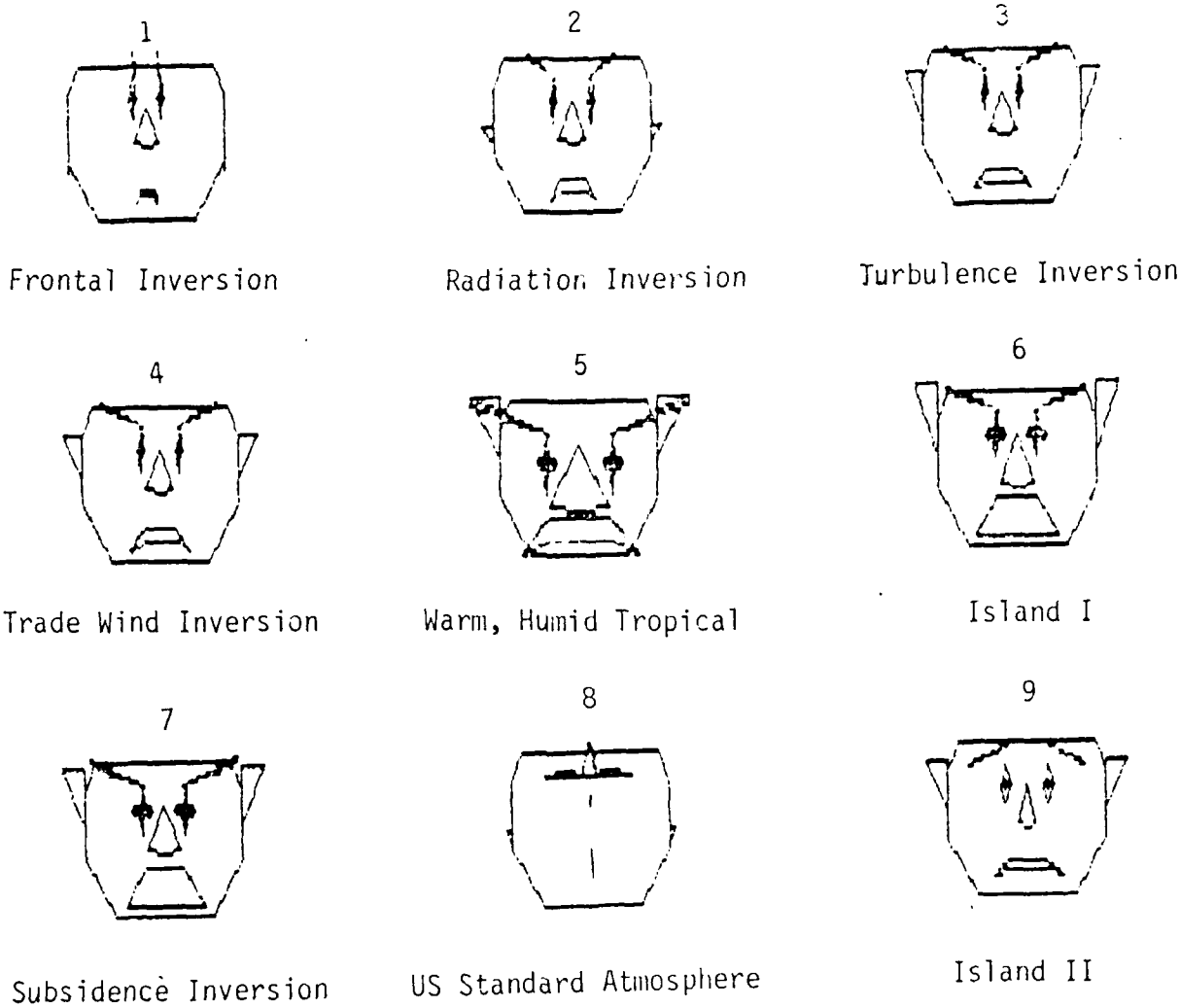

Figure 6.3. Chernoff faces representing nine seed soundings in training data.

are reflected in corresponding satellite observations and therefore in the facial expressions. Coarse and fine structure differences can be detected. Seed soundings that meteorologically are similar (or different) in basic structure are seen as faces with similar (or different) expressions. Coarse differences can be seen in the expressions on faces 5 and 8; the seed soundings from which these satellite observations were computed also are most different in temperature and moisture profiles. Fine differences among specific facial features suggest satellite channels which are responsible for discriminating among similar observations. The expressions on faces 2 and 3 are similar, but the ear characteristics are different. The ear variables are assigned to surface window channels, and the ears on faces 2 and 3 suggest that one fundamental difference in satellite observations of radiation and turbulence inversions is surface temperature. Further, the eyebrows on faces 2 and 3 are similar but of different length and slant. The eyebrows are assigned to water vapor channels and suggest another fundamental distinction. In a similar fashion, the satellite channels which explain the distinctions among synoptic regimes are revealed.

The eyes represent the 15 μm temperature channels. Eye vertical width corresponds to channel 3 (100 hPa temperature). The eye vertical width in face 8 is narrow; all others are nearly the same. The same (colder) climatological value was used for 100 hPa temperature in all soundings except 8, the standard atmosphere. Eye (not pupil) horizontal width represents channel 4 (400 hPa temperature). Faces 1-7 have nearly the same eye width; the rest have wider eyes; in face 8, the eye width is not measurable. The soundings are constructed with cold 400 hPa temperature profiles, except sounding 8 which is coldest of all. Iris size corresponds to channel 5 (600 hPa temperature). The

iris size in faces 1-4 and 9 is nearly equal; the irises in faces 5-7 and possibly 8 are larger. The 600 hPa temperature is nearly the same in soundings 1-4, much warmer in sounding 5, somewhat warmer in 6, 7 and 9, and colder in 8. Eye spacing represents channel 6 (800 hPa temperature). The eyes in face 5 are spaced wider than other faces. The 800 hPa temperature in sounding 5 is warmer than other soundings. In contrast, the 800 hPa temperature in sounding 8 is considerably cooler than the others, and no significant change in eye spacing is seen in face 8.

Analysis of other facial features offers insight into why the sounding groups classify as they do and which channels reveal the subtleties of classification. For example, the ears suggest that surface window channels differentiate between radiation and turbulence inversions.

There are two fundamental advantages to investigating satellite observations using Chernoff faces. First, satellite observations can be classified by grouping together faces with similar expressions. Second, simultaneous evaluation of 17 variables is difficult, and subtle brightness temperature changes from one satellite observation to another are hard to detect. Chernoff faces reveal relationships and trends among the variables and suggest which satellite channels reflect differences among satellite observations of atmospheric features. For example, soundings 5 and 8 represent extremes of temperature and dewpoint temperature throughout the troposphere. Faces 5 and 8 exhibit the greatest contrast in expression. In an analogous fashion, soundings 3, 4 and 5 represent similar synoptic conditions; faces 3, 4 and 5 reflect the similarities as they appear to come from the same "family."

Faces were drawn for all 450 observations in the training data set. The minor perturbations in brightness temperature vectors within regimes are

revealed in slight changes in facial expressions among the 50 faces in each regime. Fig. 6.4 shows faces representing satellite soundings of the first six perturbations of the trade wind inversion.

Like looking at relatives within the same human family, both the similarities and subtle differences among faces are clear. Faces drawn from one computational run to another have limited value. The BMDP algorithm treats each computational run as a separate exercise; faces from one computational series cannot be compared with those from another.

2. Canonical discriminant analysis

a. Background

Canonical discriminant analysis (CDA) is a data reduction and analysis technique related to factor analysis and principal component analysis (PCA) (SAS, 1982). In contrast with PCA, CDA seeks not to explain the total data variance but rather the between-class variance which defines the differences among classes of similar data. The ability to maximize between-class variance makes CDA a useful method to examine the construction of the regime training data set; the value of CDA for classification of unknown observations is limited.

CDA derives canonical variables which are linear combinations of the satellite channel brightness temperature vectors that summarize between-class variation in much the same way that principal components summarize total variation. Thus CDA accounts for within class means and serves to discriminate among groups by responding to between-class variance. Separation of synoptic regimes is attributed to structured and measurable variations in satellite channel brightness temperatures which correspond to

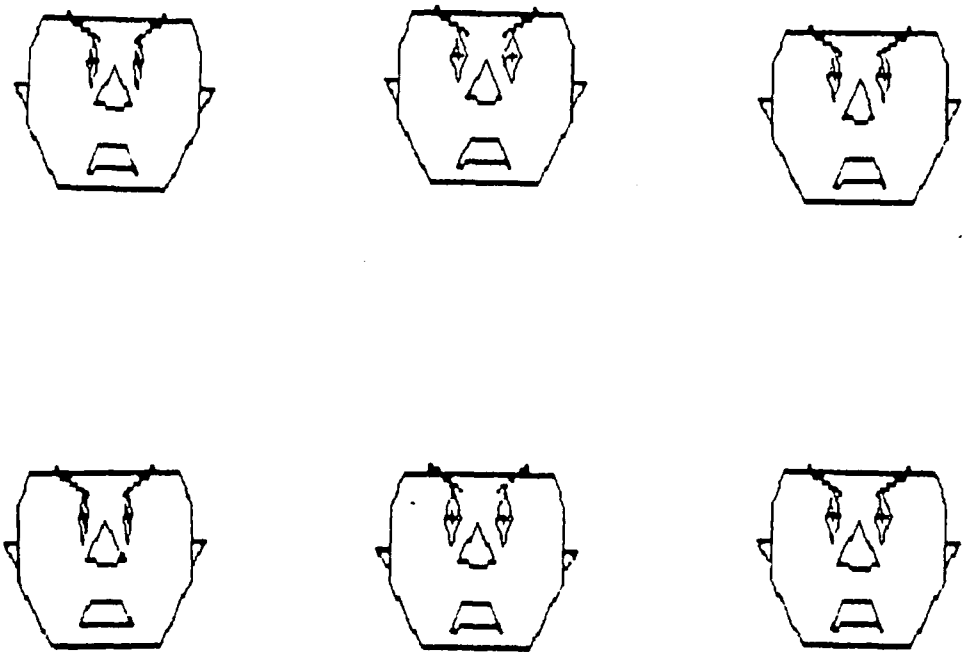

Figure 6.4. Chernoff faces representing six of 50 trade wind inversions in the training data set.

physical differences between the regimes.

The first three canonical variables and their amplitude distributions for the regime training data set are summarized in Table 6.3 and Figs. 6.5 and 6.6. Much of the between-class variance (about 58%) is contained in the first canonical variable, CAN1. This variate is dominated by satellite channels sensitive to tropospheric temperature. This result is not surprising since the structure of the upper troposphere of the seeds was nearly identical. The second canonical variate, CAN2, carries about 26% of the between-class variance and shows high correlations for channels sensitive to water vapor and to surface window channels. The third canonical variate, CAN3, accounts for just under 10% of the variance and is sensitive to temperature in the mid troposphere and temperature of the opposite sign at the surface. CAN2 and CAN3 together resemble a lapse rate signal with 2 being a moisture sensitive part and 3 being a moisture insensitive part. Rarely are more than two or three canonical variables required to explain most of the variance structure of a satellite observation data set. In contrast, in a random data set of 20 variables, each variable will explain on average 1/20 or 5% of the between-class variability.

The utility of multivariate analysis is measured in several ways. One of the simplest indicators is Wilks' lambda, the multivariate extension of R^2. It varies from one to zero and is interpreted just backwards from R^2; values near one imply low predictability, while values close to zero imply high predictability. (Wilks' lambda reduces to $1-R^2$ in the two group case.) The Wilks' lambda for the canonical structure described above is nearly zero, indicating strong confidence in regime separation.

Table 6.3. Canonical structure of the regime training data set.

CAN1 (58% of separation variance)	
Channel	Primary physical features responsible for separation
3-7	100-900 hPa temperature (15 μm)
8, 18-19	Surface window
10	900 hPa water vapor (temperature indicator?)
11-12	700-500 hPa water vapor (temperature indicator?)
13-16	700-1000 hPa temperature (4.3 μm)
22-24	700-90 hPa temperature (MSU)

CAN2 (26% of separation variance)	
Channel	Primary physical features responsible for separation
8, 18, 19	Surface window measurements
10	900 hPa water vapor (température indicator?)
11, 12	500-700 hPa water vapor
13, 14	Boundary layer temperature (4.3 μm)

CAN3 (10% of separation variance)	
Channel	Primary physical features responsible for separation
3-7	400-900 hPa temperature (15 μm)
8, 18, 19	Surface window measurements
10	900 hPa water vapor (temperature indicator?)
11	700 hPa water vapor
14-16	950-400 hPa temperature (4.3 μm)
22-24	700-90 hPa temperature (MSU)

Table 6.3 summarizes the channels that dominate each canonical variable. CAN1 (Fig. 6.5a) responds to most sensor channels and indicates that the greatest degree of separation in the regime training data arises from tropospheric average temperature differences. The most striking feature of Fig. 6.5a is that channels 3 and 24 have opposite signs than the remaining channels; this suggests a negative relationship between tropopause temperature and average tropospheric temperature. Accordingly, CAN1 appears to carry mainly an average temperature signal. If moisture remains constant but average temperature increases, radiance in channels 10-12 will increase, which indicates these channels respond primarily to average temperature in this canonical variable.

CAN2 (Fig. 6.5b) reveals the second most important physical reason for synoptic regime separation. The dominant elements of CAN2 are channels 8, 18, and 19, 10, 11 and 12, and 13 and 14. This combination of channels suggests that CAN2 responds to boundary layer temperature and tropospheric moisture. Channel 10 is described by Smith et al. (1979) as a 900 hPa water vapor sensor, although it usually is attributed to temperature because it saturates at low boundary layer moisture values. Its sign is the same as the temperature channels but is opposite to the other water vapor channels, 11 and 12, which suggests channels 11 and 12 carry the moisture signal and channel 10 senses temperature.

CAN3 (Fig. 6.5c) accounts for the remaining significant separation. The primary channels in CAN3 are 3-7, 14-16, 8 and 18-19, and 22-24. The signs of the surface-sensitive channels are opposite those channels sensitive to tropospheric temperature, indicating that this canonical variable reveals lapse rate. None of the three moisture channels contribute significantly to CAN3.

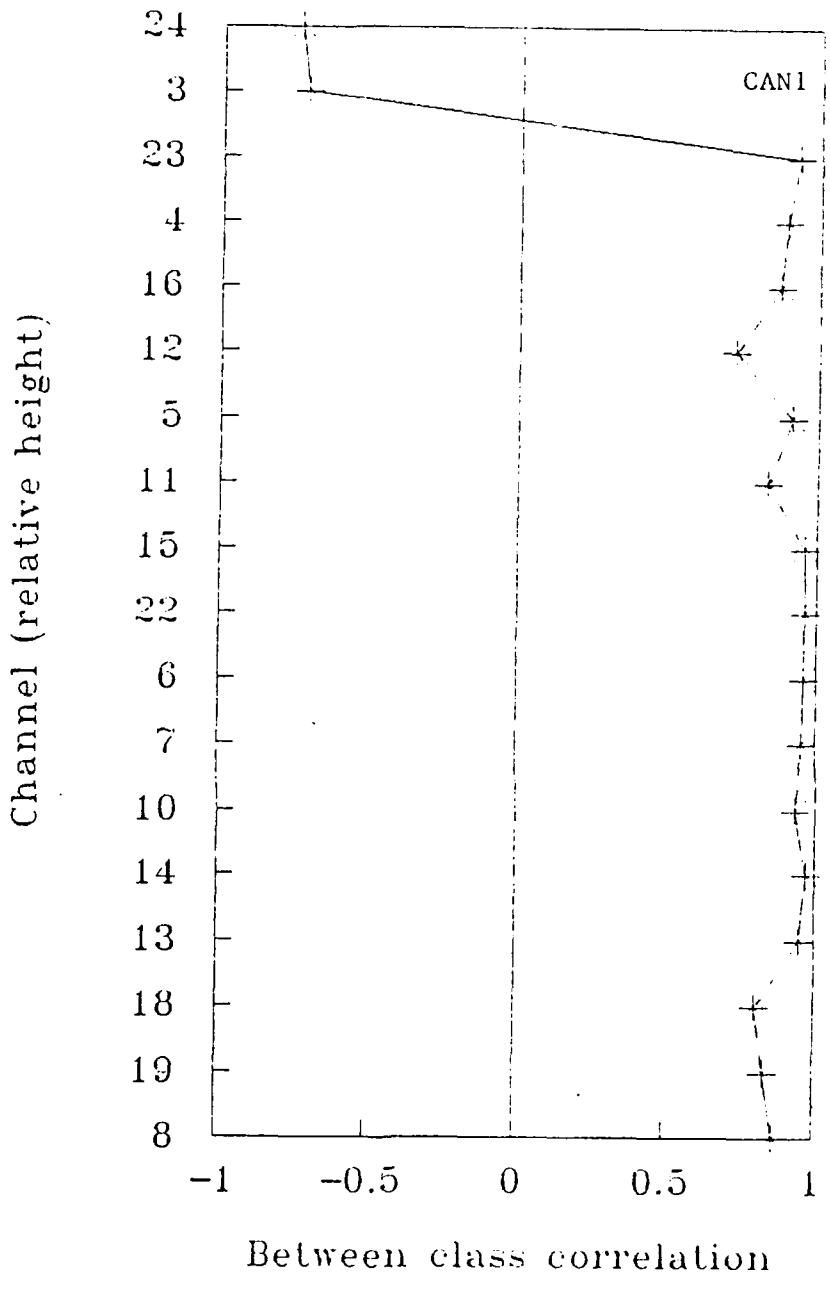

Figure 6.5a. First canonical variable, CAN1, describing between-class variance for training data based on nine seed soundings. CAN1 explains 58% of the between-class variance.

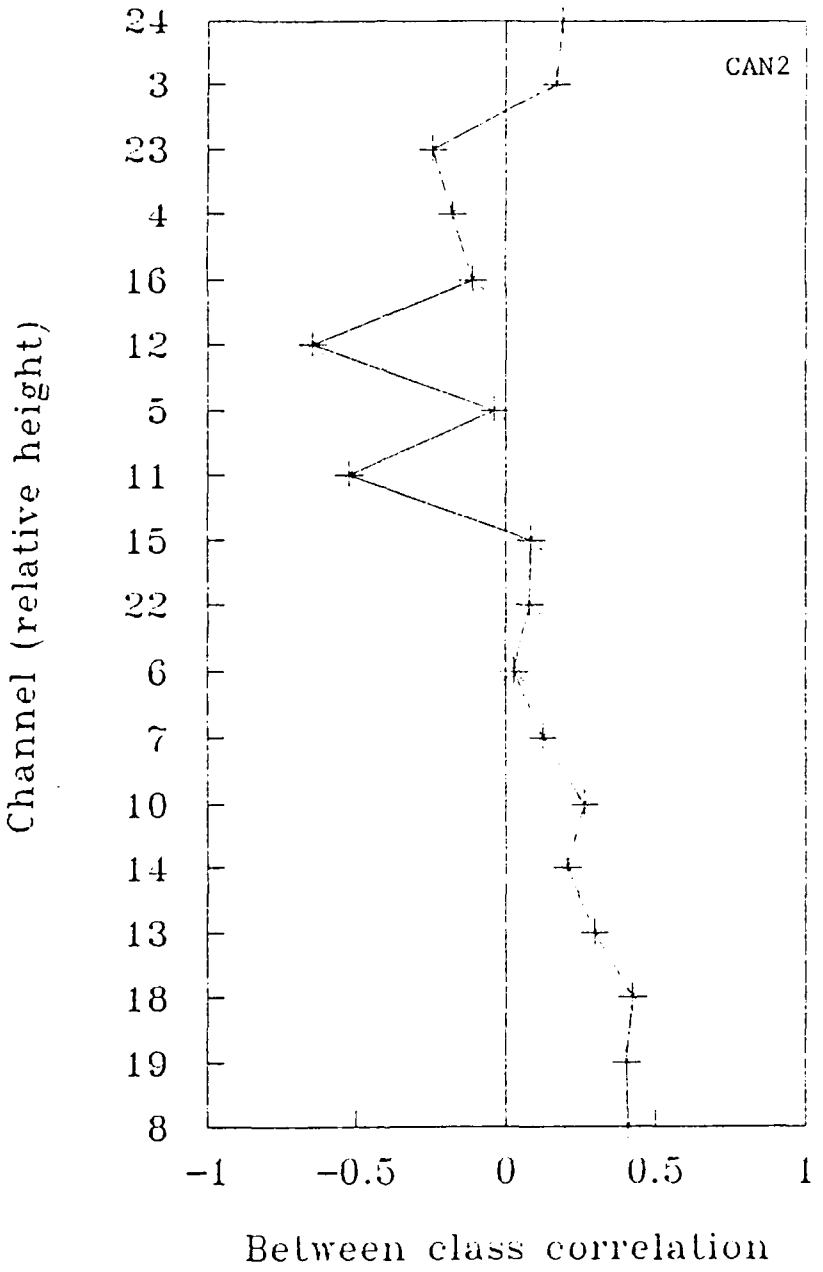

Figure 6.5b. As in Fig. 6.5a, except for CAN2. CAN2 explains 26% of between-class variance.

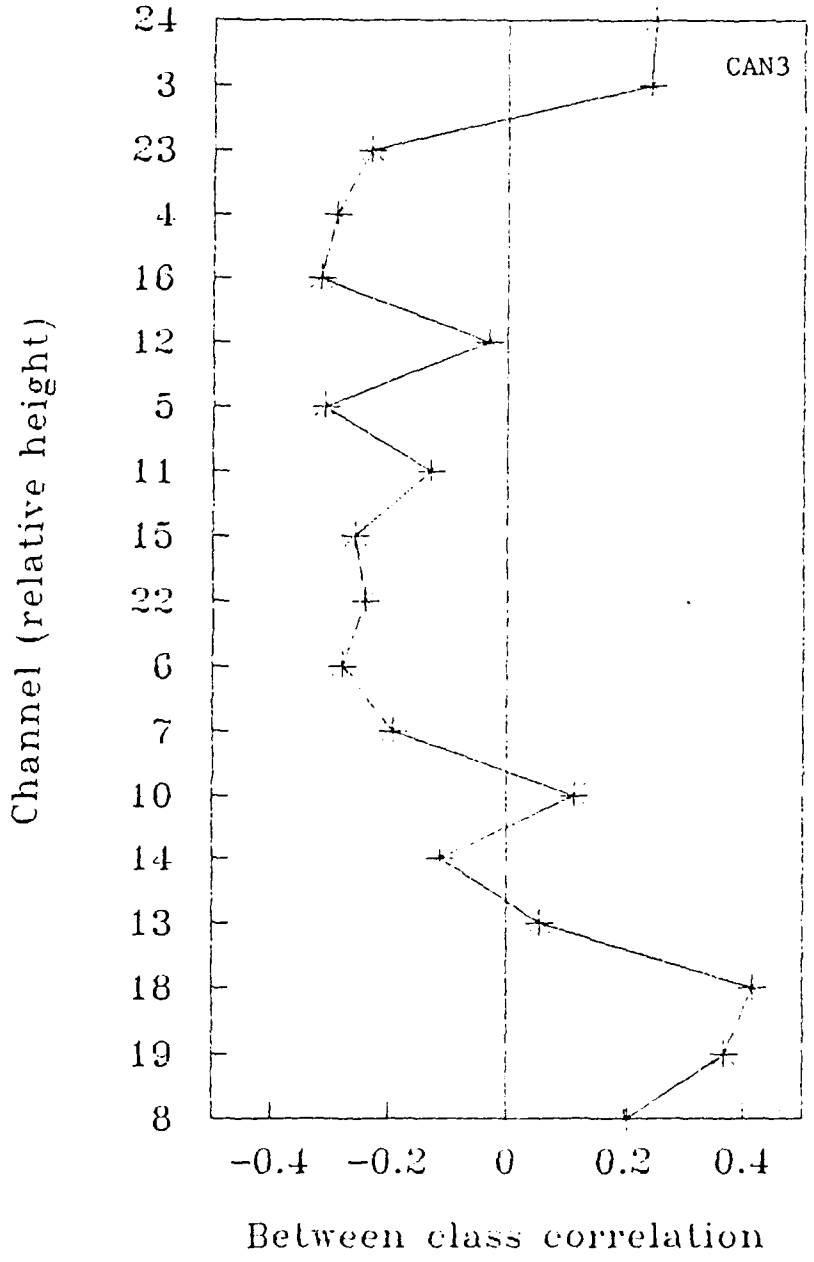

Figure 6.5c. As in Fig. 6.5a, except for CAN3. CAN3 explains 10% of the between-class variance.

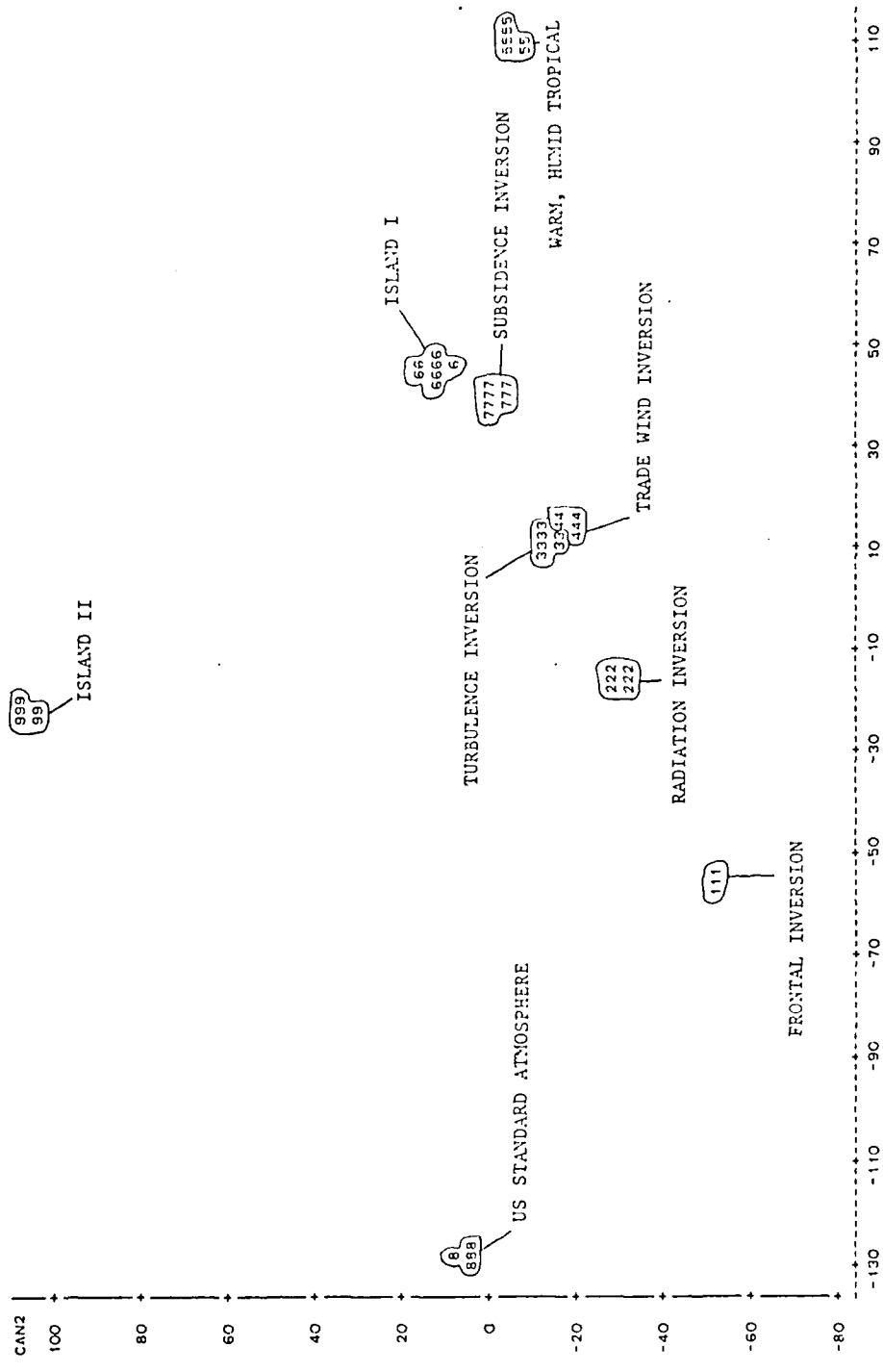

Figure 6.6a. Scatter plot of amplitudes of CAN2 vs. CAN1, illustrating synoptic regime separation of satellite observations. Regime labels were assigned through objective and *a priori* analysis methods. Data points within each label group represent 50 soundings. See text for additional details.

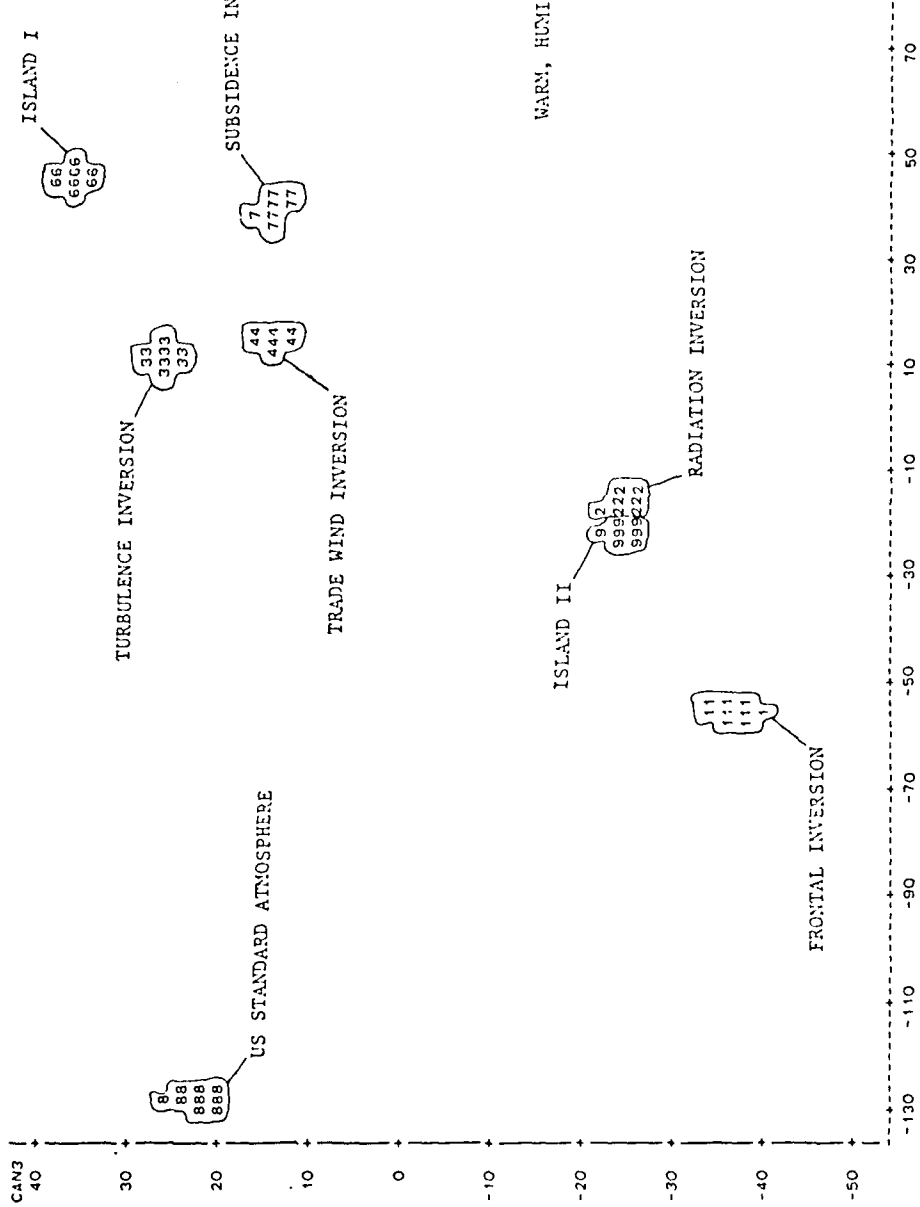

Figure 6.6b. As in Fig. 6.6a, except for CAN3 vs. CAN1.

The first three canonical variables are similar to the first three eigenfunctions of TIROS N observed radiances over the winter tropical Pacific (Anderson, 1986). The primary differences are that the moisture channels are not aliased into the tropospheric average temperature as they are in the training data and that the lapse rate function (CAN3) is not described uniquely as a single observed eigenvector but is spread across principal components 2, 3 and 4. The distribution of variances among the principal components and canonical variables is similar as well, although the moisture canonical variable carries significantly more signal than the moisture eigenvector. This correspondence gives indirect corroboration that the limited training data set simulates sounding variation typically observed over tropical oceans.

b. Classification

The relative separation of synoptic regimes can be seen as scatter diagrams of the canonical variables. For example, plots of CAN2 vs CAN1 (Fig. 6.6a) and CAN3 vs CAN1 (Fig. 6.6b) depict clusters of synoptic regimes and portray the between-group separation explained by canonical structure. These scatter diagrams are for vertically correlated seed sounding training data sets with $\pm 4\%$ perturbation. The synoptic conditions for each cluster, based on the seed, are noted in each figure; the labels assigned to the brightness temperature vectors correspond to numbers of the regime training data seed soundings and appear in the canonical variable plots. These labels were not used to cluster the data. Vectors arising from the same synoptic origin are grouped objectively according to variance structure, and they cluster together. Vectors arising from different synoptic origins cluster separately. The groups are based on physical properties extracted by CDA from the satellite radiance

soundings, and the number of displayed groups equals the number of distinct synoptic regimes.

The separation between groups is computed by CDA and measured by Mahalanobis distances, a multidimensional interval in *n*-space which provides center-to-center distances between groups. This distance is equivalent to a root mean square distance normalized by the individual channel variances. Groups that are close together have similar atmospheric origins and structures; the converse also is true. For example, the Mahalanobis distance is greatest between the dissimilar training data regimes labeled 5 (warm, humid tropical) and 8 (US Standard Atmosphere), and they appear the farthest apart in Fig. 6.6. The monsoon-like conditions of sounding 5 are warm, moist and nearly isothermal from the surface to 600 hPa. The US Standard Atmosphere (#8) is cooler and maintains a constant lapse rate from the surface to 250 hPa and a nearly constant dewpoint depression from 900 to 350 hPa. In short, these two atmospheric soundings are different in every physical respect; the same dissimilarity is reflected in their brightness temperature structure.

In contrast, training data regimes 3, 4 and 7 are similar: sounding 3 depicts a turbulence inversion; sounding 4 shows a trade wind inversion; and, sounding 7 represents a warm subsidence inversion. They appear adjacent in Fig. 6.6a and exhibit the three smallest Mahalanobis distances (Table 6.4). The Chernoff faces corresponding to regimes 3, 4 and 7 also are similar. Faces 3 and 4 differ only in corner mouth length (channel 14, 950 hPa temperature). Face 7 has higher ears (channel 19, surface window channel), broader nose and eye pupils (channel 23, 300 hPa MSU and channel 5, 600 hPa temperature, respectively) and larger mouth open amount (channel 15, 700 hPa temperature.) The eyebrows (water vapor channels) of faces 3, 4 and 7 are

similar which suggests the moisture profiles of the synoptic regimes they represent are similar, and, indeed, that is the case.

Chernoff faces and CDA are complementary tools of classification which reveal different aspects of data structure. Chernoff faces graphically depict channel differences, sensitivities and trends. They give direction to further exploration of the data by other methods. CDA objectively explains structural differences in the satellite observations and gives physical definition to the separation structure.

Since the first canonical variable, CAN1, carries most of the variance, it differentiates regimes most effectively. The regime training data can be differentiated into six unique classes knowing just CAN1 alone. Regimes 2 and 9, 3 and 4, and 6 and 7 blend together and may not be distinguished unambiguously by CAN1. CAN2 differentiates only 1 and 9, with 2 through 8 spreading almost continuously through mid-range amplitudes. Although some characterizations can be made within the CAN2 region (soundings 2 and 6 can be well differentiated, for example), classification on the basis of CAN2 alone would be of limited value.

Combining CAN1 and CAN2 leads to the nearly unambiguous delineation of seven of the nine sounding groups. Only the two lowest level inversions (subsidence and turbulence) fail to separate acceptably. Additionally, for slightly larger error tolerances, 6 and 7 (an island and warm subsidence inversion soundings), might not be classified uniquely. Even though CAN2 is not essential for differentiating most classes, it does increase separation so that accuracy may be increased when attempts are made to classify new soundings. CAN3, though accounting for less variance, is still of some use; 3 and 4 can be distinguished as unique and the separation between 6 and 7 is enhanced

Table 6.4. Mahalanobis distances for training data set.

SOUND	1	2	3	4	5
1	.	51.4416	100.9389	94.7514	181.0252
2	51.4416	.	62.9922	51.9183	135.6455
3	100.9389	62.9922	.	19.5773	123.5338
4	94.7514	51.9183	19.5773	.	112.2319
5	181.0252	135.6455	123.5338	112.2319	.
6	139.9755	98.8196	48.3318	53.4637	102.6830
7	120.7788	74.0603	37.2494	31.6367	88.3401
8	120.9601	132.2770	148.4492	150.3870	243.1051
9	163.9059	139.1299	134.9330	137.6068	179.7653

SOUND	6	7	8	9
1	139.9755	120.7788	120.9601	163.9059
2	98.8196	74.0603	132.2770	139.1299
3	48.3318	37.2494	148.4492	134.9330
4	53.4637	31.6367	150.3870	137.6068
5	102.6830	88.3401	243.1051	179.7653
6	.	34.3421	180.0023	132.7455
7	34.3421	.	172.2328	132.2409
8	180.0023	172.2328	.	161.6830
9	132.7455	132.2409	161.6830	.

significantly.

It is possible, however, to create a training data set of satellite observations that no technique will resolve. Recall that the original seed soundings were increased in number by replicating the original sounding and adding a small, vertically correlated perturbation (distributed as white noise) to the temperature and dewpoint temperature value at each level. The degree of perturbation of the original seed soundings was chosen to mimic random variation found in nature, but the perturbation range directly determines how well the satellite observations separate in later analysis. A perturbation range of $\pm 4\%$ was chosen as a typical natural range; it is shown as an envelope in Fig. 5.4. If the perturbation envelopes become sufficiently broad, the original sounding classes can be made to overlap and lose their identity, and the resulting satellite observations appear to result from the same atmospheric feature. To determine how broad the perturbation envelope can become before resolution is lost in satellite observations, the perturbation range of the original soundings was extended from $\pm 4\%$ to $\pm 8\%$ and finally $\pm 12\%$, at which point CDA fails to resolve any but the most widely different regimes.

When the perturbation range reached $\pm 12\%$, the overlap of physical features in the atmospheric soundings produced some classes of satellite observations in which the between-class variance cannot be resolved clearly. For example, seed soundings 3, 4, 5 and 7 smear together as shown in Fig. 6.7 in which three inversions and a warm-moist monsoon-like sounding start resembling each other. The $\pm 12\%$ perturbation range permits seed soundings that initially were similar physically to wander within such a broad range that the regime cross-over is not surprising. In this case, the resolution achieved by using all three canonical variables aids in regime distinction.

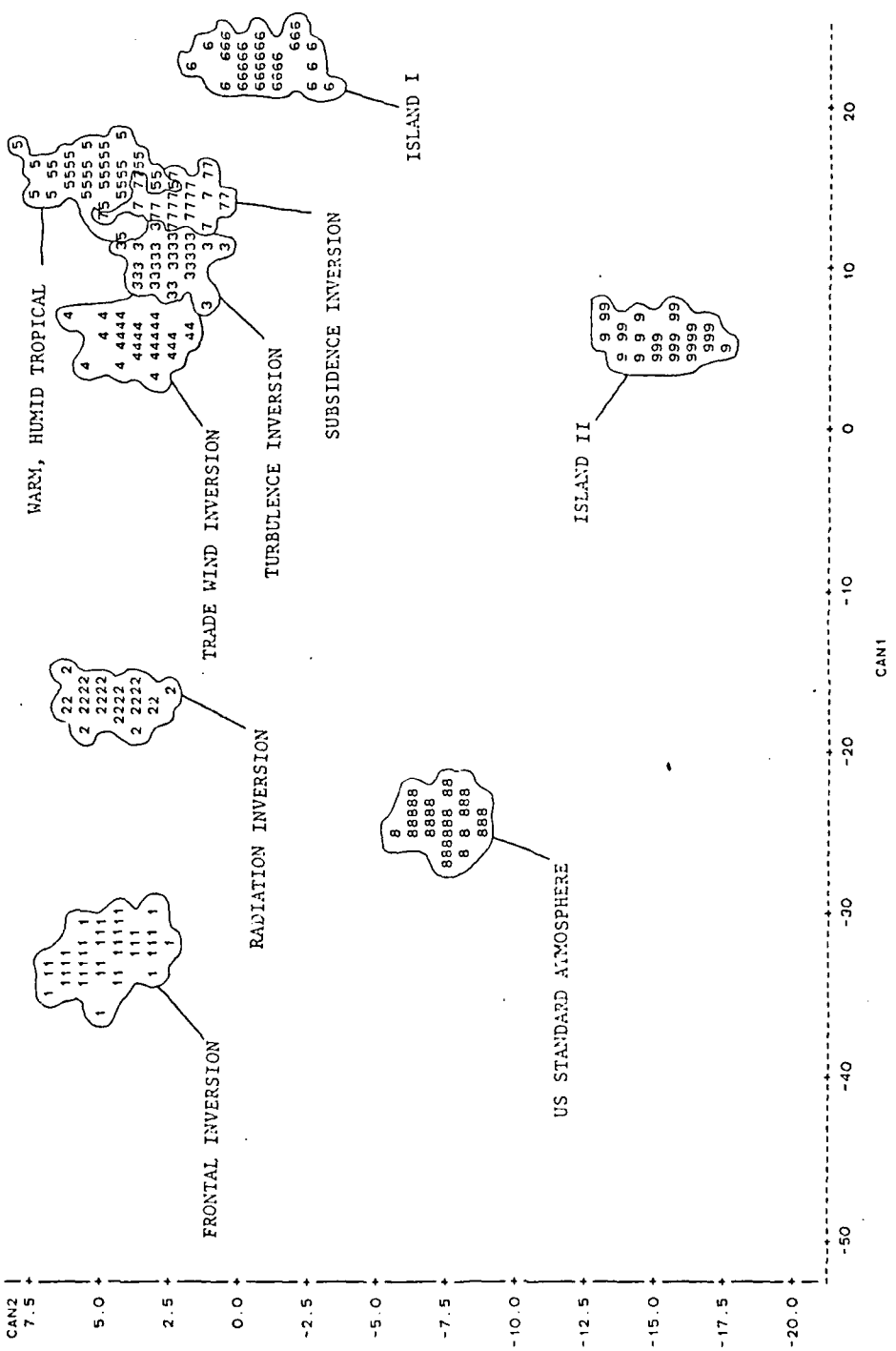

Figure 6.7a. As in Fig. 6.6a, except that perturbations to seed soundings lie within an envelope of ±12%. Sounding groups 3, 4, 5 and 7 are beginning to lose differentiation.

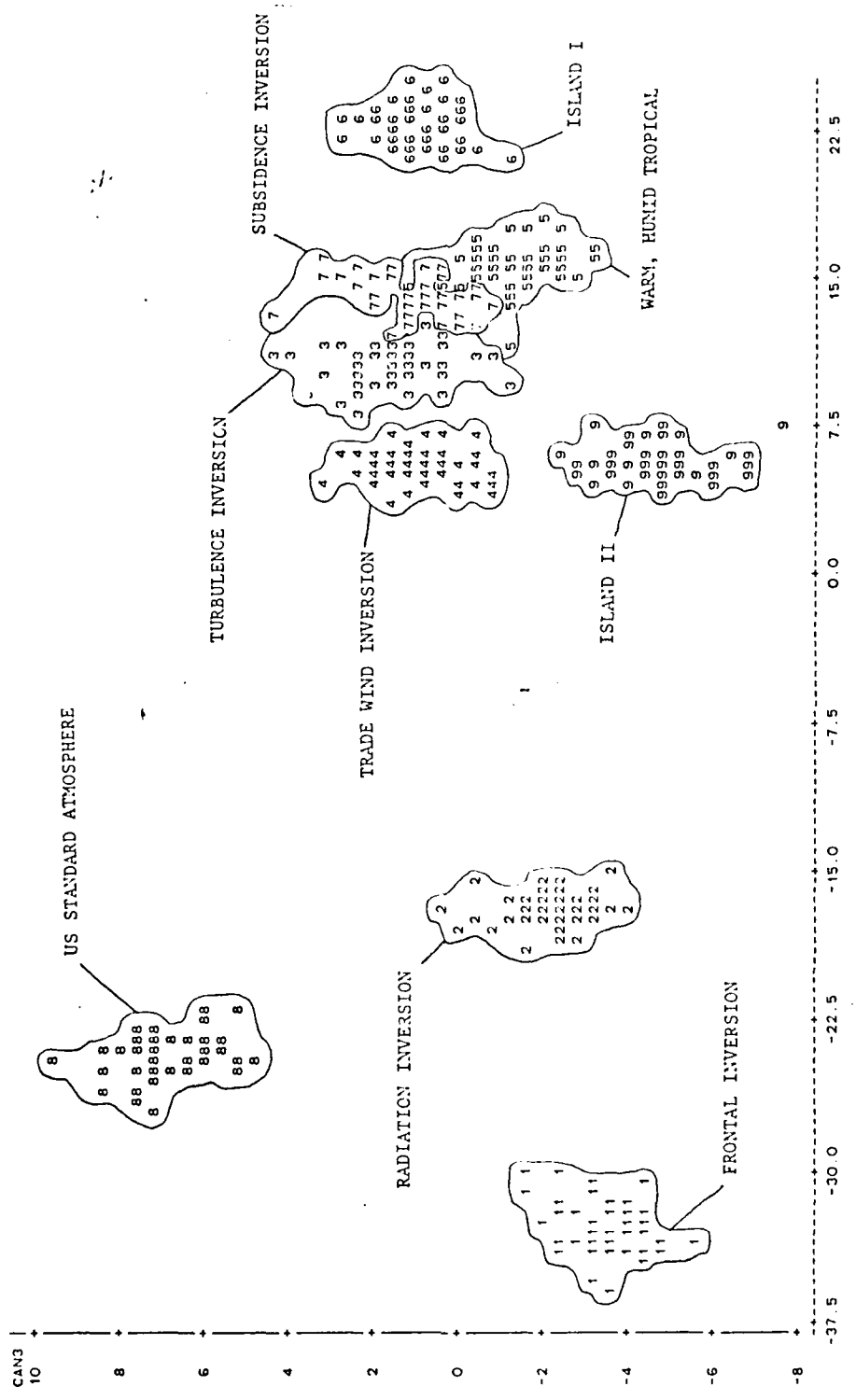

Figure 6.7b. As in Fig. 6.7a, except for CAN3 vs. CAN1.

The principal advantage to CDA is that it offers a simple, quantitative, but computationally intensive, objective method for verifying data classification. The shortcoming of the CDA algorithm is that, in its current form, quantitative prediction relationships between the regime training data set and unknown data to be classified cannot be constructed[2]. That task is left to discriminant analysis.

3. Discriminant analysis

a. Background

The third classification method is the discriminant technique, a procedure which resembles multiple regression analysis but treats data as having discrete rather than continuous distributions. It is statistical, objective and predictive; after evaluation of regime training data, the resulting linear discriminant function coefficients may be used to predict regime classification of unknown data. Discriminant analysis resembles multiple regression analysis with an important difference: In multiple regression analysis, the dependent variable is assumed to be continuous; in discriminant analysis, the dependent variable is assumed to be discrete. The independent variables are treated the same in both methods.

Discriminant analysis partitions satellite brightness temperature data according to their variance structure and assigns satellite soundings to membership in synoptic regimes (classes). The assumption of a discrete dependent variable is not a disadvantage when dealing with meteorological

---

[2] W. B. Smith, Department of Statistics, Texas A&M University; personal communication.

data. While the distribution of most atmospheric variables is continuous, meteorologists have, for convenience, created classes of many atmospheric phenomena such as climate zones, precipitation and wind measurements (for example, Griffiths and Driscoll, 1982). Additionally, these data often are reported in statistical-interval measure, for example, number of occurrences of wind speed between two discrete values. Partitioning synoptic regimes in tropical oceanic regions is a logical extension of existing analytical techniques; bogus soundings already are assigned for numerical weather prediction reporting and archival methods based on discrete cloud configurations (Haltiner and Williams, 1980).

The training data set of nine regimes and 450 satellite soundings was evaluated by discriminant analysis. During initial assignment, it was assumed that a sounding had a prior probability (equal chance) of being assigned to any of the regimes; the prior probability was set to 1/9 for each regime. All 450 soundings were classified correctly into their original regime assignments; no initial mis-classifications were identified.

C. Test sounding data classification

The classification methods described are shown to separate and classify unambiguously the 450 satellite observations in the training data set. To be useful operationally, the procedures should extend to classification of unknown satellite soundings having synoptic origins similar to observations in the training data.

Seven test satellite soundings (labeled A-G, see Chapter V) were evaluated by the three classification methods. The test soundings are representations of actual soundings; some contain complex and multiple synoptic features. They

first were analyzed by hand and were classified according to primary and, in some cases, secondary synoptic features present in the atmospheric sounding from which the satellite sounding originated. The hand analysis provides a baseline for comparison with the results of analysis by Chernoff faces, CDA and discriminant analysis.

1. Facial representation

A series of Chernoff faces was computed from observations in the regime training data (Fig. 6.3). The series was repeated after inclusion of the test soundings (Fig. 6.8). The results of subjective classification are summarized in Table 6.5. The best classification is given first, followed by possible classifications in parentheses.

Table 6.5. Summary of test sounding classifications.

	Predicted classification			
Test sounding	CDA	Discriminant	Faces	Hand analysis
A	9 (3, 4)	9	7 (6, 9)	7 (4)
B	9 (3, 4)	9	7 (6, 9)	4 (7)
C	9	9	7 (6, 9)	7 (4)
D	8	8	8 (1)	4 (7)
E	3 (4, 6, 7)	3	3 (4, 7)	4 (7)
F	6 (3, 4, 7)	3	5 (6, 7)	7 (4)
G	3 (4, 6, 7)	6	7 (6)	6 (3)

Test Sounding A

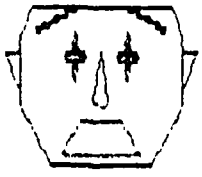

Test Sounding B

Test Sounding C

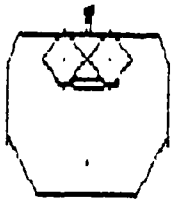

Test Sounding D

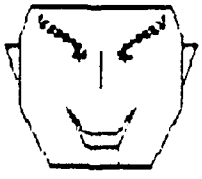

Test Sounding E

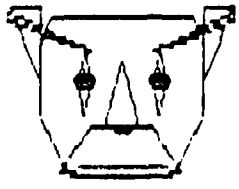

Test Sounding F

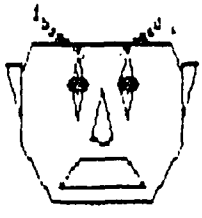

Test Sounding G

Figure 6.8. As in Fig. 6.1, except for test soundings.

2. CDA

The test sounding data were classified according to rules established by the regime training data. The Mahalanobis distance chart (Table 6.6) provides objective regime assignments; a summary of best and possible assignments is given in Table 6.5. The best classification is that training regime closest to the test sounding as measured by the Mahalanobis distance. Alternative classifications, also based on Mahalanobis distances, were deemed likely if the distances were within one standard deviation of the best classification.

3. Discriminant analysis

The regime training data set was used to establish linear discriminant functions for classification of additional satellite sounding data; test soundings were evaluated with respect to these discriminant functions. The results of the discriminant analysis are given in Table 6.5. The internal probability that discriminant analysis assigned the correct classification was calculated to be nearly 100% for each test sounding.

4. Discussion

Results of classifications of the test soundings by three statistical methods compared with the hand analyses are summarized in Table 6.5. None of the test soundings is defined exactly by any of the training regimes; the goal of classification is regime representation.

Until the training data contain soundings representing every conceivable synoptic regime, classification of unknown soundings will retain some ambiguity; the degree of ambiguity is a function of the complexity of the training data. Evaluation of Chernoff faces and the results of CDA reveal why

Table 6.6. Mahalanobis distances among seed sounding and test data synoptic regimes.

SOUND	A	B	C	D	E	F	G	1
A	.	23.9226	90.0039	96.2175	119.0374	121.6981	103.8838	139.3566
B	23.9226	.	83.2624	97.8772	116.7989	118.1533	96.3911	146.3045
C	90.0039	83.2624	.	104.4679	172.3236	175.3797	136.9866	191.4254
D	96.2175	97.8772	104.4679	.	139.3368	168.9852	129.9540	127.5957
E	119.0374	116.7989	172.3236	139.3368	.	57.8387	54.3201	113.0905
F	121.6981	118.1533	175.3797	168.9852	57.8387	.	62.0978	150.4015
G	103.8838	96.3911	136.9866	129.9540	54.3201	62.0978	.	128.3525
1	139.3566	146.3045	191.4254	127.5957	113.0905	150.4015	128.3525	.
2	119.1190	124.3485	176.7746	131.7260	87.3823	111.0775	100.0826	51.1668
3	110.2288	109.3896	163.8729	139.4360	54.2177	57.1875	53.2175	100.9483
4	113.5234	113.1137	171.1966	144.0057	60.2486	65.3399	65.5180	94.5585
5	173.9512	169.9756	226.5498	232.8268	151.9281	123.7958	150.0424	180.7302
6	121.7065	114.0672	161.2341	163.4333	80.4459	56.0741	54.9845	139.7828
7	117.2005	114.3992	169.9591	160.3561	77.0561	59.2251	70.4070	120.4521
8	148.5592	148.6508	171.4282	77.7088	135.1410	178.0925	148.6511	121.2797
9	81.9044	78.7592	69.4565	108.6751	158.5777	155.2456	128.9887	164.3306

SOUND	2	3	4	5	6	7	8	9
A	119.1190	110.2288	113.5234	173.9512	121.7065	117.2005	148.5592	81.9044
B	124.3485	109.3896	113.1137	169.9756	114.0672	114.3992	148.6508	78.7592
C	176.7746	163.8729	171.1966	226.5498	161.2341	169.9591	171.4282	69.4565
D	131.7260	139.4360	144.0057	232.8268	163.4333	160.3561	77.7088	108.6751
E	87.3823	54.2177	60.2486	151.9281	80.4459	77.0561	135.1410	158.5777
F	111.0775	57.1875	65.3399	123.7958	56.0741	59.2251	178.0925	155.2456
G	100.0826	53.2175	65.5180	150.0424	54.9845	70.4070	148.6511	128.9887
1	51.1668	100.9483	94.5585	180.7302	139.7828	120.4521	121.2797	164.3306
2	.	63.4493	52.1185	135.6850	98.9470	74.0657	132.3839	139.6377
3	63.4493	.	19.8017	124.1713	48.2317	37.3862	148.4992	135.7551
4	52.1185	19.8017	.	112.7230	53.4743	31.6643	150.3002	138.2981
5	135.6850	124.1713	112.7230	.	103.4053	88.8264	243.2467	179.7138
6	98.9470	48.2317	53.4743	103.4053	.	34.4263	179.8995	133.2083
7	74.0657	37.3862	31.6643	88.8264	34.4263	.	172.1511	132.6467
8	132.3839	148.4992	150.3002	243.2467	179.8995	172.1511	.	162.7162
9	139.6377	135.7551	138.2981	179.7138	133.2083	132.6467	162.7162	.

a clear classification choice does not always exist: *different classification criteria result in different regime assignments.* For example, classification assignments made on the basis of layer average temperature do not always agree with assignments made using moisture characteristics or with lapse rate. Although CDA indicates that nearly 55% of sounding separation is due to layer average temperature, the remaining 45% of separation is due to the synoptic detail sought in this research. Classifications made by Chernoff faces are dependent on satellite channel assignment to facial feature and on subjective choices made by the analyst. CDA offers objective Mahalanobis distances and subjective canonical variable scatterplots. Of the three methods, only discriminant analysis is completely objective; however, this objectivity is based on statistical, not physical, arguments.

D. Improvements in classification analysis

The faces representing test soundings contain features which compete for various classification assignments. For example, does the mouth (4.3 μm temperature) take precedence over the eyes (15 μm temperature) or the ears (surface temperature) or the eyebrows (water vapor) or the nose (MSU channels)? Clearly, the purpose of faces is to force the analyst to "look at" the data and seek ways to qualify and quantify the sounding separation process. Since CDA reveals which brightness temperature channels contribute to regime separation, the combination of CDA and faces establishes a powerful analytical technique.

Between-class separation of satellite soundings is quantified by CDA. In particular, Fig. 6.5 reveals the important structure in the canonical variables which explains sounding separation. Clearly, CAN1 (Fig. 6.5a) discloses that

the bulk of the between-class variance is due to layer average temperature throughout the troposphere; if satellite sounding separation is made on the basis of average temperature alone, little useful information is gained. However, almost 45% of the additional between class variance structure is present in the remaining meaningful canonical variables, CAN2-CAN3 (Fig. 6.5b-c).

A subjective classification of the training data set also may be made using CDA scatterplots of canonical variables. Fig. 6.9 shows a second CDA computation made with the 450 training soundings and seven (unperturbed) test soundings combined. Using the layer average temperature criterion of CAN1, test soundings A, B and E most closely align with regimes 9 and 2. Test sounding C aligns with regime 1. Test sounding D aligns with regime 8. Test sounding F nearly is indistinguishable from regimes 6 and 7. Test sounding G could be a member of regimes 3, 4, 2 or 9.

Using the moisture criterion of CAN2 as a classification method, test soundings A, B, and C are aligned loosely with regime 9. Test sounding D does not present a clear choice; it is nearest regime 6 but could be a member of 5, 6, 7, 8 or 9. Test sounding E is aligned closely with regimes 2 or 4. Test sounding F aligns with regimes 5, 7 and 8. Test sounding G aligns with regime 6.

CAN3 describes sounding separation by lapse rate. Test sounding A is nearest regime 9 but could be a member of 4, 7, or 8. Test soundings B, C, and D align with regimes 4, 7 or 8. Test soundings E, F and G are nearest regime 6.

The test sounding classifications by canonical variable plot are shown in Table 6.7.

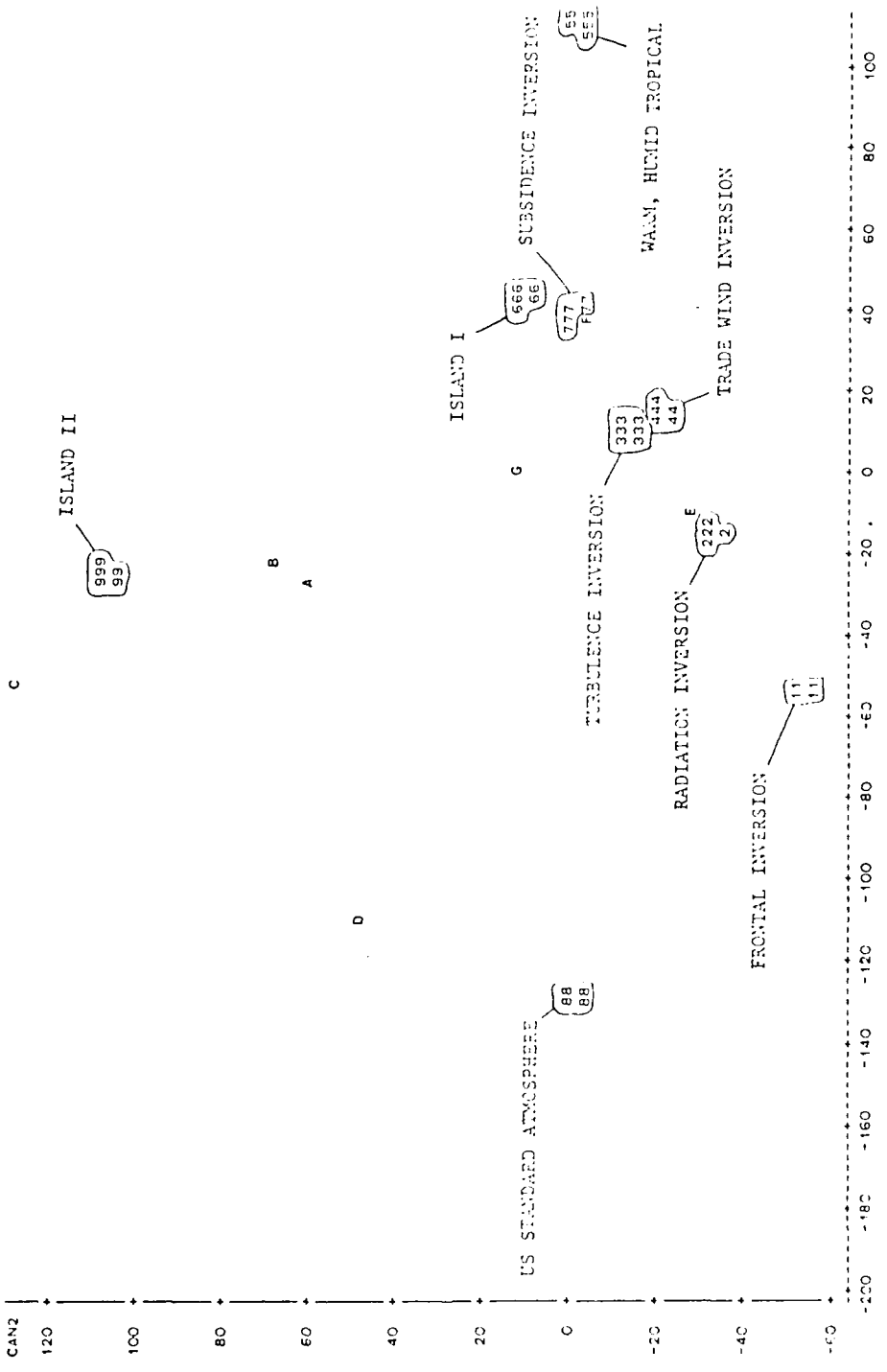

Figure 6.9a. As in Fig. 6.6a, except that the canonical discriminant analysis was performed a second time to include six (unperturbed) test soundings. Test sounding classification based on proximity to known training data sounding classes.

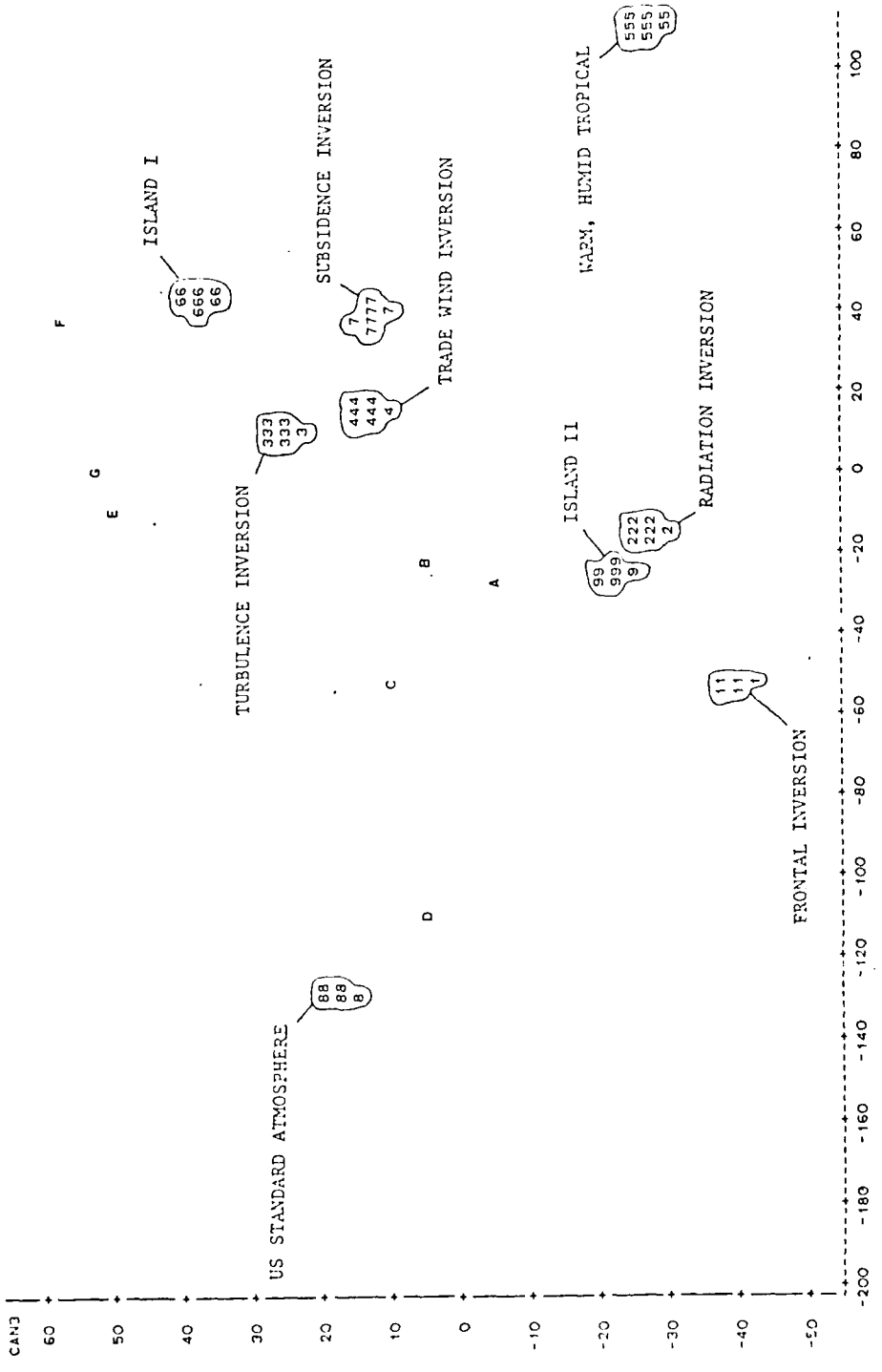

Figure 6.9b. As in Fig. 6.9a, except for CAN3 vs. CAN1.

Table 6.7. Test sounding classifications by canonical variable.

Test sounding	CAN1	CAN2	CAN3	Hand analysis
A	2, 9	9	7, 8, 9	7 (4)
B	2, 9	9	4, 7, 8	4 (7)
C	1	9	4, 7, 8	7 (4)
D	8	5, 6, 7, 8, 9	4, 7, 8	4 (7)
E	2, 9	2, 4	6	4 (7)
F	6, 7	5, 7, 8	6	7 (4)
G	2, 3, 4, 9	6	6	6 (3)

Discriminant analysis was reaccomplished using the structural separation information gained from CDA; the results are presented in Table 6.8.

E. Fine structure analysis

Satellite observations are classified into synoptic regimes by analysis of between-class variance. Once a satellite observation is classified, the next step is to study its synoptic characteristics by analysis of *within-class* variance. Once inside the synoptic regime, what are the differences among satellite soundings?

The trade wind and frontal inversion training data sets (see Chapter V) were evaluated by factor analysis, a procedure similar to PCA. Factor analysis seeks to reduce the number of variables by finding a few weighted averages (factors) of the original variables that summarize parsimoniously the information they contain. For example, the 22 satellite brightness temperature channels may be approximated by only a few factors. The factors are

Table 6.8. Discriminant analysis classifications of test soundings by canonical variable.

	Classification based on:			
Test sounding	CAN1	CAN2	CAN3	Hand analysis
A	9	9	3	7 (4)
B	9	3	3	4 (7)
C	9	9	3	7 (4)
D	8	8	8	4 (7)
E	3	3	3	4 (7)
F	7	6	9	7 (4)
G	6	3	3	6 (3)

constructed to retain as much of the information contained in the original variables as possible. The channels are retained selectively as the factors are created. Often, physical meaning can be assigned to individual factors.

The weighted coefficients are called *loadings* and take on values between -1 and 1. The signs of the loadings are not important, but the relative signs among variables are and reveal relationships among the channels.

The factors are rotated orthogonally. The original factor loadings normally are not interpretable readily; the usual practice is to rotate them until a simpler structure is found. Rotation does not change the information content; rather, it is like sharpening the focus on an optical device. The same information is present, but after focusing, it appears with greater clarity.

The procedures for analyzing within-class variance are specific for synoptic regime and are not applicable unless a satellite sounding first is identified as a member of the correct group, for example, the trade wind inversion class.

1. Analysis of trade wind inversion structure

Four factors (Fig. 6.10) explain almost 93% of the total within-class variance. The first factor (Fig. 6.9a) can be interpreted as depicting boundary layer lapse rate and average tropospheric temperature. The second factor (Fig. 6.9b) contains the mid tropospheric water vapor channel, and the surface and near-surface temperature channels. The third factor (Fig. 6.10c) shows contributions by the surface temperature channels and weak signals in water vapor channels. Contributions from the fourth factor (Fig. 6.10d) resemble the first except that 500 and 700 hPa water vapor channels have opposite signs, and there is little contribution from the upper troposphere. Together, these factors illustrate variations among soundings within the trade wind inversion

family. In the discussion that follows, it should be remembered that cold radiative temperatures imply moistness and vice versa.

Factor 1 (Fig. 6.10a) explains just over 50% of the variance. In the rotated factor loading, the surface window channels (8, 18 and 19) are positive but of small amplitude. Most of the tropospheric temperature sensing channels (3-7 and 13-16) are strongly negative. The moisture channels (11 and 12) make a lesser contribution and all are negative, suggesting modest influence of moisture aloft. Channel 10, designed as a 900 hPa moisture sensor but accepted also as a temperature channel, makes no contribution. This factor pattern describes near surface inversion structure and tropospheric layer average temperature. There is little moisture signal in factor 1.

Factor 2 (Fig. 6.10b) carries just under 29% of the variance. The surface temperature channels (8, 18-19) and the 700 hPa tropospheric moisture channel (11) are negative. Channel 10 is strongly negative. Its interpretation often is controversial because the channel senses either boundary layer temperature or moisture depending on the synoptic situation. In this case, it appears to sense moisture, and together with channel 11, implies moist conditions from the boundary layer through 700 hPa. The remaining tropospheric temperature channels are negative but tend toward positive from the surface upward. Channel 12 makes no contribution, but its sign is more positive than either of the other moisture channels which suggests that, by 500 hPa, the atmosphere is drier than in the lower layers. These relationships suggest that if the atmosphere is cool at the surface, it coincidently is warm and moist at the mid troposphere. This factor appears to represent the structure of the trade wind inversion: the temperature inversion; the moist boundary layer; and, the dry layer in the upper portion of the troposphere.

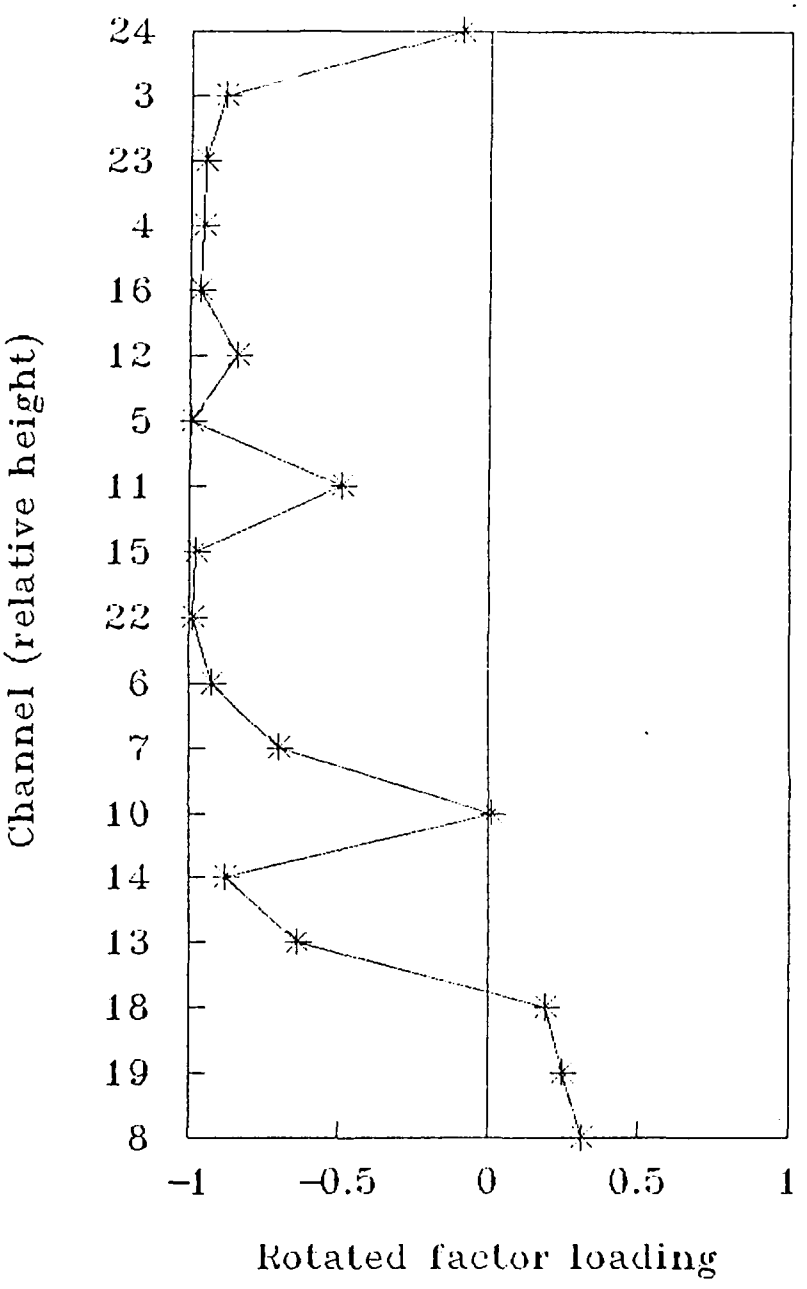

Figure 6.10a. Rotated factor loading from analysis of trade wind inversion data set. Factor 1 carries 50% of the variance and describes near-surface inversion structure and tropospheric layer average temperature.

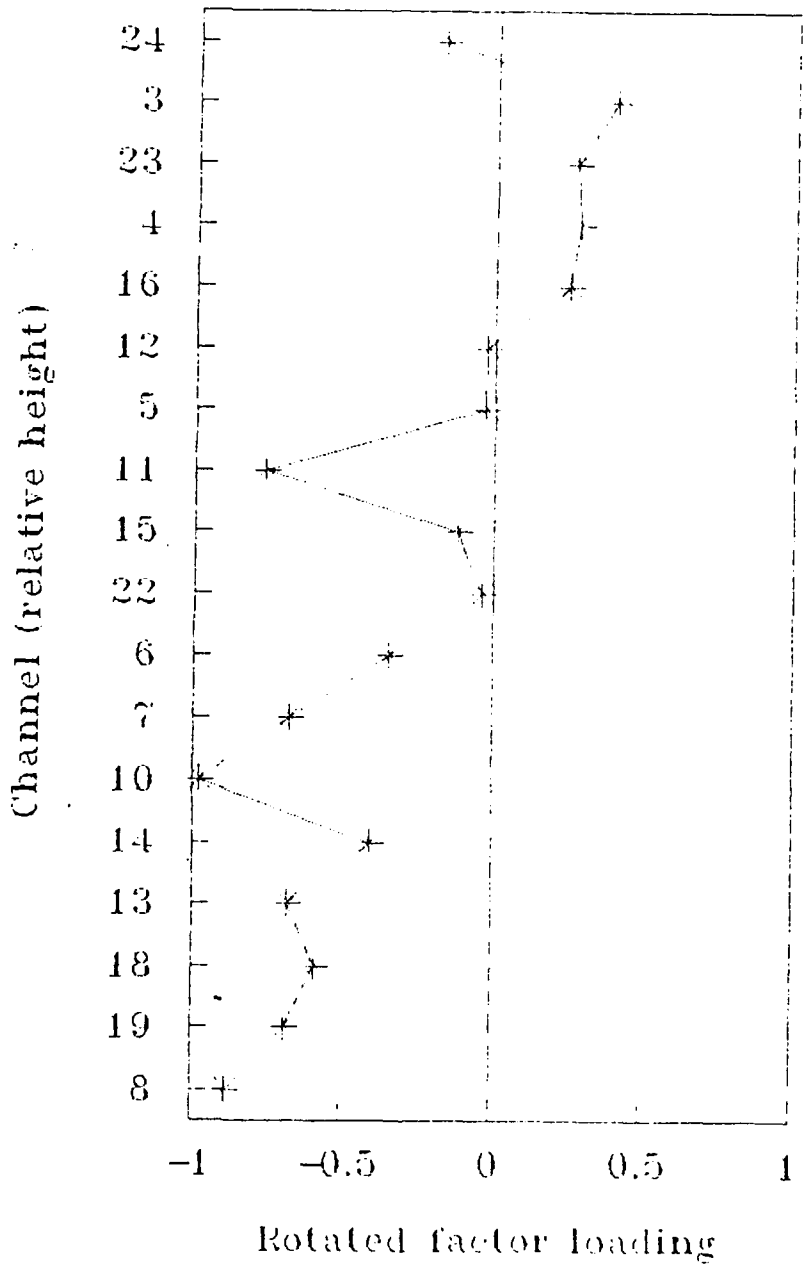

Figure 6.10b. As in Fig. 6.10a, except for factor 2 which may be interpreted to describe the structure of the trade wind inversion. Factor 2 carries about 28% of the variance.

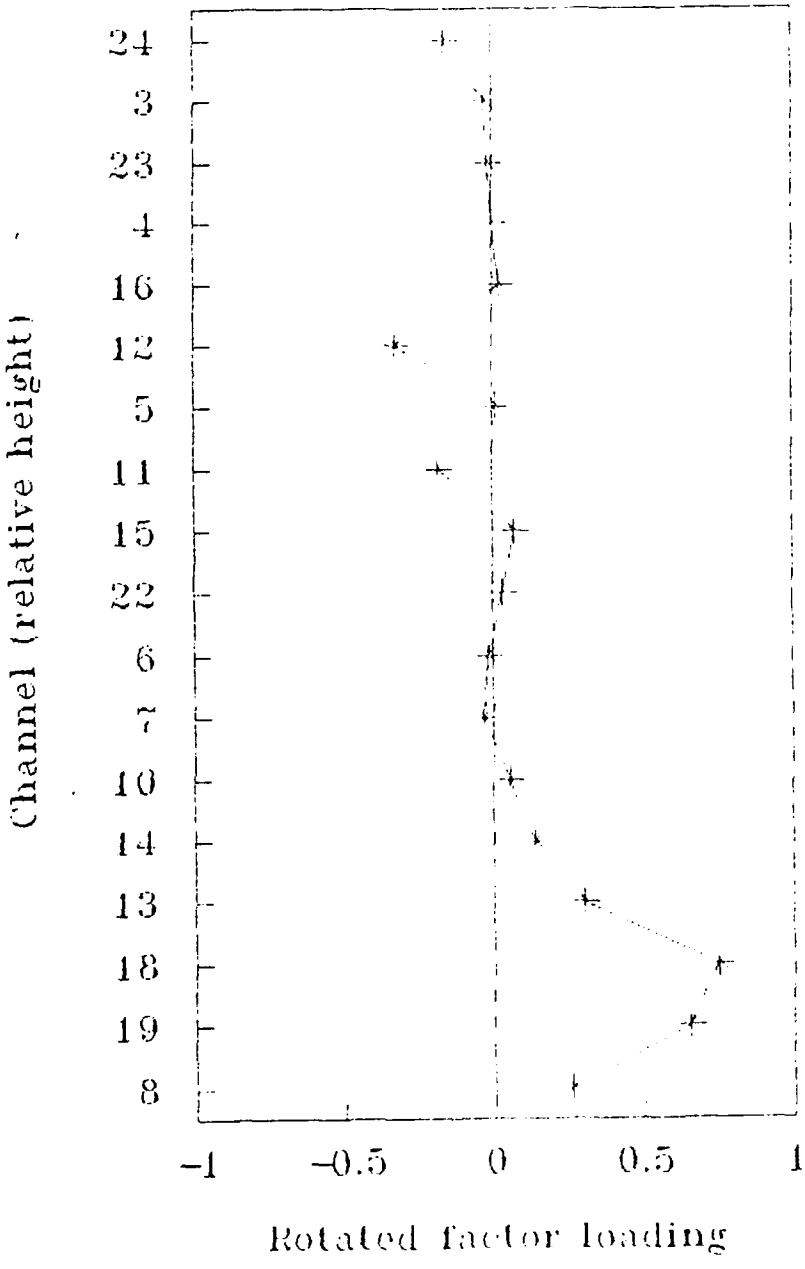

Figure 6.10c. As in Fig. 6.10a, except for factor 3 which yields little structural information. Factor 3 accounts for almost 9% of the variance.

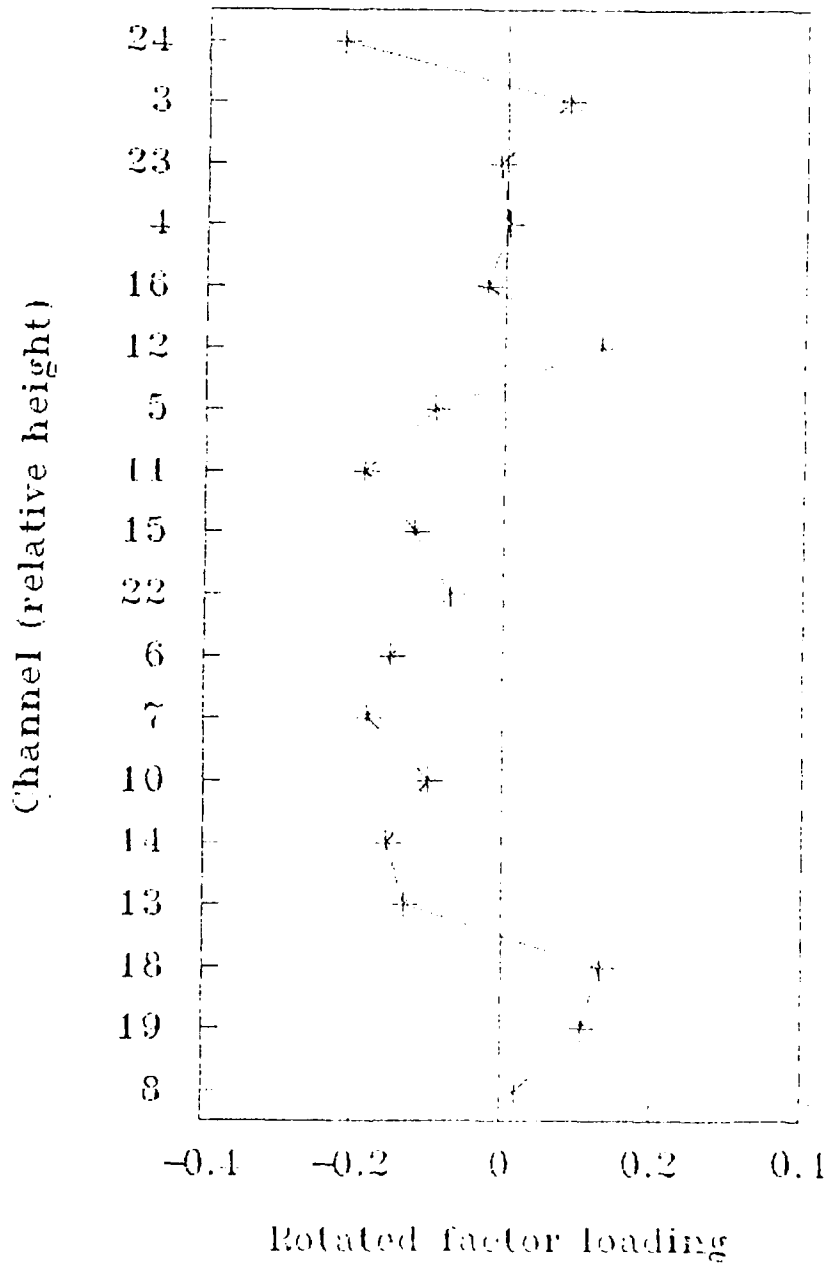

Figure 6.10d. As in Fig. 6.10a, except for factor 4 which represents the moisture profile through the inversion. Factor 4 represents barely 5% of the variance.

Factor 3 (Fig. 6.10c) resolves almost 9% of the variance. Few channels make significant contribution to this factor. The surface and boundary layer temperature channels (8, 13-14, 18-19) are positive; the moisture channels (11-12) contribution is negative and weak. Little structural information is gained.

Factor 4 (Fig. 6.10d) explains less than 5% of the variance. Most of the same surface and mid to lower tropospheric temperature sensing channels in factor 1 appear in factor 4 in much the same pattern and suggest a weak lapse rate signature. However, the significant feature of factor 4 is that the signs of moisture channels 11 and 12 are opposite. Channel 11 senses moisture at 700 hPa and channel 12 senses moisture at 500 hPa. The signs of the loading for these two channels suggest that when the atmosphere is moist at 700 hPa, it is, at the same time, dry at 500 hPa. These are the conditions expected in a trade wind inversion.

2. Analysis of frontal inversion structure

Four factors (Fig. 6.11) accounted for over 94% of the variance in the frontal inversion structure. Factor 1 (Fig. 6.11a) can be interpreted as describing describing lower tropospheric average temperature. Factor 2 (Fig. 6.11b) suggests the relationship between temperature and moisture in the mid and upper troposphere. Factor 3 (Fig. 6.11c) is strictly a weak tropopause signal and is not relevant in this research. Factor 4 (Fig. 6.11d) appears to be a temperature lapse rate signal.

Factor 1 (Fig. 6.11a) carries almost 52% of the variance and is composed of channels which describe layer average temperature in the lower half of the troposphere, the boundary layer, and the surface (5-7, 10, 13-15, 8, 18-19, 22).

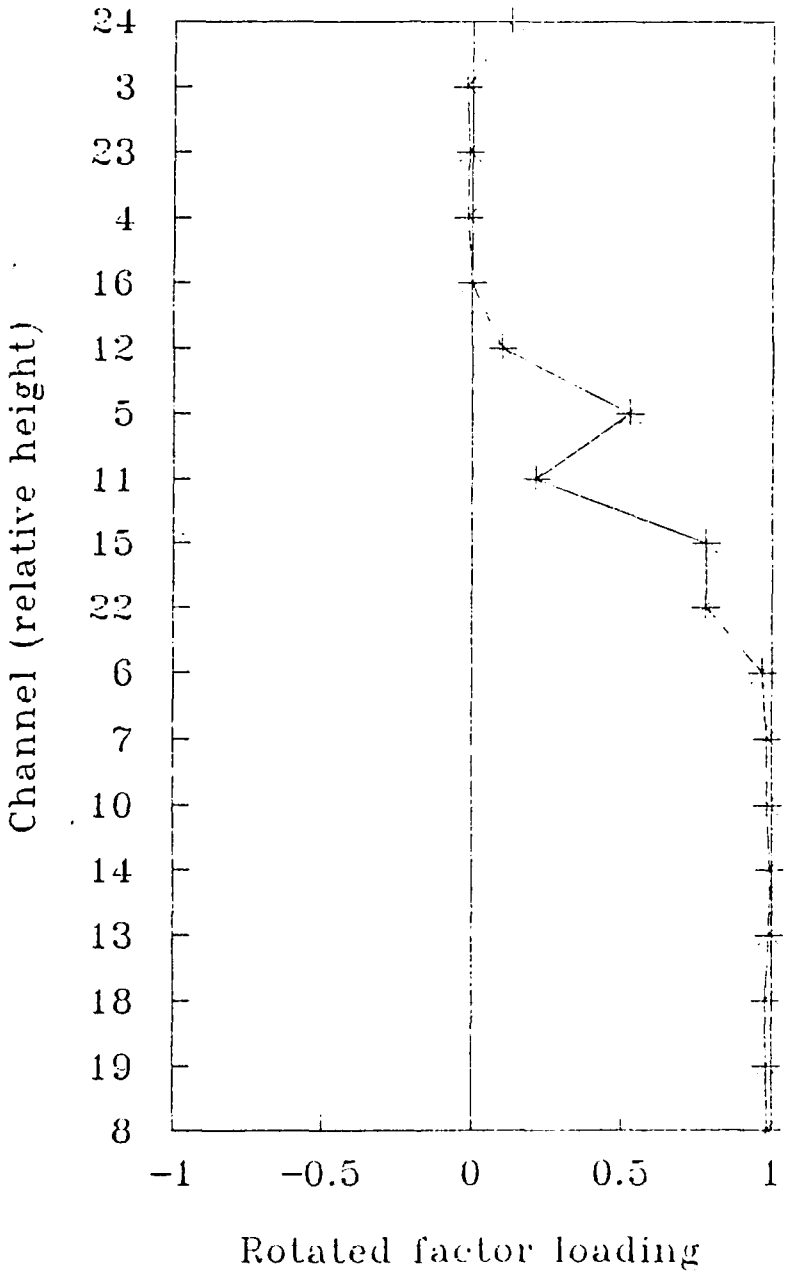

Figure 6.11a. As in Fig. 6.10a, except for frontal inversion data set. Factor 1 is influenced by lower tropospheric average temperature and accounts for almost 52% of the variance.

The signs of all contributing channels are positive.

Factor 2 (Fig. 6.11b) explains over 32% of the variance. It describes the relationship of temperature and moisture in the mid and upper troposphere and is composed of mid to upper temperature channels (3-5, 15-16, and 22-24) and moisture channels (11-12). The signs of the loadings of temperature and moisture are opposite indicating a warm and moist or cool and dry middle troposphere. This relationship suggests the ability to distinguish between pre-frontal/post-frontal conditions.

Factor 3 (Fig. 6.11c) has little useful structure although it carries over 6% of the variance. The main contribution arises from channels 1 and 2 which are sensitive to temperature in the stratosphere and are not a part of this study.

Factor 4 (Fig. 6.11d) carries only 4% of the variance and appears to be a weak lower tropospheric temperature lapse rate signature. The surface channels (18-19) are positive while mid tropospheric channels (4-6, 15-16) are negative. The MSU channels (22-24) suggest a lapse rate as well.

3. Fine structure measurement

The factors resulting from the preceding analyses are important because they reveal structure in the satellite observations. Taken collectively, patterns emerge which explain how synoptic regimes differ in terms of their brightness temperature signatures. For example, Fig. 6.10 and 6.11 illustrate the differences between the signature patterns of a group of trade wind inversions and a group of frontal inversions. The differences arise from temperature and moisture profiles which are present in the natural atmosphere and discerned in the satellite observations; the structural detail is different for each regime. This information may be combined with additional analysis techniques to

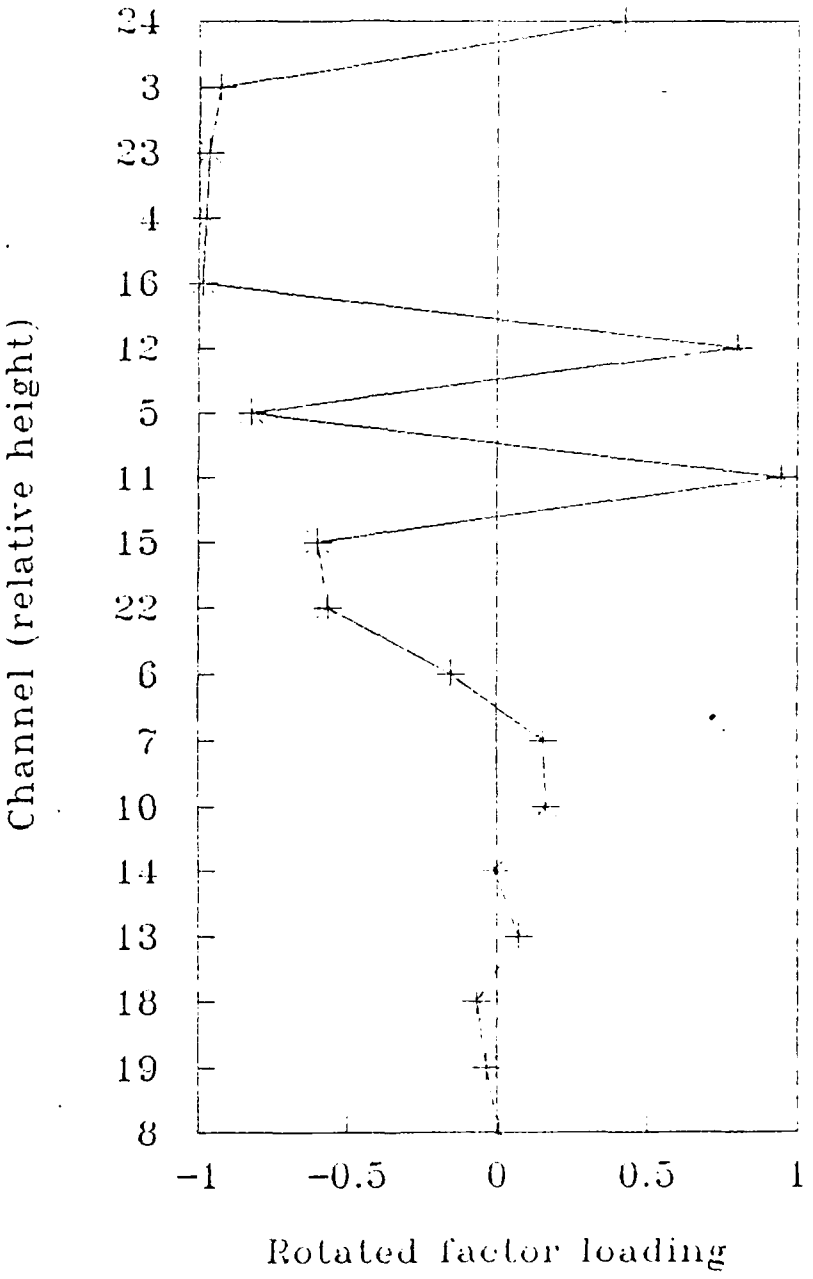

Figure 6.11b. As in Fig. 6.11a, except for factor 2 which describes the relationship of temperature and moisture in the mid and upper troposphere and carries over 32% of the variance.

investigate satellite observations that have been classified into a synoptic regime but whose structures have not been deciphered.

A curious paradox of multivariate analysis is that often the first canonical variable or factor contains most of the variance but little useable information. In the canonical discriminant analysis of regime separations and factor analysis of specific inversion features, CAN1 or factor 1 differentiate among layer average temperatures even though an effort was made to minimize those differences when constructing the training and choosing the test data sets. The synoptic subtleties that contribute to regime separation and feature measurement appear primarily in the lower order canonical variables and factors, and it is those which are most useful.

It is possible to estimate the physical characteristics of synoptic features directly in satellite observation data if models are constructed from sufficiently complete training data. In the following example, it is assumed that a sounding has been identified previously and contains a trade wind inversion. The trade wind inversion training data set was analyzed by discriminant analysis and was used to establish a set of rules to measure the strength and height of the trade wind inversions in the test sounding data set. Trade wind inversions are present in four of the seven test soundings: A, B, C and D. The height and strength of the inversions were analyzed by hand, and the results were used as reference. Discriminant models designed to predict inversion height and strength were created for each factor using the particular combinations of channels identified by factor analysis. For example, the loadings used in the discriminant model suggested by factor 1 include channels 5-7, 10, 13-15, 8, 18-19, and 22.

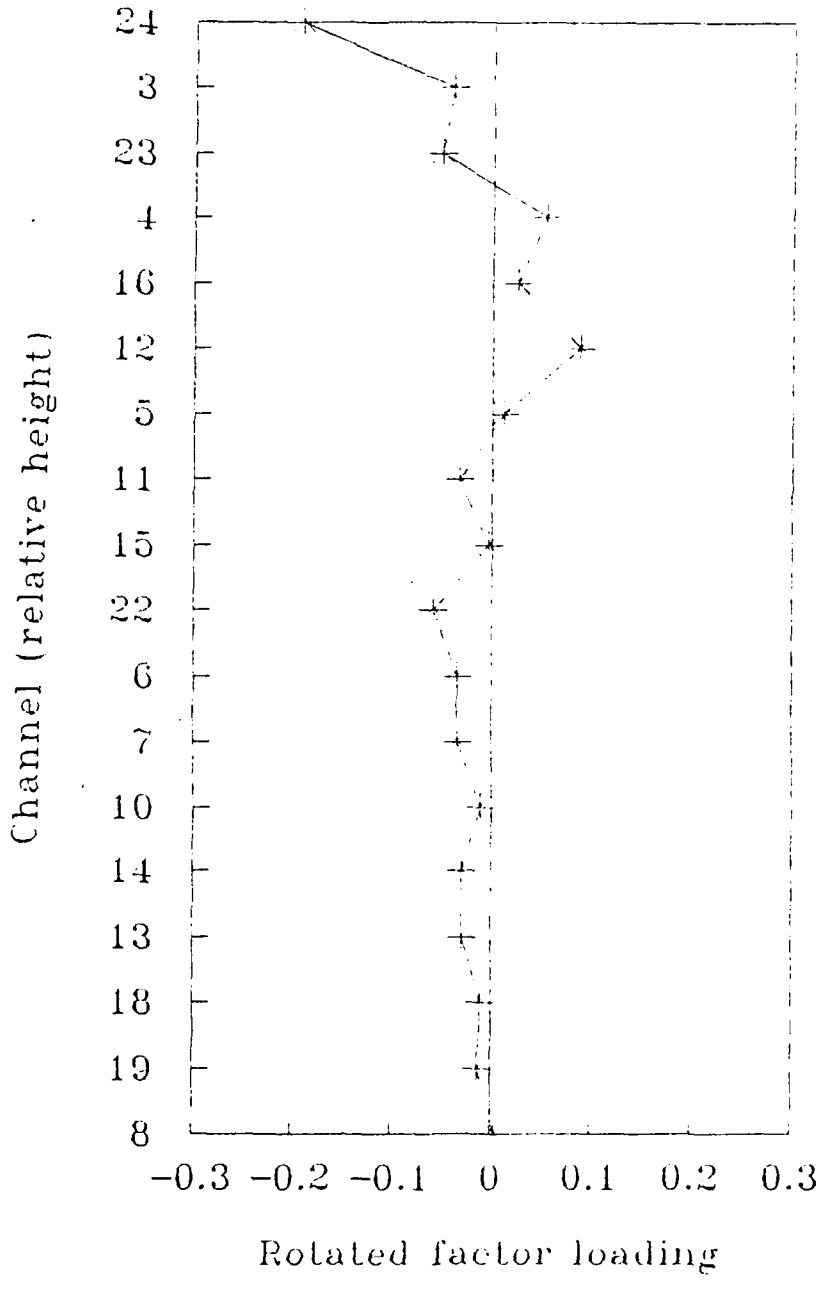

Figure 6.11c. As in Fig. 6.11a, except for factor 3 which reveals information from channels not used in this research. Factor 3 carries about 6% of the variance.

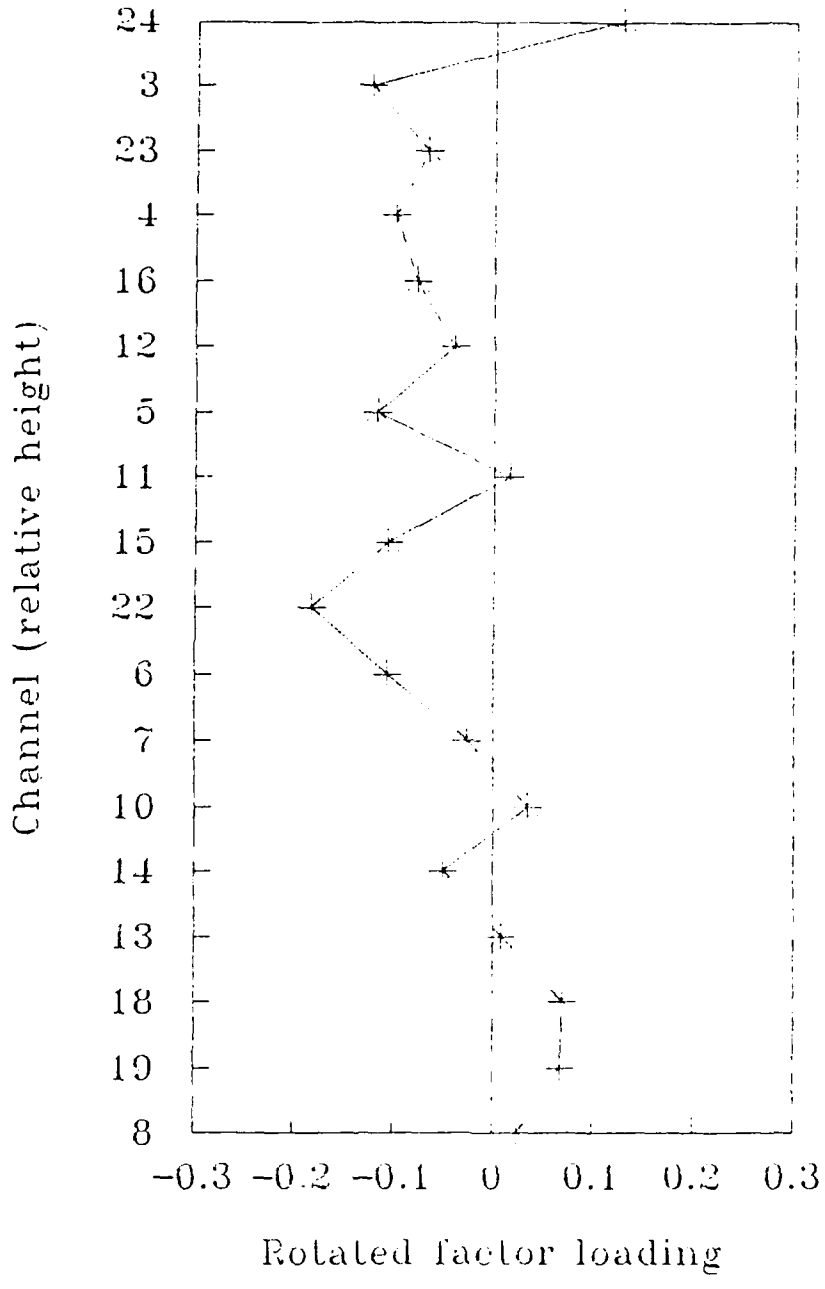

Figure 6.11d. As in Fig. 6.11a, except for factor 4 which appears to have a temperature lapse rate signal and carries just over 4% of the variance.

In the height and strength analysis of the trade wind inversion, factor 1 explains layer average temperature, and factor 3 reveals surface temperature. Factors 2 and 4 are expected to differentiate most successfully among satellite observations containing trade wind inversions. The training data are not yet complete enough to produce high resolution discriminant models. In the analysis of test soundings A-D, factor 2 appears most sensitive to inversion height.

Table 6.9 summarizes the discriminant analysis prediction results using models created from factors 1-4. The models are constructed from analysis of synthetic satellite observations of only 24 trade wind inversions. The soundings are drawn carefully to illustrate inversions of eight varying heights and three varying strengths, but they are formed from a limited data base. Expansion of the training data base to include normal variation as found in the atmosphere is expected to yield improved results. Test soundings E-F contained no trade wind inversion structure and were not included in the analysis.

F. Spatial coherence analysis

Two vertical cross sections (Figs. 5.7 and 5.8) were analyzed using the fine structure measurement method and frontal inversion discriminant functions described in Section E. Only the first two factors of the frontal inversion analysis were used to establish the predictive discriminant functions. Each cross section was taken from across a front; six atmospheric soundings were taken through A, and five were taken through B (see Chapter 5). The sections were analyzed by hand to determine the actual height and strength of the inversions present in the individual panels; the atmospheric soundings were

Table 6.9. Hand analyzed and predicted trade wind inversion features.

	Hand[a] analysis		Predicted by Factor1		Factor2		Factor3		Factor4	
Test snd	Hgt[b]	Str[c]	Hgt	Str	Hgt	Str	Hgt	Str	Hgt	Str
A	750	.2	600	.04	700	.04	600	.04	800	.04
B	850	.04	600	.04	650	.04	600	.04	600	.04
	700	.04								
C	800	.04	600	.04	600	.04	600	.04	600	.04
D	800	.1	650	.1	600	.1	600	.04	600	.1
	700	.04								

[a] Soundings may contain more than one inversion.
[b] Height of base of the inversion (hPa).
[c] Strength of inversion (°C hPa^{-1}).

evaluated by the RTM; and, brightness temperature vectors were produced. The analysis was performed to determine whether the spatial coherence of the frontal structure could be followed in the satellite observation taken across the vertical sections.

Soundings from vertical cross section A (Fig. 5.7) depict a well-defined, gently sloping cold front that begins at (base height) 300 hPa (Fig. 5.7a) and reaches the surface (Fig. 5.7e). Soundings from vertical cross section B (Fig. 5.8) depict a similar frontal structure. The base of the frontal inversion is at 450 hPa (Fig. 5.8a) and slopes to the surface (Fig. 5.8c). There is little remnant of the frontal inversion structure shown in Fig. 5.8d and less in Fig. 5.8e. The upper and lower boundaries of the front are shown in Figs. 5.7 and

5.8 by the heavy horizontal lines. The results of spatial coherence analysis are shown in Table 6.10.

The inversions in vertical cross sections A and B are frontal; the structure of cross section A is organized better than that of section B. Discriminant functions derived from the frontal inversion training data set were used to make predictions of the inversion structure of the sections. The characteristics of the frontal inversion factor loadings suggest that factor 2 is the better predictor of frontal inversion height and strength.

There are two temperature and moisture patterns in Fig. 5.7b which resemble the frontal inversion; however, in neither does the temperature increase or remain constant with height. As in Fig. 5.7a, the temperature discontinuity with the 300 hPa base is missed, but a weaker feature with base at about 850 hPa is predicted. In Fig. 5.7c, the inversion base is between 800 and 700 hPa; 900 hPa was predicted. In Fig. 5.7d-f, the frontal inversion is at the surface and varies only in strength. The factor 2 prediction places the inversion base height at 900 hPa for three soundings; however, the procedure fails to detect the change in relative inversion strength.

Vertical cross section B (Fig. 5.8) contains a competing, secondary temperature discontinuity which appears prominently in Fig. 5.8b-c. The frontal inversion structure is not defined as clearly as in section A. The inversion in Fig. 5.8a more resembles a trade wind inversion; there is some frontal inversion temperature/moisture structure near the surface. Discriminant analysis predicts an inversion height of 900 hPa in the sounding shown in Fig. 5.8a. The frontal inversion clearly appears in Fig. 5.8b; its base is at 750 hPa. The best predictor fails to detect the inversion at this height and, instead, predicts the base to be at 900 hPa. Factor 1 correctly predicts the

Table 6.10. Hand analyzed and predicted spatial coherence of inversion structure.

Vertical cross section A

	Hand analysis		Predicted by Factor1		Predicted by Factor2	
Test Snd	Hgt[a]	Str[b]	Hgt	Str	Hgt	Str
a	300	.02	850	.02	750	.05
b[c]	350	.1	950	.02	850	.05
	800	Weak				
c	800	.02	850	.02	900	.02
d	900	.1	950	.02	900	.02
e	900	.02	950	.02	900	.02
f	SFC	.02	950	.02	900	.02

Vertical cross section B

	Hand analysis		Predicted by Factor1		Predicted by Factor2	
Test Snd	Hgt	Str	Hgt	Str	Hgt	Str
a	500	.01	950	.02	900	.05
b	750	.02	750	.02	900	.02
c	SFC	.02	750	.02	900	.02
d	SFC	Weak	750	.02	850	.02
e	SFC	Weak	750	.02	850	.02

[a] Height of base of the inversion (hPa).
[b] Strength of inversion (°C hPa^{-1}).
[c] More than one inversion.

inversion height at 750 hPa; however, this likely is coincidence. The inversion in Fig. 5.8c is at the surface and is predicted as 900 hPa. In Fig. 5.8d-e the inversion begins to lose organization and remains in the boundary layer structure. The discriminant analysis continues to predict an inversion in the boundary layer at 850 hPa.

Inversion strength predictions did not fare well. Possibly the additional structure in the soundings suggested added temperature discontinuity which the model interpreted as inversion strength. Only the general trend of the characterization is expected to result when the discriminant analysis models are constructed from more complete training data.

CHAPTER VII

SUMMARY AND CONCLUSIONS

A. Summary

The quality of data retrieved from satellite observations is dependent, in part, on methods used to convert satellite observations into conventional atmospheric data. To improve the spatial resolution of satellite observations, new techniques for identification and quantification of synoptic scale features directly in satellite data were found. These methods exploit the vertical variance structure of individual satellite channel brightness temperature data and use advanced multivariate statistical techniques, some of which treat the data as having discrete rather than continuous distributions.

Current operational retrieval methods exploit the same between-class variance structure used in this research to separate satellite observations into synoptic regimes. An underlying, second-level variance structure was identified within each synoptic regime. The second-level structure is unique for each synoptic regime and can be used to estimate details of synoptic features in satellite retrieved atmospheric soundings.

A series of atmospheric soundings were taken from data summaries to be representative of certain synoptic regimes typically found over the tropical eastern Pacific Ocean. The soundings were altered, within prescribed limits, to introduce variance normally found in nature. A radiative transfer model (RTM) was procured and prepared; the soundings were evaluated by the RTM, which computed, for each sounding, the equivalent TOVS channel brightness temperature data set that would have been produced had the satellite observed the atmospheric sounding in nature. Varying aerosol, cloud and hydrometeor

effects were ignored. In this fashion, a training data set of 450 soundings representing nine distinct synoptic regimes was prepared.

The introduction of Chernoff faces, a multivariate graphical technique, allowed 17 individual satellite channel brightness temperatures to be viewed simultaneously in two dimensions. Normalized channel brightness temperatures govern the size, shape and placement of facial features on the caricature of a human face. Chernoff faces were used for two purposes: first, similar faces were grouped, allowing satellite observations to be classified according to facial expression; and, second, by observing changing facial features representing a series of satellite observations, the channels which carried the variance were identified.

The satellite channel brightness temperatures were clustered objectively to determine the number of distinct regimes represented by the data. Next, the variance structure that gave rise to the regime separation was quantified by canonical discriminant analysis which gave physical definition to the separation structure. Separation was found to be the result of three primary factors: (1) tropospheric average temperature; (2) tropospheric moisture; and, (3) tropospheric lapse rate.

After determining the pattern for regime separation, the structure of two individual synoptic features, identified as the trade wind inversion and the frontal inversion, were examined. A training data set of trade wind inversion soundings at various heights and strengths was created and evaluated by the RTM. The satellite channel brightness temperatures were analyzed by two methods, factor analysis and discriminant analysis.

Factor analysis revealed that the synoptic signature of trade wind inversions is described by three factors: (1) tropospheric layer average

temperature; (2) the temperature profile at the inversion; and, (3) the temperature and moisture relationship characteristic of the trade wind inversion. The signatures of these factors are unique to the trade wind inversion.

The frontal inversion data set was evaluated in a similar fashion and is described also by three factors: (1) lower tropospheric average temperature; (2) temperature and moisture in the middle troposphere; and (3) temperature lapse rate in the lower and mid troposphere. The signatures of these factors are unique to the frontal inversion.

In addition to quantifying variance, factors define variable relationships. Individual satellite channels that comprise each factor are identified, and the relationships among channels and factors may be used to form discriminant models which infer physical characteristics of synoptic features directly from brightness temperature data.

Linear discriminant functions were computed for the trade wind inversion data set and used to create predictive equations which quantified inversion structure. In a similar fashion, the spatial coherence of a sloping frontal inversion structure was studied in two vertical cross sections. Success was only modest, but, in general, the existence of the inversion structure was followed through most of the cross section.

B. Limitations

The new techniques developed in this research are sound in concept and have been demonstrated satisfactorily in controlled data. It is emphasized that this research concentrates on technique development and uses synthetic data. The vagaries of "real" data are certain to introduce additional variance that

may be challenging to interpret or neutralize; of special significance are multiple sounding features, aerosols, hydrometeors, non-synoptic moisture influences, and varying surface quality which always will contaminate the more subtle radiance signals.

The linear discriminant functions used (1) to predict inversion characteristics and (2) to measure spatial coherence of frontal features were derived from a limited training data set. As a result, the accomplishment of these two objectives was limited. Expansion of the training data set to include more varied synoptic features should lead to more accurate predictions.

C. Significance

The research produced several new techniques by which satellite observations may be identified and quantified. Advances were made in four areas: (1) determination of the signatures of synoptic features directly in satellite channel brightness temperatures without the use of conventional retrieval algorithms; (2) introduction into the atmospheric sciences of a heretofore unused multivariate graphical technique for qualitative data analysis as well as comparison with other state-of-the-art classification procedures; (3) testing of a procedure for quantification of the fine structure of synoptic features; and, (4) groundwork for expansion of the new techniques developed in this research to the operational realm.

REFERENCES

Anderson, L. L., 1986: Multispectral analysis of a tropical radiance set from the TIROS operational vertical sounder. PhD Dissertation, Texas A&M University, 229 pp.

Andrews, D. F. 1972: Plots of high dimensional data. *Biometrics, 28*, 125-136.

Atkinson, B. W., 1981: *Meso-scale Atmospheric Circulations.* Academic Press, New York, 495 pp.

Blackwell, K. B., 1987: Synoptic scale sensitivity of TIROS-N moisture channels in the tropics. M.S. Thesis, Texas A&M University, 124 pp.

BMDP, 1988: *SOLO User's Guide and IBM Computer Software.* BMDP Statistical Software, Inc., Los Angeles, 286+69 pp.

Chatfield, C., 1984: *The Analysis of Time Series.* Chapman and Hall, New York, 286 pp.

Chernoff, H., 1973a: Using faces to represent points in k-dimensional space graphically. *J. Am. Statistical Assoc., 68*, 361-368.

_____, 1973b: The use of faces to represent points in k-dimensional space graphically. *J. Am. Statistical Assoc., 70*, 548-554.

Fleming, H. E., M. D. Goldberg and D. S. Crosby, 1986: Minimum variance simultaneous retrieval of temperature and water vapor from satellite radiance measurements. Preprint from Second Conference on Satellite Meteorology/Remote Sensing and Applications, Williamsburg, VA, Amer. Meteor. Soc., 20-23.

_____, _____, and _____, 1988: Operational implementation of the minimum variance simultaneous retrieval method. Preprint from Third Conference on Satellite Meteorology and Oceanography, Anaheim, CA, Amer. Meteor. Soc., 16-19.

Goldberg, M. D., J. M. Daniels and H. E. Fleming, 1988: A method for obtaining an improved initial approximation for the temperature/moisture retrieval problem. Preprint from Third Conference on Satellite Meteorology and Oceanography, Anaheim, CA, Amer. Meteor. Soc., 20-23.

Griffiths, J. F. and D. M. Driscoll, 1982: *Survey of Climatology*. Charles E. Merrill, Columbus, OH, 358 pp.

Haltiner, G. J. and R. T. Williams, 1980: *Numerical Prediction and Dynamic Meteorology*. John Wiley and Sons, New York, 477 pp.

Houghton, J. T., F. W. Taylor and C. D. Rodgers, 1984: *Remote sounding of atmospheres*. Cambridge University Press, Cambridge, England. 343 pp.

Johnson, R. A. and D. W. Wichern, 1982: *Applied Multivariate Statistical Analysis*. Prentice Hall, Englewood Cliffs, NJ, 594 pp.

Karson, M. J., 1982: *Multivariate Statistical Methods*. The Iowa State University Press, Ames, IA, 307 pp.

Koopmans, L. H., 1981: *An Introduction to Contemporary Statistics*. Duxbury Press, Boston, 599 pp.

Lipton, A. E., D. W. Hillger and T. H. Vonder Haar, 1986: Water vapor vertical profile structures retrieved from satellite data via classification and determination. *Mon. Wea. Rev., 114*, 1103-1111.

McGuirk, J. P., L. L. Anderson and A. H. Thompson, 1985: Satellite-derived synoptic climatology in data-sparse regions. *Adv. Space Res., 5(6)*, 45-48.

_____, A. H. Thompson and L. L. Anderson, 1986: Wintertime disturbances in the tropical Pacific: FGGE IIIb and satellite comparisons. Preprint from National Conference on Scientific Results of the First GARP Global Experiment, Miami, Jan. 1986, Amer. Meteor. Soc., 4 pp.

McMillin, L. M., 1986: The use of classification procedures to improve the accuracy of satellite soundings of temperature and moisture. Preprint from Second Conference on Satellite Meteorology/Remote Sensing and Applications, Williamsburg, VA, Amer. Meteor. Soc., 1-4.

_____, 1988: Retrieval of air surface temperatures over oceans from satellite radiance measurements using stratification techniques. Preprints from Third Conference on Satellite Meteorology and Oceanography, Anaheim, CA, Amer. Meteor. Soc., 10-12.

Moine, P., A. Chedin, N. A. Scott and G. Rochard, 1986: Automatic air masses classification for satellite temperature retrievals. Preprints from Second Conference on Satellite Meteorology/Remote Sensing and Applications, Williamsburg, VA, Amer. Meteor. Soc., 5-10.

Neter, J., W. Wasserman and M. H. Kutner, 1983: *Applied Linear Regression Models*. Richard D. Irwin, Inc., Homewood, Illinois, 547 pp.

Riehl, H., 1979: *Climate and Weather in the Tropics*. Academic Press, 611 pp.

Rodgers, C. D., 1976: Retrieval of atmospheric temperature and composition from remote measurements of thermal radiation. *Rev. Geophys. Space Phys., 14*, 609-624.

SAS Institute, 1982: *SAS User's Guide: Statistics*. SAS Institute, Cary, 584 pp.

Smith, W. L. and H. M. Woolf, 1976: The use of eigenvectors of statistical covariance matrices for interpreting satellite sounding radiometer observations. *J. Atmos. Sci., 33(7)*, 1127-1140.

_____, _____, C. M. Hayden, D. Q. Wark and L. M. McMillin, 1979: The TIROS-N operational vertical sounder. *Bull. Am. Meteor. Soc., 58*, 1177-1187.

Susskind, J., J. Rosenfield, D. Reuter and M. T. Chahine, 1982: The GLAS physical inversion method for analysis of HIRS2/MSU sounding data. NASA Tech. Memo. 84936, Goddard Space Flight Center, Greenbelt, MD, 101 pp.

_____, _____ and _____, 1984: Remote sensing of weather and climate parameters from HIRS2/MSU on TIROS-N. *J. Geophys. Res.*, *89*, 4677-4697.

Thompson, O. E., M. D. Goldberg and D. A. Dazlich, 1985: Pattern recognition in the satellite temperature problem. *J. Climate Appl. Meteor.*, *24*, 30-48.

Uddstrom, M. J. and D. Q. Wark, 1985: A classification scheme for satellite temperature retrievals. *J. Clim. and Appl. Meteor.*, *24*, 16-29.

Wang, P. C. C., ed., 1978: *Graphical Representation of Multivariate Data.* Academic Press, New York, 278pp.

Westwater, E. R. and O. N. Strand, 1968: Statistical information content of radiation measurements used in indirect sensing. *J. Atmos. Sci.*, *25*, 750-758.

_____, M. T. Decker, A. Zachs and K. S. Gage, 1983: Ground-based remote sensing of temperature profiles by a combination of microwave radiometry and radar. *J. Climate Appl. Meteor.*, 22, 126-133.

VITA

G. Anderson White, III

G. Anderson (Andy) White, III [redacted] Andy graduated from Chapel Hill High School in 1968 and from the University of North Carolina at Chapel Hill in 1972 with a degree in chemistry. He worked as a research physicist until he accepted a commission in the United States Air Force. He completed the basic meteorology program at Texas A&M University in 1979. His first Air Force assignment was to Wright Patterson AFB, Ohio where he worked as staff meteorologist to the Air Force Wright Aeronautical Laboratories. In 1981, Andy returned to Texas A&M under the sponsorship of the Air Force Institute of Technology and, in 1983, received the M.S. degree in meteorology.

In 1983, he was assigned to Headquarters, Second Weather Squadron, Andrews AFB, Maryland. He served there until 1985 when he returned to Texas A&M for additional studies and to conduct the research descibed in this document. [redacted]